A Numerical Study of a Highway Embankment on Degrading Permafrost

By

Arash Gholamzadehabolfazl

A Thesis submitted to the Faculty of Graduate Studies of

The University of Manitoba

in partial fulfilment of the requirements of the degree of

MASTER OF SCIENCE

Department of Civil Engineering
University of Manitoba
Winnipeg, Manitoba

ABSTRACT

Degradation of permafrost is the major cause of damage to transportation infrastructure in cold regions. This research uses numerical modeling to understand the operating mechanisms of deformations of a fully-instrumented test section along an existing highway embankment in northern Manitoba, Canada. The initial instruments were installed in 2008. Strings of thermistors were placed beneath the toe and the mid-slope of the road embankment to monitor ground temperatures. Vibrating wire piezometers and a stand-pipe were installed beneath the toe to measure changes in pore water pressures. A slope indicator and settlement plates were also installed to measure lateral and vertical deformations respectively. Additional instruments were installed in 2012. The new instruments included thermistor strings beneath the shoulder and centreline, and vibrating wire piezometers beneath the centreline. Shape-Accel-Arrays (SAAs) were installed vertically beneath the shoulder and horizontally beneath the embankment from the toe to the centreline to continuously measure lateral and vertical displacements respectively. The data acquisition system was upgraded with satellite communication to improve the earlier data collection arrangements.

In this research, two comprehensive numerical models were developed using ABAQUS/CAE Finite Element (FE) software: 1) geothermal model, and 2) coupled thermo-hydro-mechanical model. In the first model, a purely heat transfer analysis was performed to reproduce the conditions at the site and investigate the subsurface thermal regime beneath the road embankment. The existence of a frozen section (frost bulb) underneath the embankment and its size and location were investigated by the model. The second model concentrated on the mechanical behaviour of the road embankment.

Temperature-dependent thermal and mechanical properties were used for all the materials. Model parameters were calibrated using the results of the triaxial and oedometer tests which have been conducted by previous researchers. A fully-coupled and a sequentially-coupled analysis were conducted. The results of the two analyses were compared to each other and to the field measurements. This thesis is presented in the form of two journal publications corresponding to each developed numerical model.

The geothermal model simulated the ground thermal regime under the embankment with reasonable accuracy. The model results show a region of frozen soil under the embankment and its shape, location, and seasonal changes were simulated reasonably well by the model. Based on the predicted future air temperatures, the model results show that the frost bulb will disappear completely within 20 years, and perhaps much sooner. The stress-deformation model was also able to simulate the vertical and lateral deformations of the embankment reasonably well. The model shows that the gradual degradation of the frost bulb affects the mechanical behaviour of the embankment. Fully-coupled analysis was found to simulate slightly lower displacements compared to the sequentially-coupled analysis. This is attributed to the colder ground temperatures simulated in the fully-coupled analysis compared to those using sequentially-coupled analysis.

ACKNOWLEDGEMENT

First and foremost, I would like to thank my supervisor Dr. Marolo Alfaro for his support, guidance and encouragements throughout the project. He always made time for my questions from the beginning until the end of the project. Thank you also to Dr. Jim Graham for his invaluable and encouraging feedbacks and for his reviews of the papers. Financial support is also acknowledged, via Dr. Alfaro, from the University of Manitoba.

I would like to thank my wife, Nazanin Motevalli, for her love and support and her patience during difficult times despite the distance. Thanks also to my parents for their endless encouragements and unfailing support of my endeavours. I owe a great deal to my wife and my parents.

TABLE OF CONTENTS

LIST OF FIGURES

CHAPTER 1: INTRODUCTION

1.1 BACKGRHOUND

Permafrost areas occupy 24% of the land in northern hemisphere (Nelson, 2003) and around 40% to 50% of Canada's total land surface of 10 million square kilometers (Brown, 1960). Railroads, highways, pipelines and airport runways have been, and continue to be, constructed in this large area of permafrost land. In Canada, this area is the home of First Nation communities which rely on the transportation infrastructures to connect them to the southern parts of the country. Northern Canada has a lot of natural resources such as minerals and hydrocarbons. There is a substantial need to construct more transportation networks, communication lines, pipelines, buildings and other types of infrastructure to bring these resources to southern markets. These infrastructure systems rely on the underlying permafrost for their foundation support. Frozen soils are less compressible than unfrozen soils. The pore ice in a frozen soil acts like cement that binds the solid soil particles together and therefore, if remain frozen, frozen soils have much higher shear strength compared to unfrozen soils. Warming temperatures can reduce the ability of frozen soils to support a load. Moreover, if a fine-grained frozen soil starts to melt, the melted water can generate excess pore water pressure which upon consolidation, large thaw settlements can occur. This can inflict serious damages to the overlying structures. Thawing can be the consequence of the climate warming, human activities or both. Clearing land of shaded trees, any excavation in the permafrost region and the added heat from a house are examples of human activities that can cause permafrost to melt. The effect of thawing is much more noticeable in ice-rich permafrost areas where extensive thaw settlements can occur due to the melting of the ice lenses

or ice chunks in the ground. This can cause serious problems for houses, roads, pipelines and other infrastructures built in these areas. A comprehensive assessment of the permafrost and the conditions of its active layer is essential prior to any project in northern regions (Ling and Zhang, 2004). Without an in-depth site investigation, an infrastructure can be vulnerable to short term or long term damage due to permafrost degradation.

When a road embankment is constructed, it alters the natural ground surface in two ways: the topography of the terrain and the surface material. Each of these changes can significantly alter the surface energy balance within the constructed embankment area. As an example, the embankment disrupts the gentle topography of the ground and acts as a snow fence which can accumulate snow on the embankment shoulders and toes (Fortier et al., 2011). Moreover, the shoulders of a road embankment can be subject to new patterns of wind and solar radiation. In addition to topographic changes, new material of the embankment has different surface albedo, heat capacity and thermal conductivity. The combined effect of these changes can substantially alter the thermal regime of the ground beneath the road embankment. In permafrost regions, these alterations can cause deeper thawing of the underlying permafrost table and trigger thaw consolidation which can then lead to severe differential settlements on the road surface.

A highway embankment constructed in a permafrost region is usually prone to two different types of damage from its foundation soil. One is frost heaving, which is caused by the growth of ice lenses in fine-grained soils, and the other is thaw settlement caused by degradation of the permafrost and the ice lenses. Each of these diseases can inflict

serious damages to a road and cause serviceability and safety issues. Identifying problematic sections of a road requires regular checks and reporting any major symptoms. The two main symptoms can be lateral spreading and settlement of the road embankment, both of which are common in regions of discontinuous permafrost (Alfaro et al., 2009). For more detailed investigations, instrumentation and field measurement programs should be performed to monitor and understand the behaviour of the problematic sections of the road and possibly take remedial measures. However, areas of permafrost are usually remote areas with unfavorable weather conditions and therefore field investigation and instrumentation in these areas are not always possible. In such conditions, a comprehensive numerical model can help by simulating the field conditions and investigating the causes and consequences of the problem. Moreover, a numerical model makes it possible for some predictions of the future behaviour of the road embankment. It is important to note, however, that problems related to freezing/thawing soils are inherently complex. This is mainly because freezing/thawing soils are multiphase materials consisting of ice, water, soil grains and air. Therefore, a comprehensive and reliable numerical model to simulate a degrading permafrost problem requires an in-depth knowledge of the process and advanced numerical modeling platforms.

1.2 HYPOTHESIS AND OBJECTIVES

This research has the following hypotheses:

1- Degradation of the existing frozen bulb (frost bulb) beneath the road embankment can be simulated reasonably well with the geothermal model developed in this study.

2- The irregular settlements of the road embankment are caused by the combined effects of thaw consolidation and lateral movements of the unfrozen soil at the side of the frost bulb.

Two numerical models were developed, a geothermal model and a stress-deformation model to examine the two hypotheses. In the geothermal model, the ground thermal regime under the road embankment was simulated using the thermal properties of the soils at the site measured in earlier studies. The modeled temperatures were compared with the recorded ground temperatures. The existence of the frost bulb was verified and its approximate size and location was illustrated by the geothermal model. In the second model, the deformation of the embankment was simulated using the mechanical properties of the soils at the site which were measured in earlier studies. Two types of numerical analyses were conducted in the second model: a fully-coupled analysis and a sequentially-coupled analysis. The vertical and lateral deformations modeled by the two analyses were compared to each other and to the recorded values. The model was used in order to examine the effects of the frost bulb degradation on the deformation behaviour of the road embankment.

1.3 ORGANISATION OF THE THESIS

This thesis is organised as a Sandwich Thesis format which includes two journal papers. The thesis consists of the following chapters:

Chapter 2: This chapter provides a literature review with a focus on early and recent thermo-hydro-mechanical numerical models. The review also includes a description of the role of numerical modeling in geotechnical engineering and how using a numerical model can be useful in a geotechnical engineering research program.

Chapter 3: This chapter is dedicated to the development of the geothermal model in the form of a journal publication for the *Journal of Cold Regions Science and Technology*.

Chapter 4: This chapter is dedicated to the development of the stress-deformation model in the form of a journal publication for the *ASCE Journal of Geotechnical and Geoenvironmental Engineering*.

Chapter 5: In this final chapter, a summary of all the findings and conclusions are presented. Recommendations for future research in order to better understand the behaviour of the embankment and to improve the results of the models are also provided.

CHAPTER 2: LITERATURE REVIEW

2.1 INTRODUCTION

In this chapter, a literature review is first conducted on permafrost, its types and distribution. This review will be followed by defining the role of numerical modeling in geotechnical engineering and explaining the advantages of a numerical model over a physical model. In the subsequent sections, the focus will be on the numerical modeling of highway embankments in permafrost regions. The literature review is organised in two parts. First, a review is conducted on thermal numerical modeling. An in-depth literature review is then presented on the early and recent coupled stress-deformation numerical models for simulating heat and water flow in freezing/thawing soils.

2.2 PERMAFROST

The term ‘permafrost’, is a ground that remains at or below 0°C for at least two consecutive years (Van Everdingen, 1998). This term can be used regardless of the material composition, phase of water substance or cementation (Neslon et al., 2003). In northern hemisphere, the thickness of permafrost is maximum near the arctic border and thins out toward its southern borders (Brown, 1960). The occurrence and thickness of permafrost can increase during colder climatic periods and decrease during warmer periods. The surface of permafrost is usually overlaid by an active layer (a layer that freezes in winter and thaws in summer seasonally), a vegetative layer, a seasonal snow cover and a complex boundary layer in the air (Osterkamp and Lachenbruch, 1990). Active layer, permafrost table, permafrost base and permafrost thickness are some key definitions in a layer of permafrost soil which have been illustrated in Figure 1 (Van Everdingen, 1998). The distribution of permafrost is classified based on its lateral

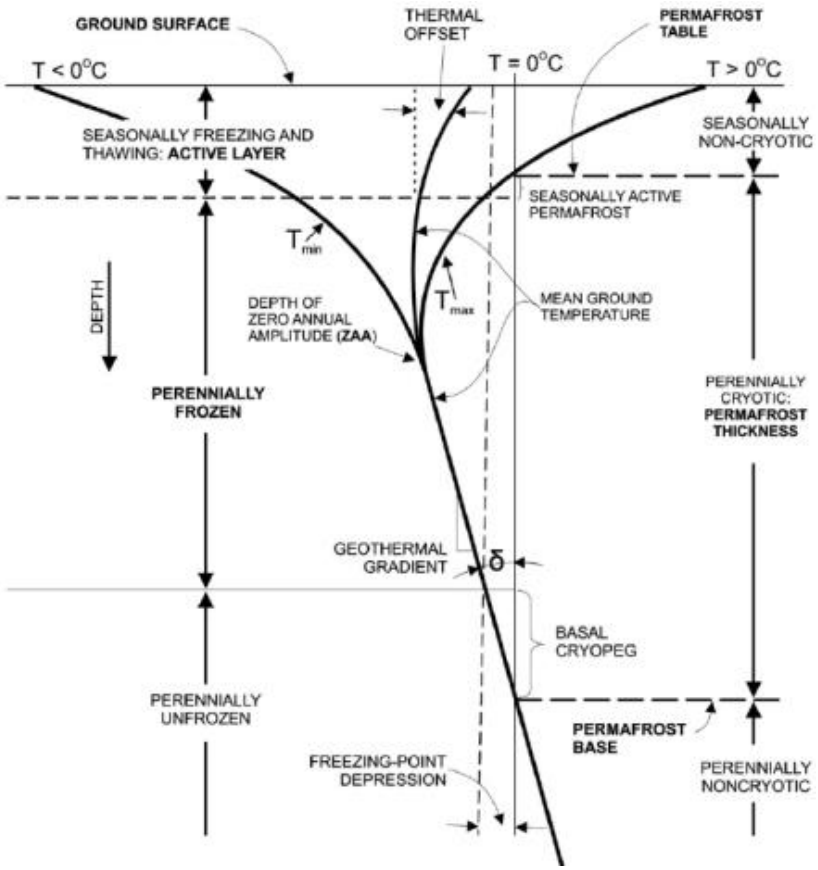

Figure 1: Key terms used to describe the ground temperature relative to 0°C in a permafrost environment (courtesy of Van Everdingen, 1998, supplied by the National Snow and Ice Data Center, University of Colorado, Boulder). Used with permission.

continuity (Neslon et al., 2003) and is also affected by many factors such as climate, the presence of large water bodies, snow cover, vegetation, soil conditions, and topography (Anisimov and Reneva, 2006).

2.2.1. Permafrost Types

Generally, permafrost is divided into three major categories. Continuous permafrost is a type of permafrost that exists under all land surfaces, except large bodies of water, and can be hundreds of feet thick (Brown, 1960). Mean annual ground temperature in the northernmost zone of continuous permafrost can be typically between -8°C to -13°C

(Anisimov and Reneva, 2006). Discontinuous permafrost, is the type that co-exists with unfrozen ground and is not uniformly distributed. The geography of this kind of permafrost is influenced by local factors such as vegetation and thermal properties of the local soil. Mean annual ground temperature in discontinuous permafrost is typically between -3°C to -7°C (Anisimov and Reneva, 2006). The third type of permafrost is a completely localised type which can only be found in patches and in places where the conditions for its occurrence and maintenance is favorable. Mean annual ground temperature in the third type of permafrost can be typically between 0°C to -2°C in the southern sporadic zones (Anisimov and Reneva, 2006). Figure 2 shows the distribution of permafrost types in Canada (photo was retrieved from Natural Resources Canada (NRC)).

2.2.2. The Effect of Global Warming on Permafrost

The twenty-first century will be a period of global warming and according to the Intergovernmental Panel on Climate Change (IPCC), it is estimated that the temperature rise will be 1.4°C to 5.5°C over the next century (IPCC taken from http://climate.nasa.gov/effects/). Anthropogenic climate warming, or the type of warming that is caused by human activities, have considerable effects on higher latitudes in northern regions (Nelson et al., 2003). In permafrost regions, the effect of climatic warming can be serious and different for continuous and discontinuous permafrost areas. For continuous permafrost, the effect can be restricted to warming the permafrost and increasing the depth of the active layer. This can eventually lead to thawing of the base of the permafrost but after several centuries later (Osterkamp and Burn, 2003). For discontinuous permafrost, however, the effect is more severe: the permafrost can

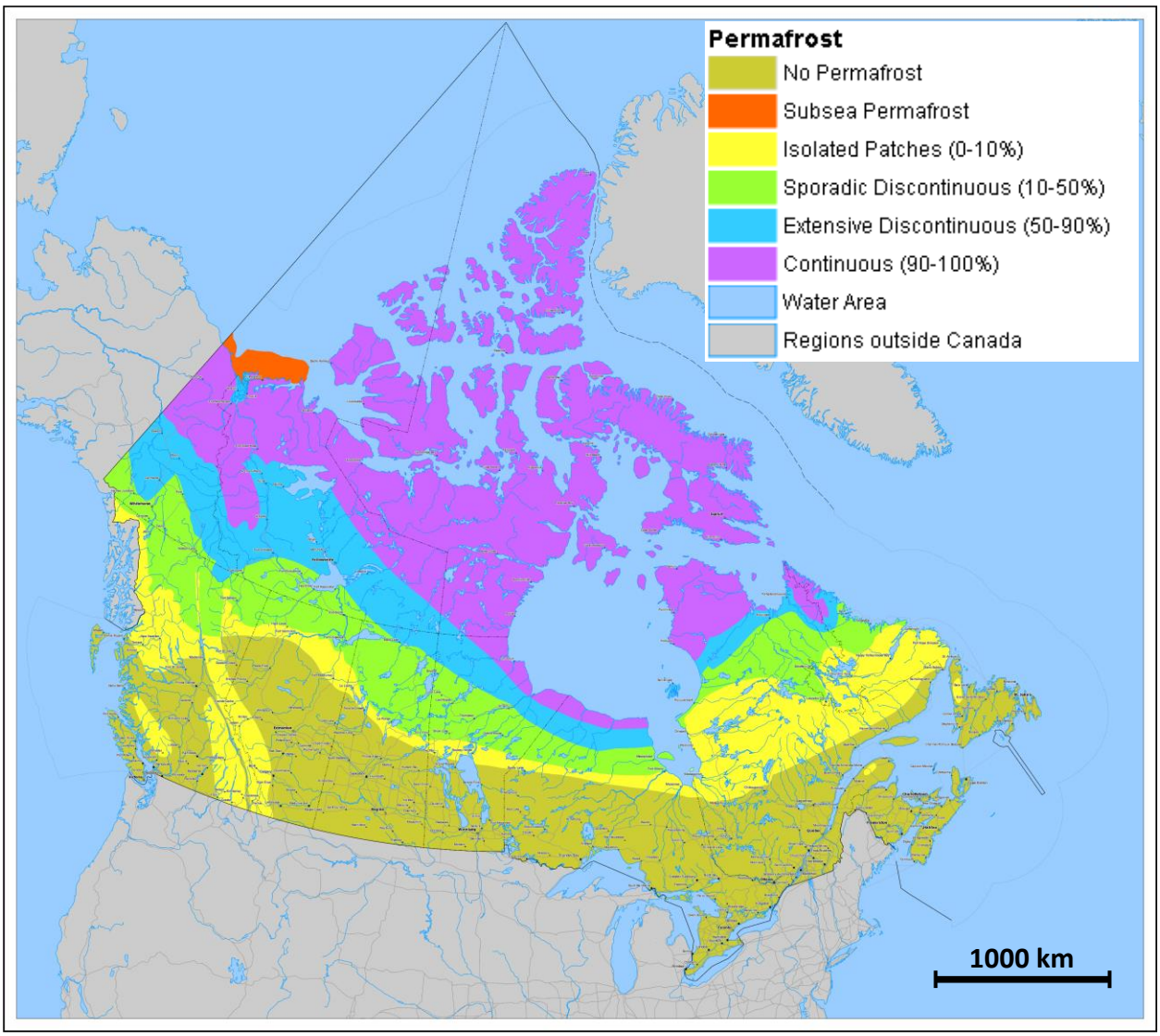

Figure 2: Distribution of permafrost types in Canada (Photo obtained from NRC, 2012). Used with permission.

disappear completely and it can start melting from both top and bottom at the same time (Osterkamp and Burn, 2003).

It is now believed that permafrost has been more extensive in the past and has retreated northward during the last 100-150 years (Vitt et al., 1994). In China, for example, where permafrost constitutes around 20% of the land area, it is estimated that the southern limits of permafrost are moving northward at around 1.5-3 km per year

(Ding, 1998). Other studies also show patterns of permafrost degradation in regions such as Mongolia and Alaska. Thawing of permafrost has also caused the southern boundary of permafrost to move northward in Canada (Kwong and Gan, 1994).

2.2.3. Permafrost in Manitoba

As mentioned previously, northern Canada comprises a large portion of the permafrost in northern hemisphere (Figure 2). A large area of Manitoba province is also occupied by permafrost of different types. Permafrost in Manitoba starts from the Hudson Bay shore to the north-east of the province as continuous and ends up towards the centre of the province as isolated patches, as illustrated in Figure 3. Many infrastructures such as road and railway embankments and pipelines have been, and continue to be, constructed in this large area of permafrost land in Manitoba. When the permafrost starts to degrade, severe damage is inflicted to these infrastructures which results in serviceability and safety issues. Provincial Roads (PR) 391 and PR 290 are two examples of road embankments in Manitoba that have recently experienced large irregular settlement deformations due to the degradation of the underlying permafrost. Research has recently focused on the maintenance of these road embankments by responsible organisation bodies such as Transport Canada and Manitoba Infrastructure and Transportation (MIT). PR 391, which is the only road connection to mining towns and First Nation communities in north-western Manitoba, is located 18 km north-west of city of Thompson and is the focus of this research project.

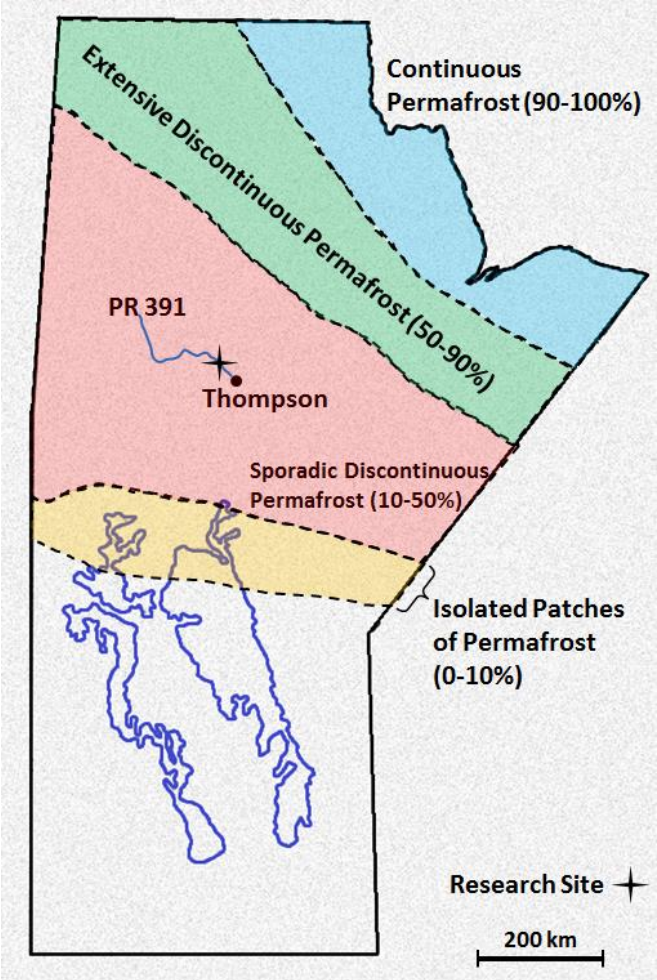

Figure 3: Permafrost types and distribution in Manitoba and the location of the site

2.3 NUMERICAL MODELING

The 20th century was the time of many scientific discoveries in engineering and mathematics. Civil, mechanical and electrical were the engineering fields that experienced unprecedented advances within a rather short period of time. New ways to solve engineering problems in these fields became possible by new discoveries in mathematics. In 1950's and 1960's, the use of computer simulation in engineering started by the advent of numerical methods such as Finite Element Method (FEM) and

Finite Difference Method (FDM). These mathematical methods can be regarded as revolutions because they helped all engineering fields in many ways.

By definition, a numerical model is a mathematical simulation of a real physical process (Geostudio, 2010a). By using a numerical method to solve a physical process, the real world is represented by discretized volumes or “elements” of material. A numerical model is a mathematical concept and therefore it is completely different from building an actual scaled model in the laboratory. Advances in the 21st century in electrical and computer science engineering completed the final missing piece of numerical modeling which was the lack of fast computing power. Nowadays, numerical modeling has become an indispensable part of many engineering fields, from modeling small components of an airplane engine in mechanical engineering to modeling reinforced soil structures in geotechnical engineering.

2.3.1. Numerical Modeling in Geotechnical Engineering: Why Numerical?

Barbour and Krahn (2004) provide a simple definition for numerical modeling:
‘Numerical modeling is a process by which we extract from a complex physical reality an appropriate mathematical reality on which we can base a design.’ Numerical modeling in engineering has many benefits which makes it a powerful and reliable tool in engineering research. Among all the advantages, the following are the most highlighted (Geostudio, 2010c):

- A large amount of output data can be obtained from a numerical model, at any point or cross section. Physical models require instrumentation at limited specific points in order to observe the response

- Unlike physical models, numerical models can consider many different types of boundary conditions and a wide variety of different scenarios
- Unlike physical models, numerical models are quick to set up and they do not require heavy equipment in the laboratory. With numerical models, health and safety of the user is not an issue

In addition to these benefits, a numerical model can help engineers to make predictions or identify the governing parameters in an engineering problem. Barbour and Krahn (2004) state that the key benefit of using a numerical model is its capability to improve the engineering judgement.

Barbour and Krahn (2004) have an informative article in which they discuss the role of numerical modeling in geotechnical engineering. In their article, they refer to Burland Triangle as the basis for understanding how and why geotechnical engineers should make use of numerical modeling. This Triangle consists of three main components: First, understanding the 'ground profile' by doing a site investigation; second, understanding the 'soil behaviour' by performing field and laboratory measurements and third, conducting 'numerical modeling'. These three components of Burland Triangle, i.e. ground profile, soil behaviour and numerical modeling, are interlinked to each other by empiricism, precedent and experience. Numerical models in geotechnical engineering are generally used for interpretation of a laboratory or field data, comparing the performance of design alternatives, or to help the engineer to predict the field behaviour (Barbour and Krahn, 2004).

Another important note on the role of numerical modeling in geotechnical engineering is that a geotechnical numerical model should 'start simple' (Barbour and Krahn, 2004).

Soils are natural geologic materials and they are considerably variable both in terms of properties and spatial distribution. Therefore, when trying to model such a complex natural material, two facts should be kept in mind: first, the purpose of modeling is 'not' to replicate all the nature's complexity, and second, all models in geotechnical engineering are data deficient. In all steps of the modeling process, the model should start simple and then complexity should be added in increments (Barbour and Krahn, 2004).

2.4 HEAT TRANSFER IN SOILS

Natural ground surface of a soil medium is exposed to different weather elements such as short and long-wave radiation, wind, precipitation and humidity. In order to develop a thermal model for a soil medium which is exposed to natural weather conditions, it is essential to first understand the thermal regime of the ground surface. This basically defines the amount of net heat flux on the ground surface, which is then considered as a top boundary condition in a thermal numerical model. The net heat flux on the natural ground surface of a soil medium is the sum of the net flux of heat arising from absorbed solar radiation and from sensible and latent heat transfer between the ground and the overlying air. In mathematical form, the net heat flux on the ground surface can be written as (Ling and Zhang, 2004):

$$(1-\alpha)Q_{si} + Q_{li} + Q_{le} + Q_h + Q_e + Q_c = \mathrm{Q_m} \qquad \text{[Eq.1]}$$

where α is the surface albedo, Q_{si} is the short wave solar radiation, Q_{li} is the incoming longwave radiation, Q_{le} is the emitted longwave radiation, Q_h is the turbulent exchange of sensible heat, Q_e is the turbulent exchange of latent heat, Q_c is the conduction heat

flux through the snow cover or ground surface and Q_m is the energy flux available for melting. Measuring each component of the ground surface energy balance equation is a difficult task. Instead, some other alternative methods are available in order to approximately measure the ground surface temperature at a specific location. The n-factor theory is one of these methods which has been used extensively for construction and engineering purposes for decades (Hildebrand, 1983). A thawing n-factor (n_t) is used in thawing seasons and is defined as the ratio of ground surface thawing index (I_{st}) to the air thawing index (I_{at}). Similarly, a freezing n-factor (n_f) is used in freezing seasons and is defined as the ratio of ground surface freezing index (I_{sf}) to the air freezing index (I_{af}). It is important to note that a thawing or freezing n-factor is highly site-specific and it is dependent on many factors. Ground surface material type, vegetation, topography and snow cover can be named as some of the most important factors affecting the n-factors at a site (Andersland and Ladanyi, 2004). Typical values of n-factors for different surface types and site locations have been published in the literature by different researchers (For example Lunardini, 1981).

In permafrost soils, the temperature of permafrost is dependent on the energy balance at the ground surface and any change in energy balance can make the permafrost warmer or cooler (Osterkamp and Romanovsky, 1999). In cold regions, surface energy balance is a function of different and complex variables such as seasonal snow cover, vegetation, atmospheric radiation, temperature and surface moisture content. As an example, snow cover, because of its low thermal conductivity, has a significant effect on the ground thermal regime and the depth of the active layer (Ling and Zhang, 2004).

In a volume of soil medium, the conservation of energy dictates that the amount of heat energy entering the medium must be equal to the amount of energy stored plus the amount leaving the medium. The heat storage consists of two main components: first, the amount of energy that is used to increase the temperature of the medium, which is associated with the heat capacity of the materials, and second, the energy used for phase change, which is associated with the latent heat of fusion. Mathematically, transient heat transfer in a soil medium can be written as:

$$\nabla(\lambda\nabla T) + Q = \left(\rho c - L\rho_i \frac{\partial \theta_i}{\partial T}\right)\frac{\partial T}{\partial t} \qquad \text{[Eq.2]}$$

Where T is the temperature, Q is the applied boundary heat flux, t is the time, ρc is the volumetric heat capacity of the soil mixture, ρ_i is the density of ice, θ_i is the volumetric fraction of ice, L is the latent heat of fusion per unit mass of water, $\nabla = \frac{\partial}{\partial x} + \frac{\partial}{\partial y} + \frac{\partial}{\partial z}$ is the gradient operator, and λ is the effective thermal conductivity of the soil mixture. This equation, referred to as the basic heat conduction equation, is based on the assumption that heat flows solely via conduction.

2.5 THERMAL MODELING OF DEGRADING PERMAFROST

Temperature plays the most significant role in frozen ground engineering. The variation of the ground thermal regime with time can significantly affect the thermal and mechanical properties of frozen soils. In the case of highway embankments in permafrost regions, the thermal stability of the embankment is the most important factor that directly affects the serviceability of the road (Li and Yu, 2008). Therefore, thermal modeling has become the focus of many researchers of permafrost.

In a research conducted by Alfaro et al. (2009), degradation of permafrost is studied beneath a gravel road embankment in northern Manitoba, Canada. They successfully calibrated a geothermal model with the ground temperature measurements for a 3-year monitoring period. Their thermal modeling shows that the permafrost degradation occurs beneath the road embankment and the climate warming accelerates the degradation process. In their research, Alfaro et al. (2009) predict that in a 30-year period, a large area of the permafrost beneath the embankment will degrade.

Darrow (2011) has performed numerical analysis of a highway embankment located in an ice-rich permafrost region in Alaska. Finite Element TEMP/W (Geo-Slope International, 2010) software was used as the modeling tool and the theory of n-factors was used to convert the air temperature to ground surface temperature. In her research, she successfully calibrated a numerical model using the measured field temperatures. A sensitivity analysis was also performed in order to determine the effects of surface boundary condition and thermal conductivity on the overall model results. The results of the research show that the ground surface temperature is the most critical input parameter and thermal conductivity had very little effect on the model results. Therefore, Darrow (2011) indicated that careful estimation of thermal conductivity would suffice in a thermal modeling. It is also found that when using the results of the modeling for design purposes, the depth of the active layer is an important parameter. Darrow (2011) stated that the modeled active layer thickness should closely match or be overestimated for a safe embankment design in permafrost regions.

Fortier et al. (2011) conducted a comprehensive research to evaluate the differential settlements of a road embankment in Nunavik, Quebec. Their research included

developing a thermal numerical model in order to investigate the thermal regime of the road embankment, the subgrade and the permafrost condition at the site. Surface n-factors were used for applying the thermal boundary condition on the ground surface. The results of their thermal modeling show that snow cover has a major effect on degradation of the permafrost underneath the road embankment. Fortier et al. (2011) stated that snow cover acts as an insulator on the ground surface and decreases the heat loss from the ground in winter seasons. This inhibits the permafrost to be able to 'freeze back' again in winter seasons. They further stated that when the thermal insulation effect combined with the warming climate, it would result in a deep thawing of the underlying permafrost.

Latent heat is a key material property in problems where the soil is subject to phase change. Zhu and Michalowski (2005) investigated the effect of latent heat by developing a heat transfer numerical model in a freezing soil medium using FE software ABAQUS/CAE® (a registered trademark of Dassault Systemes or its affiliates). In their research, they simulated a chilled pipeline which is embedded in a saturated unfrozen soil medium. The objective of their research was to numerically investigate the effect of including/excluding latent heat of fusion on the resulting ice/water content in the soil medium. Their model consisted of a 2-D soil medium which underwent a sudden decrease in temperature originating from a circular boundary (chilled pipe). The results of their research show that latent heat has a significant effect on the frost penetration depth in the medium. Zhu and Michalowski (2005) show that ignoring the latent heat effect produces lower temperatures and results in deeper frost penetration.

2.6 STRESS-DEFORMATION MODELING OF DEGRADING PERMAFROST

Heat transfer in freezing soils is inherently a complex process and this is mostly due to the multi-phase nature of a partially frozen soil mixture (Zhu and Michalowski, 2005). In such a multi-phase material, all the thermal, hydraulic and mechanical solutions affect each other simultaneously, and therefore they should be coupled in a stress-deformation numerical modeling. A coupled numerical model of a degrading permafrost problem can be either fully- or sequentially-coupled. In a fully-coupled approach, thermal and consolidation analyses are performed in a fully-coupled manner in one single analysis. Therefore, the simultaneous effects of the thermal, mechanical and hydraulic properties are considered and they are assigned to the model at the same time. In a sequentially-coupled approach, a purely heat transfer thermal modeling is first performed in order to induce a temperature distribution in the soil medium. The results of the thermal modeling are then used to perform a consolidation analysis in which all the mechanical and hydraulic material properties are temperature-dependent. In the first stage, the thermal material properties and in the second stage the mechanical and hydraulic material properties are assigned to the model. While the basic concepts of the fully-coupled and sequentially-coupled approaches are similar, the results of their analyses can be different. In the current research, both of these analysis approaches are performed and their results are compared to each other.

The governing partial differential equation for moisture flow in soils can be written as the following (Li et al., 1998):

$$\frac{\partial}{\partial x}\left(K_x \frac{\partial \psi}{\partial x}\right) + \frac{\partial}{\partial y}\left(K_y \frac{\partial \psi}{\partial y}\right) = \frac{\partial \theta_u}{\partial t} + \frac{\rho_i}{\rho_w}\frac{\partial \theta_i}{\partial t} \qquad \text{[Eq.3]}$$

where ρ_w and ρ_i are the densities of water and ice respectively; t, x and y denote the time and two space coordinates; θ_i and θ_u are the volumetric fractions of the ice content and the unfrozen water content, K_x and K_y are the hydraulic conductivities in the x and y directions; T is the temperature; C is the specific heat; L is the latent heat; ψ is the total potential of water in soil (sum of the volumetric and gravitational potentials). This equation is based on the assumptions that Darcy's law is valid and the vapour transfer is omitted. θ_u should be defined as a function of temperature ($\theta_u = f(T)$) to couple the above equation with the heat transfer equation.

Many researchers have developed different coupled stress-deformation numerical models and applied it to practical engineering problems. In the following sections, first a review is conducted on the early numerical models proposed mostly in the 1970's. This section is then followed by a review on more recent and advanced numerical models which have made use of the existing Finite Element computer programs.

2.6.1. Early Coupled Numerical Models

Harlan (1973) is one of the first researchers who proposed a numerical model for simulating the coupled heat and mass transfer in freezing soils (Li et al., 1998). Harlan (1973) mathematically coupled the two basic heat and mass (water) transport equations in freezing soil medium using the interdependency of the equations when phase change occurs. Many researchers have developed and used Harlan's strategy in order to produce different models for coupling the equations. Taylor and Luthin (1978) are among the early researchers who developed and used Harlan's method in their studies.

Morgenstern and Nixon (1971) were among the first researchers who introduced a 1-D numerical model for describing the thaw settlement of a thawing soil using a moving

freeze-thaw interface boundary condition. In their numerical model, they used the solution to the heat conduction equation given by Carslaw and Jaeger (1947). Morgenstern and Nixon (1971) assumed that within the thawed region, the soil is compressible and the consolidation theory is valid. In order to validate this numerical model, Morgenstern and Smith (1973) and Nixon and Morgenstern (1974) performed comprehensive thaw-consolidation tests on remolded and undisturbed clays respectively. The results of their research support the thaw-consolidation theory developed by Morgenstern and Nixon (1971) and therefore it was concluded that this theory can be confidently applied for frozen soils under thawing conditions.

Foriero and Ladanyi (1995) developed a large-strain coupled stress-deformation Finite Element model for thaw settlement of degrading permafrost. Their FE numerical model was written in FORTRAN 77. In order to calibrate their model, they chose to use the data obtained from the performance of a warm oil test pipeline in Inuvik, NWT, Canada. In their research, they used the Gibson's consolidation theory which is capable of considering the change in void ratio as the consolidation progresses. Their argument for not using the conventional Terzaghi consolidation theory was that this theory underestimates the excess pore water pressure and thus overestimates the shear strength of the soil which leads to unsafe design (Foriero and Ladanyi, 1995). The thaw settlements predicted by their model show a good agreement with the observations made in the warm oil pipeline field. The most important part of their results is the design charts that predict the time-dependent settlements underneath heated structures in ice-rich permafrost soils.

2.6.2. Recent Coupled Numerical Models

Similar in many other geotechnical engineering topics, permafrost problems have also benefitted from the advent of advanced numerical modeling computer programs. Frost heave in frost susceptible soils, thaw consolidation of degrading permafrost and the interaction between warm pipelines and a frozen soil medium are the most important issues that have been the focus of researchers in this field. As an example, Xu et al. (2009) developed a sequentially-coupled numerical model using ABAQUS/CAE to investigate warm pipeline-permafrost interaction. Their modeling was performed in two stages. First, a purely heat transfer analysis was performed in order to model the permafrost melting process. In the second stage, the resulting temperatures were used in order to perform a consolidation analysis. Their model consisted of a warm pipeline which passes through three regions of different types of permafrost soils: a region of clay in the middle surrounded by two regions of sand. A warm liquid flows in the pipe which makes it a heat source inside the permafrost. Temperature-dependent elasto-plastic properties were used for the soil materials. Their numerical model was able to capture the significant amount of thaw consolidation settlement in the clay region. Xu et al. (2009) concludes that the pipe wall will experience bending strains within the clay region and this would cause damage to the pipeline system. The research by Xu et al. (2009) is a good example that shows the power of an advanced numerical modeling computer program and its capability to deal with a complex thawing permafrost problem.

Shoop et al. (2008) performed a comprehensive numerical modeling on thaw-weakened pavement soils under vehicle loads. Their model used the built-in capabilities of FE

software ABAQUS/CAE. Shoop et al. (2008) used Modified Drucker-Prager Cap (MDPC) model which is a built-in elasto-plastic material model in the software. The elastic and plastic material parameters were determined by performing triaxial tests. They calibrated and refined their material model parameters with triaxial test simulations with ABAQUS/CAE and further validated their model parameters with direct shear tests. After determining the required soil properties, Shoop et al. (2008) performed a 3-D dynamic analysis of a rolling wheel over the thaw-weakened soil. An important part of the results of their research is that ABAQUS/CAE was able to capture the 'plowing' of the soil at the sides and front of the wheel of a moving vehicle. Shoop et al. (2008) stated that the results matched the field observations.

Qi et al. (2012) developed a sequentially-coupled stress-deformation numerical model to simulate the thaw consolidation of permafrost beneath the Qinghai-Tibet roadway embankment. Their model consisted of two stages, a thermal analysis followed by a consolidation analysis. Qi et al. (2012) used a 3-D large strain thaw consolidation theory and used FLAC3D as their numerical modeling platform. The results of their research show that some parameters including load and effective consolidation time control the behaviour of the thawed permafrost layer. Their proposed model can also explain why in some permafrost regions the road embankment continues to settle even a long time after the permafrost has completely thawed.

Zheng et al. (2010) and Wang et al. (2015) can also be named as other researchers who proposed stress-deformation models to simulate the operation mechanisms of highway embankments built on permafrost. The focus of these models are on the performance of the railway and highway embankments built on Qinghai-Tibet

permafrost region. The effects of permafrost degradation on the performance of the embankments and the amount of thaw consolidation were successfully simulated by the models.

2.7 JUSTIFICATION OF THE RESEARCH

The large extent of the permafrost lands in northern hemisphere and their role as foundation soils for the infrastructure in these regions highlight the importance of research on degrading permafrost. Transportation infrastructure, and in specific highway embankments, can be regarded as the veins in the body of this vast area of permafrost land. The operability of transportation infrastructure is vital for the economic growth of northern regions. The regions of permafrost are usually remote areas with unfavorable weather conditions. Therefore, field investigation and instrumentation in these areas are not always possible. In such conditions, numerical modeling and simulation of the field conditions can help engineers to understand the operation mechanisms and make some future predictions of the behaviour of overlying infrastructure.

The research at the PR 391 site has been quite extensive in terms of field investigation and laboratory programs. Batenipour (2014), who started the research in 2008, Kurz (2014), and Flynn (2015a) have performed extensive field and laboratory studies to understand the behaviour of the road embankment and obtained the thermal and mechanical properties of the soil at the PR 391 site. The results of the field investigations and laboratory programs conducted by those researchers have paved the way for conducting a comprehensive numerical modeling. By simulating the field

conditions, the numerical model will help to further understand the thermal and deformation mechanisms of the road embankment.

The goal of the author's research is to develop two comprehensive numerical models: a geothermal model to investigate the thermal regime beneath the road embankment and a coupled thermo-hydro-mechanical numerical model to understand the stress-deformation behaviour of the road embankment. ABAQUS/CAE (Complete Abaqus Environment) FEM software was chosen as the modeling platform because of its powerful capabilities in dealing with degrading permafrost problems. Table 1 illustrates some of the key capabilities of the software compared to Geostudio 2007 software.

Table 1: A comparison between Geostudio 2007 and ABAQUS/CAE

DESCRIPTION	ABAQUS/CAE	GeoStudio 2007
3D Modeling	YES	NO
Fully-Coupled analysis	YES	NO
Sequential analysis	YES	YES
Built-in material constitutive models	Comprehensive	Limited
Temperature-dependent material properties	YES	NO
Post-processing capabilities	Powerful	Moderate
Range of output results	Broad	Moderate
Meshing and element type controls	Powerful	Limited
Complexity	Complex	User-Friendly

CHAPTER 3: Modeling of Permafrost Degradation under a Road Embankment

Arash Gholamzadeh, Marolo Alfaro and Jim Graham

Submitted to **Cold Regions Science and Technology**
for publication as an Article

In this chapter, the thermal modeling part of the research is presented in the form of a journal paper. The paper consists of the following sections:

1- INTRODUCTION

2- RESEARCH SITE

3- SOIL PROFILE

4- INSTRUMENTATION PROGRAMS

5- MATERIAL PROPERTIES

6- THERMAL MODELING

7- RESULTS

8- PREDICTION

9- CONCLUSIONS

ABSTRACT

Degradation of permafrost is a major cause of damage to transportation infrastructure in cold regions. Degradation of permafrost is associated with excessive and irregular deformations and instabilities. The paper describes numerical modeling developed for examining the degradation of permafrost underneath a road embankment in northern Canada. Calibration of the model used temperature data from thermistors installed at the site. Modeled and measured temperatures both show the existence of a degrading frost bulb underneath the embankment. The term ‘frost bulb’ refers to the region where the temperature is below 0°C. The model was able to estimate the size, location and rate of degradation of the bulb. It was used to assess the effects of future climate warming on the frost bulb. The results suggest the bulb will degrade in 20 years or less, and will result in safety and serviceability issues for the embankment.

3.1. INTRODUCTION

Much of the transportation infrastructure in northern Canada has been built on permafrost. Road embankments, in particular, rely on the underlying permafrost for their foundations. Any significant change in the thermal regime of the permafrost can have significant effects on the stability and serviceability of the road.

The project site for this paper is an example of a road embankment built in northern Manitoba on degrading permafrost. Here, we use ‘degrading’ to mean ongoing, long-term decrease in the vertical and horizontal extent of a permafrost zone. Superimposed on this long-term trend are annual increases in size during freezing seasons and decreases during following thawing seasons.

The availability in recent years of computer programs that use advanced numerical modeling has enabled researchers and practicing engineers to perform more comprehensive thermal numerical modeling on degrading permafrost. For example, Alfaro et al. (2009) developed a 2-D numerical model to investigate the degradation of permafrost beneath a gravel road embankment in northern Manitoba. Using the climate simulation models of the Canadian Centre for Climate Modeling and Analysis (CCCma), they predicted that by 2040 a large area of the frozen ground beneath the embankment would degrade. Several researchers, for example Fortier et al. (2011), Darrow (2011) and Li and Yu (2008) have developed numerical models and investigated the factors affecting the thermal regime of permafrost layers underlying road embankments. Snow cover, warming climate (surface air temperatures), selection of ‘n-factors’, and the type of road surface were shown to significantly affect the thermal regimes. Darrow (2011), for example, performed a sensitivity analysis of input parameters and found that, while

surface air temperatures had the largest effect on thermal modeling, values of thermal conductivity had little effect. She concluded that careful estimates of thermal conductivity would suffice in thermal modeling.

This paper presents the thermal modeling of a section of Provincial Road (PR) 391 in northern Manitoba that used the Finite Element (FE) computer program ABAQUS/CAE® (ABAQUS® is a registered trademark of Dassault Systemes or its affiliates). Flynn et al. (2015a) also worked on the same project site using a different commercially available program and somewhat different boundary conditions. Their results were similar in principle but different in scope and in detail.

The road is in a region of discontinuous permafrost. Thawing has led to large irregular deformations and resulted in safety and maintenance issues. Instruments were installed, thermal properties measured, ground temperatures monitored, and a thermal model developed to simulate the subsurface thermal regime. The model was then used to compare measured and modeled temperatures (Batenipour et al., 2014; Kurz et al., 2014, and Flynn et al., 2015a).

Measured temperatures show the existence of an ongoing frost bulb beneath the road embankment. This was confirmed by drilling at the site. The frost bulb consists of soil that is permanently frozen, plus a surrounding layer of soil that freezes in cold seasons and thaws in warm seasons. The location, size and yearly changes of the frost bulb were investigated using the modeling. The paper also describes the use of a climate-simulation model to predict future degradation of the frost bulb.

3.2. RESEARCH SITE

The site is a low road embankment on PR391, about 18 km north-west of Thompson, Manitoba, at approximately N55°50' latitude and W98°01' longitude. It is in a region of discontinuous permafrost (Figure 1). The embankment was originally constructed in the mid-1960s and converted to a gravel road in the early 1970s. After a period with an asphalt hard-top, the surface of the road was returned to gravel. Thawing of the underlying permafrost has caused severe damage to the road surface in the form of large differential settlements (Figure 2).

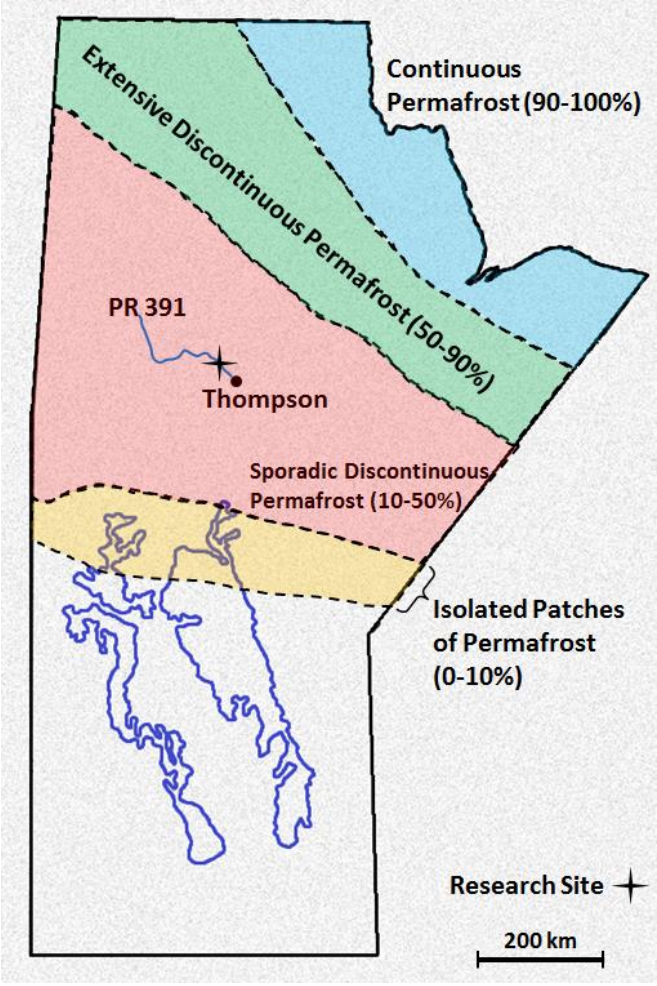

Figure 1: Permafrost types and distribution in Manitoba and the location of the research site

Figure 2: Unstable section of PR 391 in northern Manitoba (courtesy of Batenipour, 2014).

Successive drilling programs at the site over the last two decades showed ongoing decreases in the extent of the frost bulb. In 1991, drilling encountered irregular frozen soil at depths from 1.9 m to 10.5 m below the toe of the embankment. In 2005, frozen soil was found between depths of 4.6 m to 10.7 m. No frozen soil was found beneath the toe and mid-slope of the embankment in 2008. Further drilling in September, 2012 found frozen ice-rich soil beneath the shoulder between depths of 6 m and 9 m, and below the centreline between depths of 4.5 m and 11 m (Flynn et al., 2015a).

3.3. SOIL PROFILE

Observations and drillings at the site by previous researchers (Batenipour et al., 2014; Flynn et al., 2015a) produced a good approximation of the ground profile under the road embankment that was used for the numerical modeling (Figure 3). The top of the

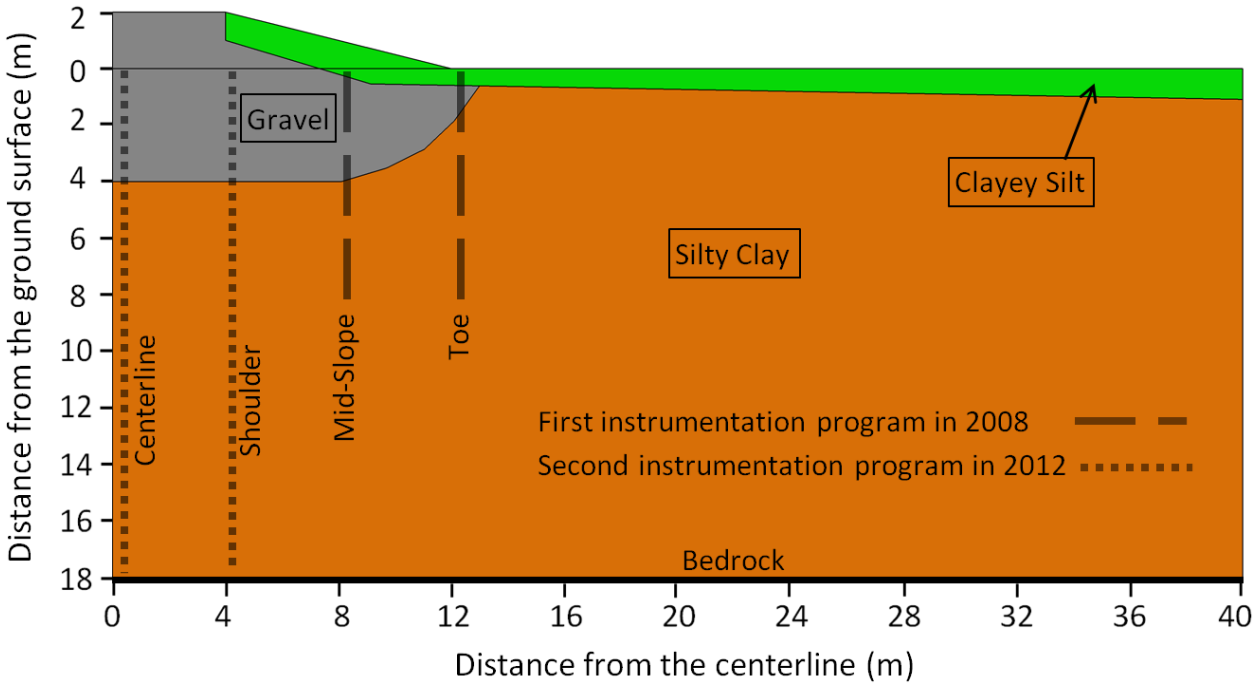

Figure 3: Ground profile at PR 391 test section and the locations of thermistors in the two instrumentation programs (2008 and 2012)

embankment is approximately 2 m above the natural ground surface. The surrounding area is poorly drained and the ground water table is at about the ground surface level all year. At the centreline, the embankment consists of 6 m of gravel. The toe of the embankment is comprised of about 1 m of clayey peat-silt and an underlying layer of plastic clay. This clay layer is underlain by bedrock at a depth of around 18 m (Batenipour et al. 2014; Flynn et al., 2015a).

3.4. INSTRUMENTATION PROGRAMS

Instrumentation of the site and monitoring of field temperatures were conducted in two related programs, with the first starting in 2008 and the second in 2012. Table 1 and Figure 3 show details of the two programs. A more detailed description of each program can be found in Batenipour et al. (2014) and Flynn et al. (2015a). Monitoring provided

Table 1: Details of the instrumentation and monitoring programs at PR 391 research site.

Field program	Start date	End date	Location	Thermistor length	Data collection	Researcher
First	October 2008	October 2014	Toe and mid-slope	9 m	Manual download	Batenipour et al. (2014)
Second	September 2012	October 2014	Shoulder and centerline	18 m	Remotely via satellite	Flynn et al. (2015a)

temperature data for 6 years below the toe and mid-slope, and for 2 years below the shoulder and centreline of the embankment. Due to logistical reasons, no measurements were taken between April 2011 and September 2012.

3.5. MATERIAL PROPERTIES

Material properties used in the modeling are latent heat, density, heat capacity and thermal conductivity. Following paragraphs describe how these material properties are handled in the numerical model.

3.5.1 Latent heat

Latent heat is a key material property in transient heat transfer analysis. It represents the energy absorbed or released when the pore fluid water in soil changes phase between ice and liquid water. In freezing soils, ignoring latent heat in a heat transfer analysis results in lower temperatures in the soil medium and deeper frost penetration (Zhu and Michalowski 2005). Phase change in soils does not occur strictly at a specific temperature and instead, it happens over a range of temperatures. The temperature range is wider in fine-grained soils such as silt and clay than in coarse-grained soils.

Based on the lower and upper limits of the temperature range, the terms ‘frozen’ and ‘unfrozen’ states can be defined. In ABAQUS/CAE, the ice and water phases are defined respectively by ‘solidus’ and ‘liquidus’ temperatures. Solidus temperature is the temperature below which the material is frozen, with a minimal amount of unfrozen water (residual water content). Similarly, liquidus temperature is the temperature above which the material is unfrozen, with a volumetric water content equal to the porosity of the soil when the soil is fully saturated. In this research, the solidus and liquidus temperatures were chosen based on our observations in the field and values reported in the literature, for example in Farouki (1985) and Geo-Slope International (2010). The recorded temperatures show that the average temperatures inside the frost bulb vary between -0.1°C and -0.3°C during the two-year period of the second monitoring program (Flynn et al., 2015a). Based on those measurements and values reported in the literature, the solidus and liquidus temperatures of the clay materials were assumed to be respectively -4°C and 0°C for the silty clay and -3°C and 0°C for the clayey silt. The solidus and liquidus temperatures of the gravel material were assumed to be -0.75°C and 0°C respectively. Small variations of these values were examined by sensitivity analyses in the modeling but were found to have only small effects.

Latent heat for a fully saturated soil can be calculated using:

$$L = \frac{\rho_d}{\rho_{bulk}} L'(w - w_r) \qquad \text{[Eq.1]}$$

where L is the latent heat of the soil per unit mass (J/kg), ρ_d is the dry density of the soil (kg/m^3), ρ_{bulk} is the bulk density of the soil (kg/m^3), L' is the latent heat of water which can be assumed as 334,000 J/kg, w is the total (gravimetric) water content (decimal)

and w_r is the residual unfrozen water content (decimal). Residual unfrozen water content is defined as the amount of liquid water that remains unfrozen in frozen soils (at solidus temperature). Unfrozen water in frozen soils mostly occurs in fine-grained soils such as silt and clay, and depends on the specific surface area (SSA, $m^2.g^{-1}$) of the soil and the presence of solutes (Anderson and Tice 1973). In this research, the residual unfrozen water content is assumed to be 5% for the clayey silt and silty clay materials (Farouki, 1985). In saturated coarse-grained soils such as gravel, almost all the water freezes (Zhu and Michalowski 2006). However, a minimal (1%) amount of residual unfrozen water content was assumed for this material to account for the possible presence of small amounts of moist fine-grained soil in the gravel.

3.5.2 Heat Capacity

The (specific) heat capacities for frozen and unfrozen states were calculated according to the following equations (Farouki, 1985):

$$c_{mu} = \left(\frac{\rho_d}{\rho_{bulk}}\right)[0.17 + 1.0(w_n)]c_{mw} \quad \text{[Eq. 2]}$$

$$c_{mf} = \left(\frac{\rho_d}{\rho_{bulk}}\right)[0.17 + 1.0(w_u) + 0.5(w_n - w_u)]c_{mw} \quad \text{[Eq. 3]}$$

where c_{mu}, c_{mf} are unfrozen and frozen specific heat capacities (J/kg·°C), ρ_d and ρ_{bulk} are the densities of the dry soil and bulk soil respectively (kg/m^3), w_n and w_u are the gravimetric water content and the gravimetric unfrozen water content (decimal), and c_{mw} is the specific heat capacity of water (4.2×10^3 J/kg·°C). Dry density and water content of the materials were measured in the laboratory as part of the measurement of thermal conductivity. Graphs of unfrozen water content function developed by Farouki (1985)

were used to calculate the heat capacities of the partially frozen states of the materials. Soil materials above the level of the surrounding natural ground surface were assumed to be moist throughout the year, with assumed gravimetric water contents of 7 % for the clayey silt and 4 % for the gravel materials. Equations 2 and 3 were also used to calculate the specific heat capacities of the moist materials.

3.5.3 Thermal Conductivity

Thermal conductivities of clayey silt and silty clay materials were measured and reported in Kurz et al. (2015). Thermal properties of the gravel material were not determined. Instead, Equations 4 and 5 were used to calculate the thermal conductivities of the gravel material for saturated frozen and unfrozen states respectively (Andersland and Ladanyi, 2004, based on work by Kersten, 1949).

$$k(frozen) = 86400 \times (0.01096(10)^{0.8116\rho_d} + 0.00461(10)^{0.9115\rho_d} \times w) \quad \text{[Eq.4]}$$

$$k(unfrozen) = 86400 \times (0.1442 \times (0.7logw + 0.4) \times 10^{0.6243\rho_d}) \quad \text{[Eq.5]}$$

where ρ_d is the dry density (g/cm^3), *w* is the water content (%) and k is the thermal conductivity in J/(day·m·°C).

The method by Johansen (1975) reported in Andersland and Ladanyi (2004) was used to calculate the thermal conductivities of all the soil materials in partially frozen states. It was also used to calculate the thermal conductivities of the moist materials above the ground surface. The method requires the thermal conductivities of the fully dry materials, which were calculated according to the following equations:

$$k_{dry}(Silt) = \frac{86400\times(64.7+0.137\rho_d)}{(2700-0.947\rho_d)} \pm 20\ \% \quad \text{[Eq.6]}$$

$$k_{dry}(Gravel) = 0.039 \times n^{-2.2} \pm 25\ \%$$ [Eq.7]

where ρ_d is the dry density (kg/m^3), K_{dry} is the thermal conductivity for the fully dry state of the material in J/(day·m·°C) and *n* is the porosity of the soil.

Thermal conductivities and specific heat capacities of the soil materials were defined at both frozen and unfrozen states. Table 2 tabulates the material properties used in the modeling.

Table 2: Material properties used in the thermal modeling.

Material	Thermal Conductivity (J/day·m·°C)		Specific Heat Capacity (J/kg·°C)		Latent Heat (J/kg)	Solidus Temp (°C)	Liquidus Temp (°C)	ρ_d (kg/m^3)
	Frozen	Unfrozen	Frozen	Unfrozen				
Moist Gravel	123000	154000	760	840	12850	-0.75	0	1900
Gravel	355000	230000	890	1160	40660	-0.75	0	1900
Moist Clayey Silt	73200	66700	800	940	21850	-3	0	1620
Clayey Silt	207000	123000	1000	1380	51180	-3	0	1620
Silty Clay	173000	117000	1020	1450	57850	-4	0	1500

3.6. THERMAL MODELING

Thermal modeling was performed for a 12-year period from 1 January 2002 until 31 October 2014. This period includes the 6-year period ending in 2014 when the ground temperatures were monitored (Table 1). The modeling began with a steady-state

analysis to produce an approximate temperature distribution in the ground on 1st January 2002. This initial steady-state analysis was followed by a 12-year transient analysis. The transient analysis was initiated in 2002 well in advance of the monitoring period so that the possible influence of the assumed initial conditions on later modeling results could be minimized. Starting the transient modeling in 2002, six years before the start of monitoring in 2008, produced an improved simulation of the first observed temperatures on October 2008.

The modeling used the 'Sweep' meshing technique (ABAQUS manual, 2012) with eight-node linear heat transfer brick elements (DC3D8). Figure 4 shows the meshed geometry of the embankment and the underlying soils down to the bedrock. Geometric symmetry about the centreline suggested it was sufficient to model only one-half of the embankment. We recognize that orientation of the side slopes, prevalent wind directions, etc. meant that the embankment is not thermally symmetric.

3.6.1 Boundary Conditions

The modeling requires (1) the ground surface boundary condition on top of the meshed domain, which is controlled mainly by mean daily air temperatures that vary seasonally with time; (2) the base boundary condition at the bottom of the cross-section, represented by a constant temperature, and (3) boundary conditions at the left and right vertical boundaries.

Ground Surface Boundary Condition:

The soil temperature just below the ground surface was directly affected by air temperatures applied on the top surface of the model. The mean daily air temperatures

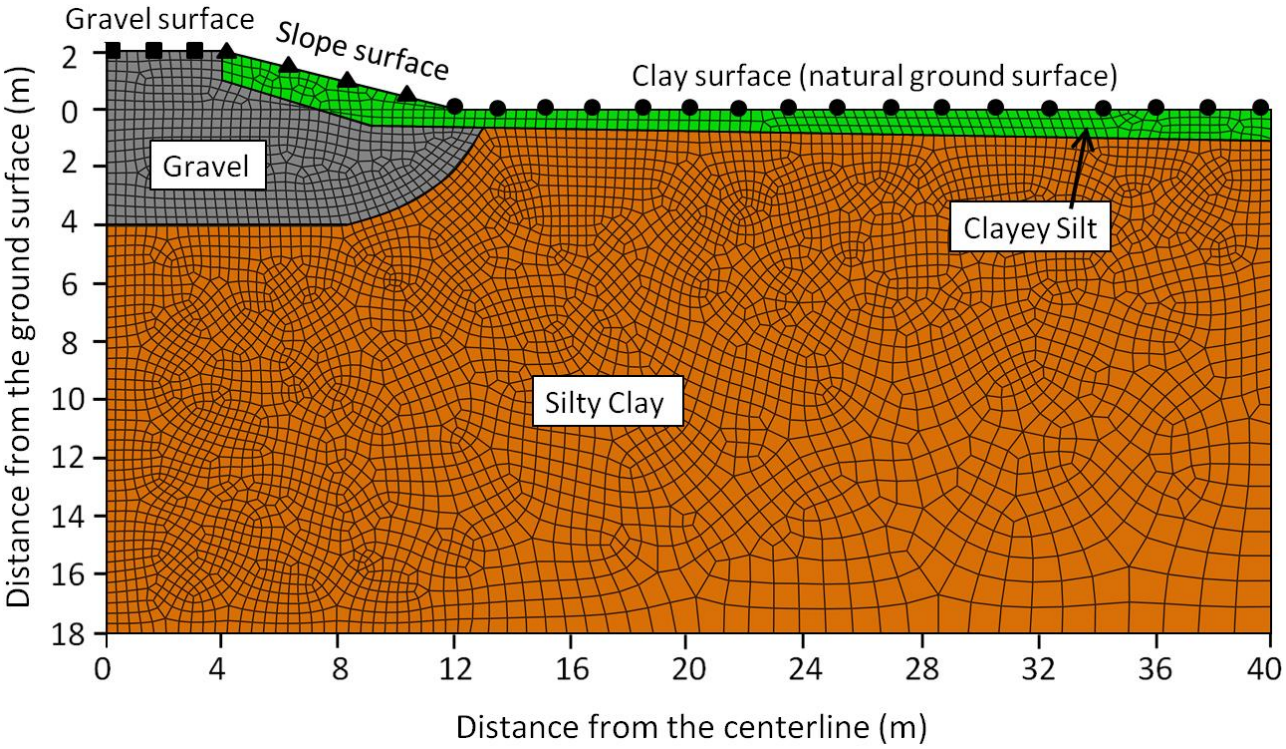

Figure 4: Finite Element mesh, soil types and surface types used in the modeling

were obtained from climate data recorded by Environment Canada at their weather monitoring station at Thompson Airport, less than 10 km away from the test site. Conversion of air temperatures to temperatures just below the ground surface used modifying n-factors. The surface modifying n-factors are site-specific and can vary depending on many factors such as surface type, wind speed (Lunardini, 1981), and snow cover (Fortier et al., 2011), among others. Three distinct surface types were identified based on the materials at the site. The surfaces are shown in Figure 4.

1. The clay surface: The surface of the surrounding natural ground. This surface is covered with snow in freezing seasons and under bushes and short plants in thawing seasons.

2. The slope surface: This is the surface from the shoulder down to the toe of the embankment. This surface is also covered with snow in freezing seasons and under bushes and short plants in thawing seasons.
3. The gravel surface: This is the surface of the road pavement. This surface is free of snow and vegetation throughout the year.

Freezing and thawing n-factors were considered for each surface type. The initial modeling used values of n-factors summarized by Andersland and Ladanyi (2004) based on publications by Lunardini (1981) and McRoberts (1974). The starting n-factors were n_f = 0.25 (freezing) and n_t = 0.73 (thawing) for the clay surface; n_f = 0.25 and n_t = 0.73 for the slope surface; and n_f = 0.9 and n_t = 1.3 for the gravel surface.

Two types of ground surface boundary conditions were used in the transient analysis:
1) daily air temperature data from Environment Canada (indicated in following sections and figures as 'Climate' data), and 2) a 'Sine Function' fitted to the raw climate data to smooth out daily irregularities.

In Figure 5, the data points represent daily mean air temperatures. The solid line represents a sine function with the form:

$$T = A + Bt + C\sin[\frac{2\pi}{365}\ (t + D)] \qquad \text{[Eq.8]}$$

where A = mean annual air temperature, B = warming rate of air temperature over time, C = amplitude of the function, t = time (days) and D = a constant representing the time shift. The calculated average freezing indices for the climate data and the sine function are -2773°C.days and -2710°C.days respectively. The corresponding calculated thawing indices are 2024°C.days and 1947°C.days for the period between October

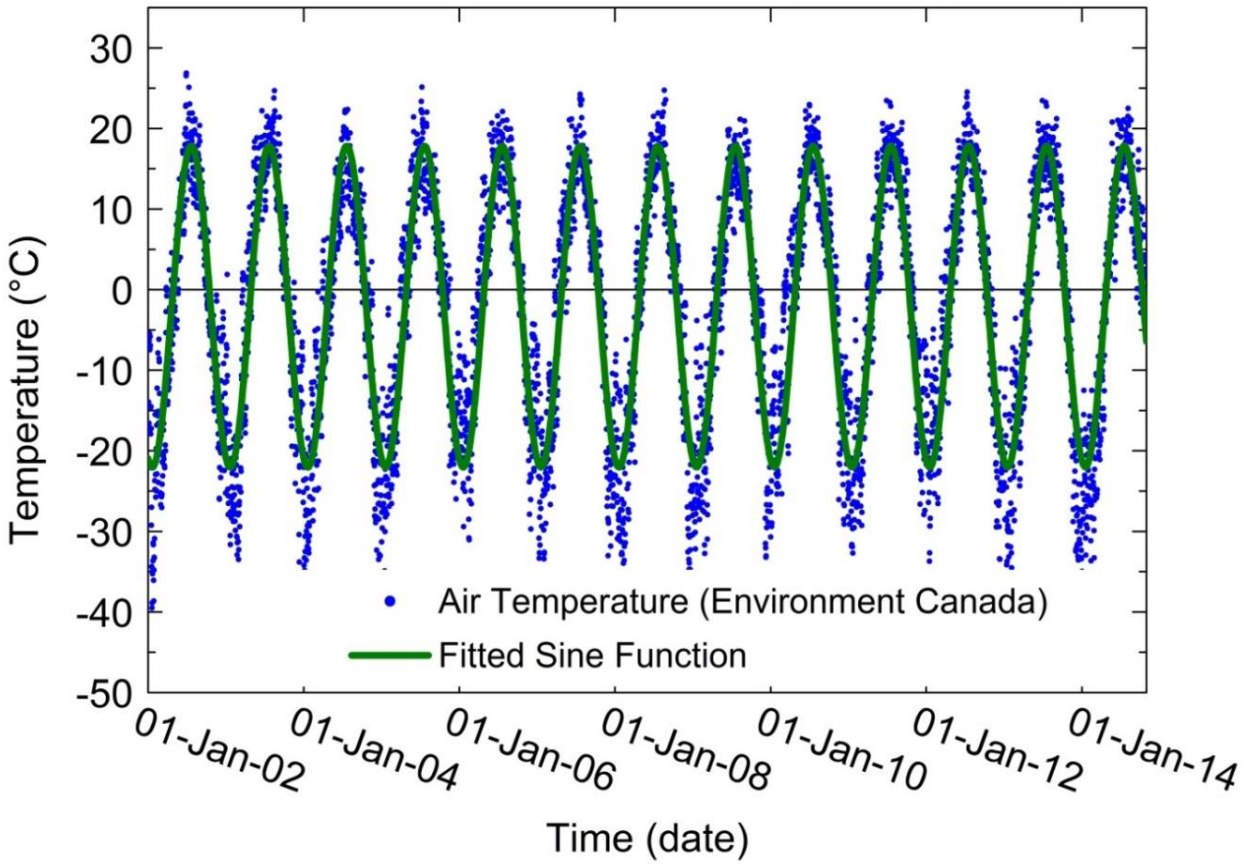

Figure 5: Measured air temperatures by Environment Canada and the fitted sine function.

2008 and October 2014. This means that the fitted Sine Function data result in slightly warmer winters and cooler summers.

Base Boundary Condition:

The base boundary condition used average measured temperatures at 18 m depth below the ground surface. Constant temperatures of 1°C and 1.9°C were applied to the bottom of the model below the centreline and toe of the embankment respectively. A linear variation of base temperature was assumed between these two locations. The constant 1.9°C temperature was also applied to the base of the model from below the toe to the right boundary of the model.

Vertical Boundaries:

The left and right boundaries were defined from symmetry as 'no-heat-flow' boundaries. This is the default condition used by the software.

3.7. RESULTS

As mentioned earlier, initial modifying n-factors were selected from Andersland and Ladanyi (2004). They were subsequently adjusted until modeled ground temperatures were in good agreement with the measured temperatures. Initial and adjusted sets of n-factors are shown in Table 3. For the gravel boundary, the adjusted n-factors are close to the initial n-factors, whereas for the slope and clay boundaries, the differences are larger. Lower adjusted freezing n-factors may be attributed to wind and solar radiation patterns at the site, snow cover in winter seasons, and other factors that are different from those for the n-factors reported in the literature.

Figure 6 compares the modeled isotherms and measured temperatures for four different dates from January 2009 to October 2014. The simulated and measured temperatures are generally in good agreement, particularly below the toe and mid-slope of the embankment. The results show a frozen zone or 'frost bulb' under the centreline and shoulder. They also show variation of the size and location of this frozen zone that are

Table 3: Initial and final adjusted modifying n-factors used for the ground surface boundary conditions

SURFACE	Initial n-factors		Adjusted n-factors	
	n_f	n_t	n_f	n_t
Clay	0.25	0.73	0.08	1
Slope	0.25	0.73	0.1	1.1
Gravel	0.9	1.3	1	1.2

consistent with observations during the drilling programs, particularly the 2012 program. Figure 6 also shows that simulations of temperature inside the frost bulb are less accurate than at other locations. We believe this may be due to uncertainties regarding changes of phase at the outer surface of the frost bulb, which is a multi-phase material consisting of water, ice, and solid soil particles. This makes heat transfer in the region a complex process (Li et al., 2010; Zhu and Michalowski, 2005). The uncertainties can cause inaccuracies in modeling ground temperatures inside the frost bulb and at other locations where phase change may occur.

3.7.1. Toe and Mid-Slope

Figure 7 and Figure 8 show the variation of measured and modeled temperatures with time at different depths beneath the toe and mid-slope of the embankment. As mentioned earlier, two cases were used for the boundary condition at the top boundary. For the modeling in Figure 7, ground temperatures, here called ‘Climate data’, were converted from recorded air temperatures using n-factors. In Figure 8, a ‘Sine function’ was fitted to the raw climate data. In both cases, good agreement was found between the modeled and measured ground temperatures. At 2 metres depth, the Climate boundary condition produced better results. As depths increased to 5 m, and then 8 m, results from both types of boundary conditions were closely similar. This means that using a best-fitted sine function for the surface boundary condition can be used as a reasonable simplification to help prevent numerical instabilities or convergence problems.

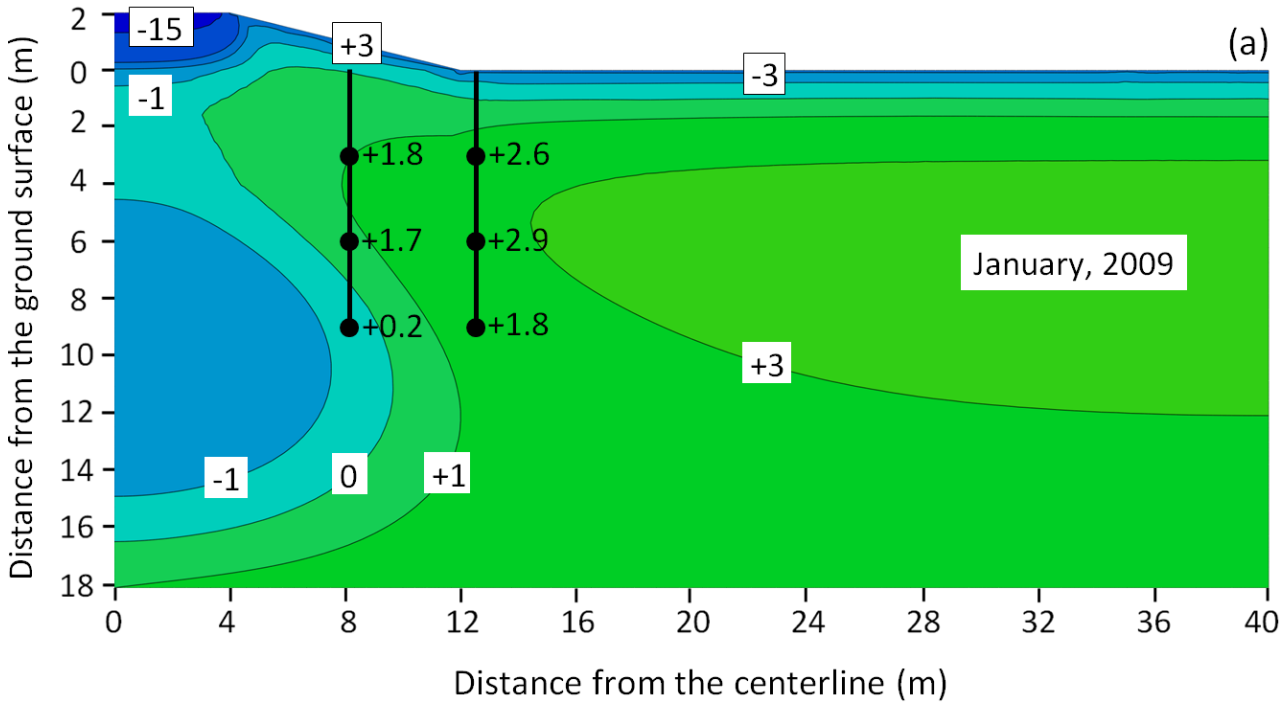
(a)
-15
+3
-3
-1
+1.8
+2.6
+1.7
+2.9
+0.2
+1.8
January, 2009
+3
-1
0
+1
Distance from the ground surface (m)
Distance from the centerline (m)
0
4
8
12
16
20
24
28
32
36
40
2
0
2
4
6
8
10
12
14
16
18

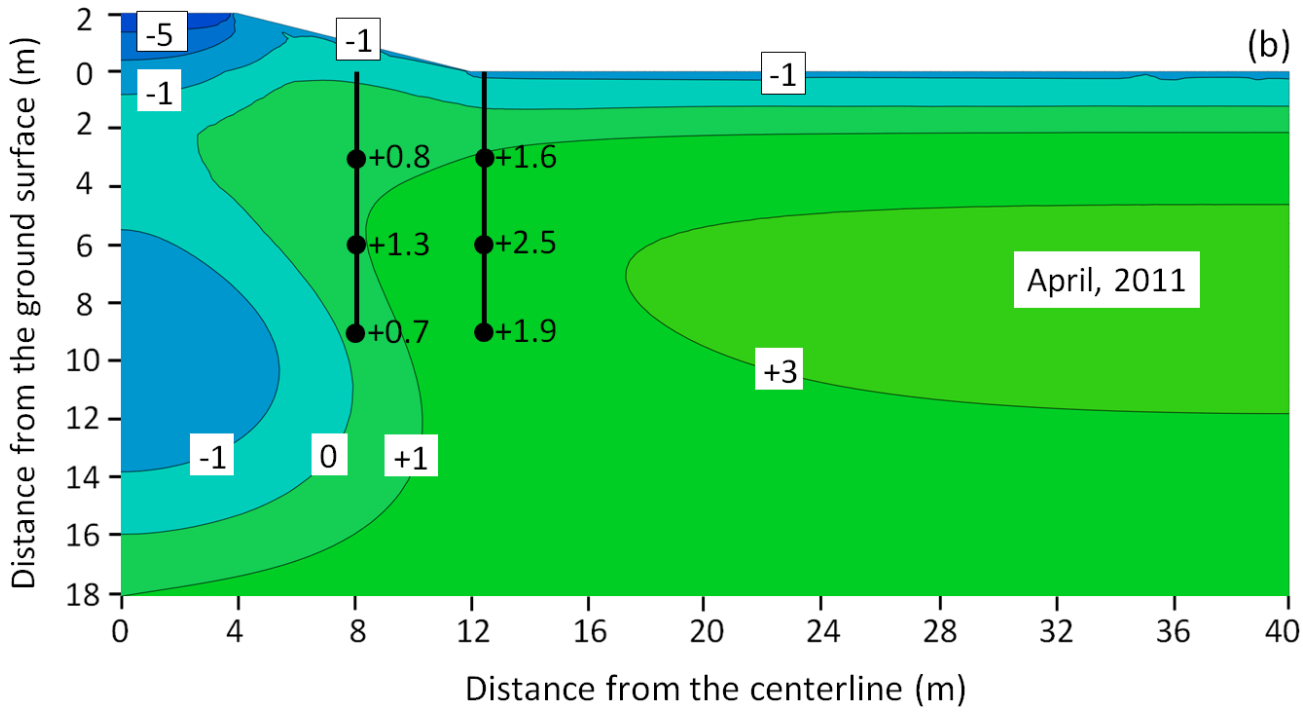
(b)
-5
-1
-1
-1
+0.8
+1.6
+1.3
+2.5
+0.7
+1.9
April, 2011
+3
-1
0
+1
Distance from the ground surface (m)
Distance from the centerline (m)
0
4
8
12
16
20
24
28
32
36
40
2
0
2
4
6
8
10
12
14
16
18

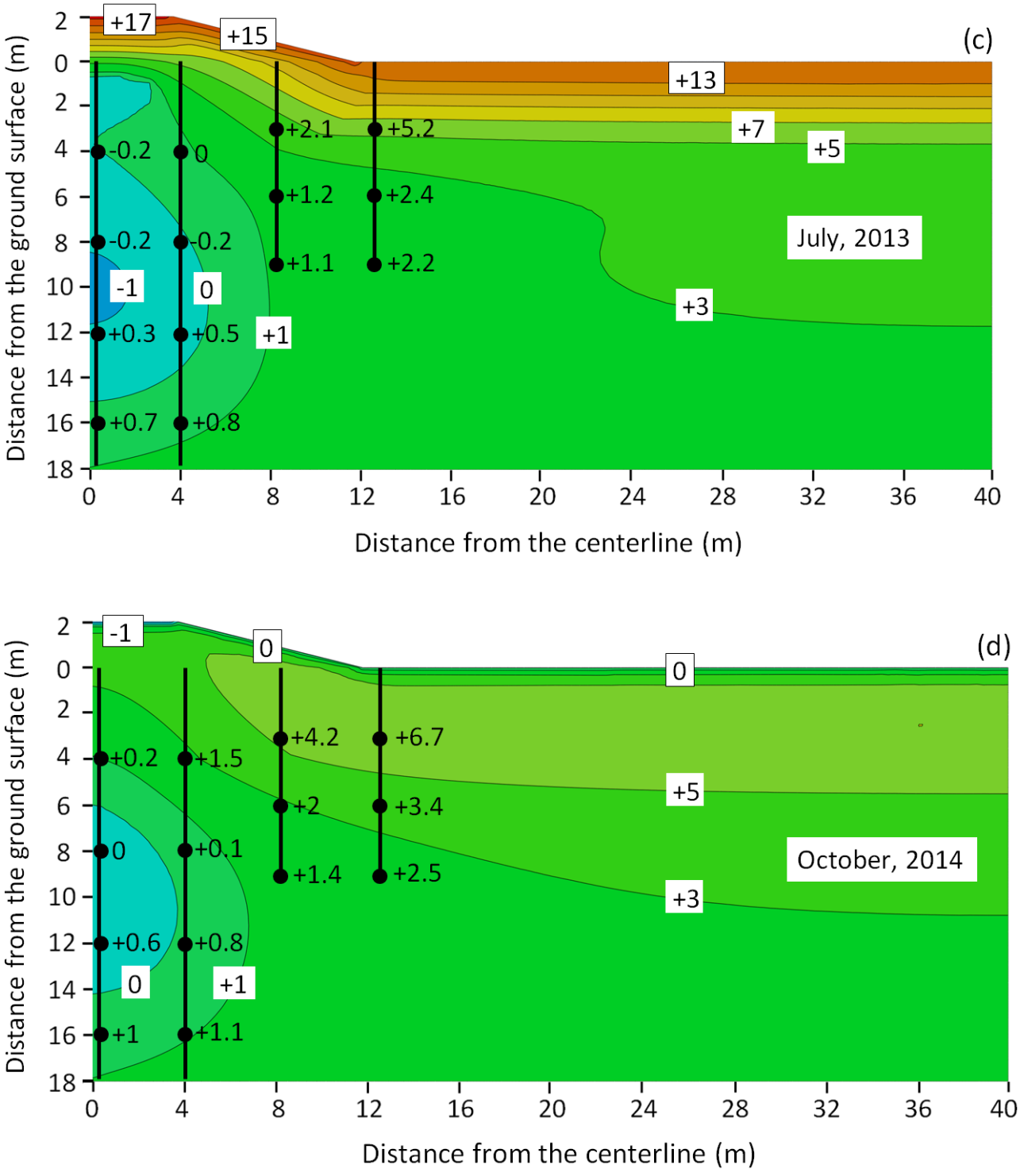

Figure 6: Measured temperatures and contours of modeled temperatures at different dates (Measured temperatures are shown next to their corresponding thermistor locations). Measured temperatures are after Batenipour et al. (2014) and Flynn et al. (2015a)

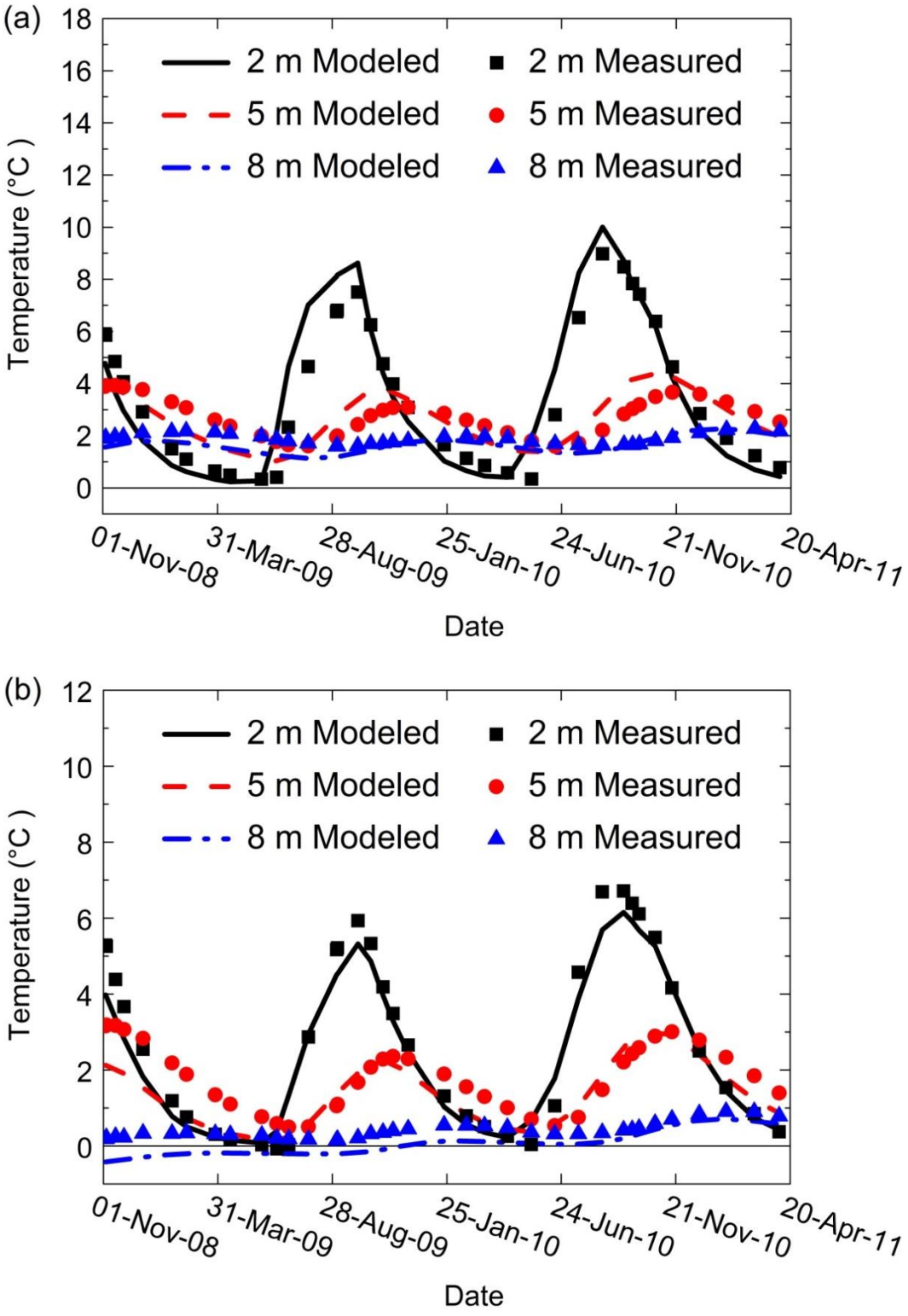

Figure 7: Measured and modeled temperatures versus time below the (a) toe and (b) mid-slope using the Climate data boundary condition. Measured temperatures are after Batenipour et al. (2014)

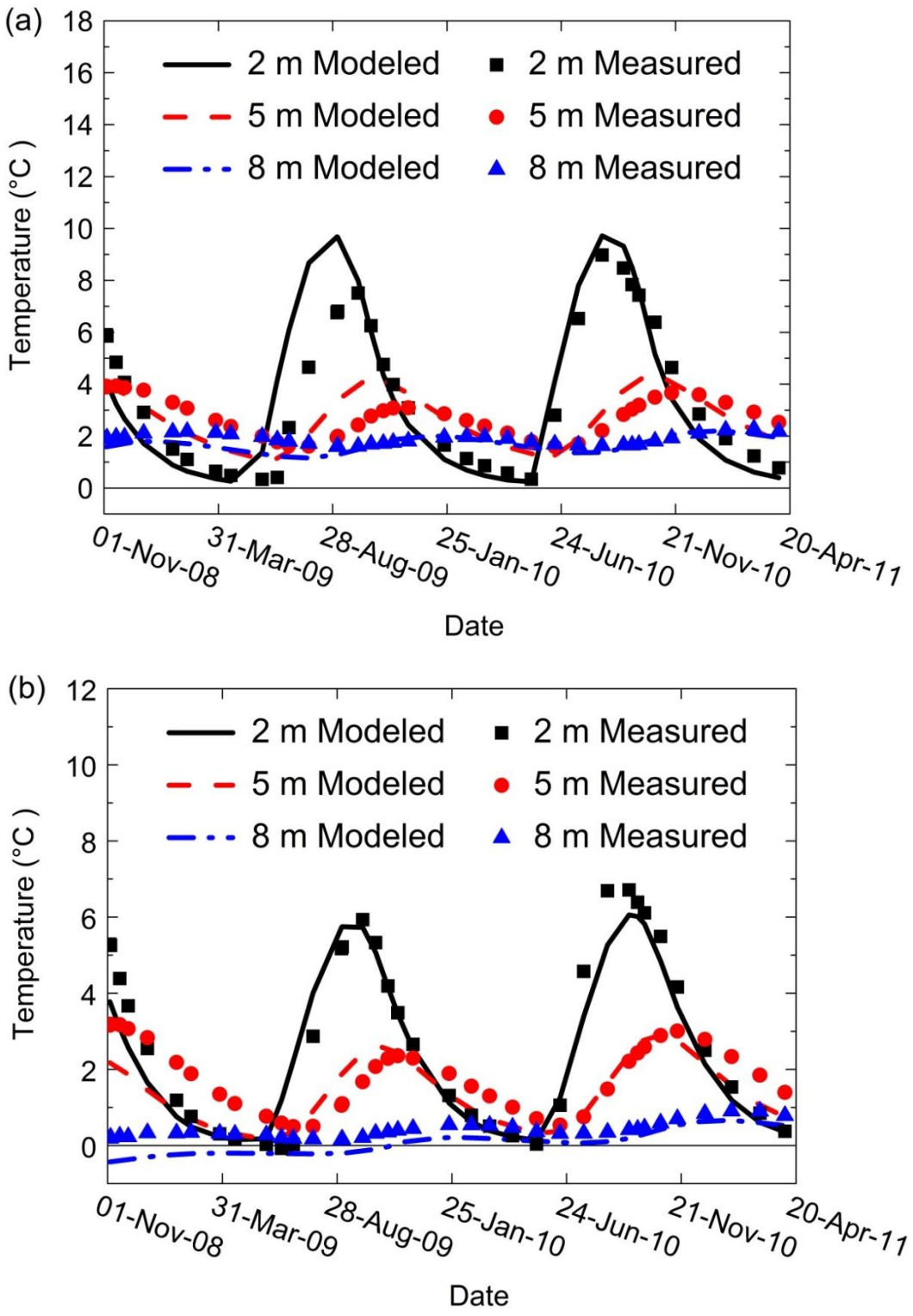

Figure 8: Measured and modeled temperatures versus time below the (a) toe and (b) mid-slope for Sine Function boundary condition. Measured temperatures are after Batenipour et al. (2014)

Figure 9 shows the variation of measured and modeled temperatures with depth below the toe and mid-slope at different times using the Climate boundary condition. The results are in good agreement with the measured temperatures. At both locations, the modeled temperatures are slightly colder than the measured temperatures by an average of 0.5°C. The temperatures become nearly constant with negligible variation at a depth of around 8 m at both locations. This depth can be taken as the depth to mean zero annual amplitude (DMZAA) (Brown, 1969).

3.7.2 Centreline and Shoulder

Figure 10 shows measured and modeled temperatures below the shoulder and centreline of the embankment. Below the shoulder, the modeled temperatures are warmer than measured temperatures by an average 1°C at 2 m to 5 m depth. At 14 m depth, however, modeled temperatures are colder than measured temperatures. A similar pattern can also be seen below the centreline of the embankment. It appears that the model has reasonably simulated the ground temperature regime, although the results are a little less accurate below the centreline than below the shoulder. We believe this may be because the former is more affected by the frost bulb.

Figure 11 shows measured and modeled temperatures plotted against depth below the shoulder and centreline of the embankment for different times in the year, one in late summer and one in late winter. Similar to the toe and mid-slope results shown in Figure 8 and Figure 9, the largest temperature variations are in the top 8 to 9 metres below the shoulder and centreline. At both locations, the modeled temperatures are reasonably accurate down to a depth of around 9 metres. From this depth downward, the modeled

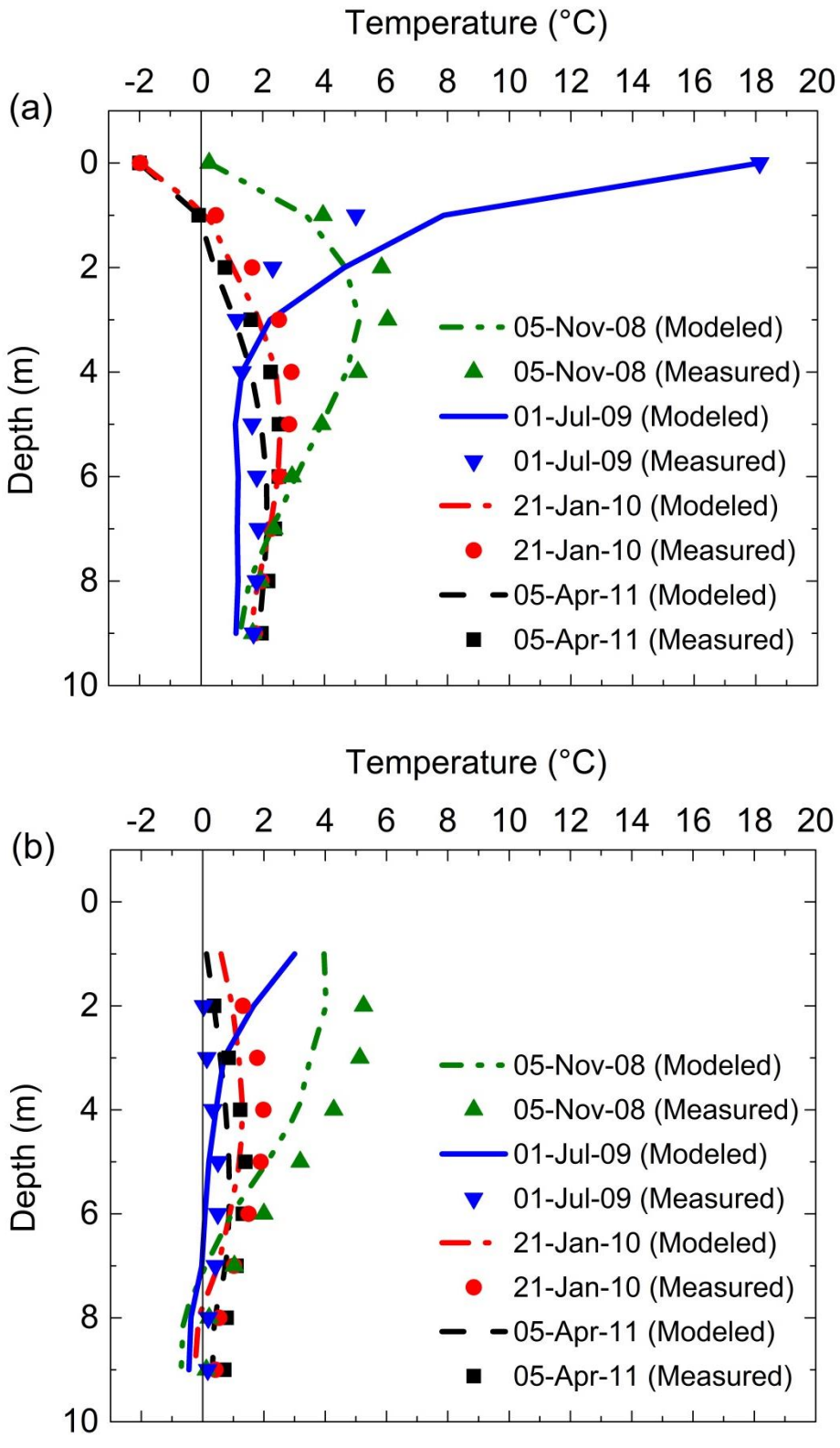

Figure 9: The measured and the modeled temperatures versus depth below the (a) toe and (b) mid-slope of the embankment at different times for Climate boundary condition. Measured temperatures are after Batenipour et al. (2014)

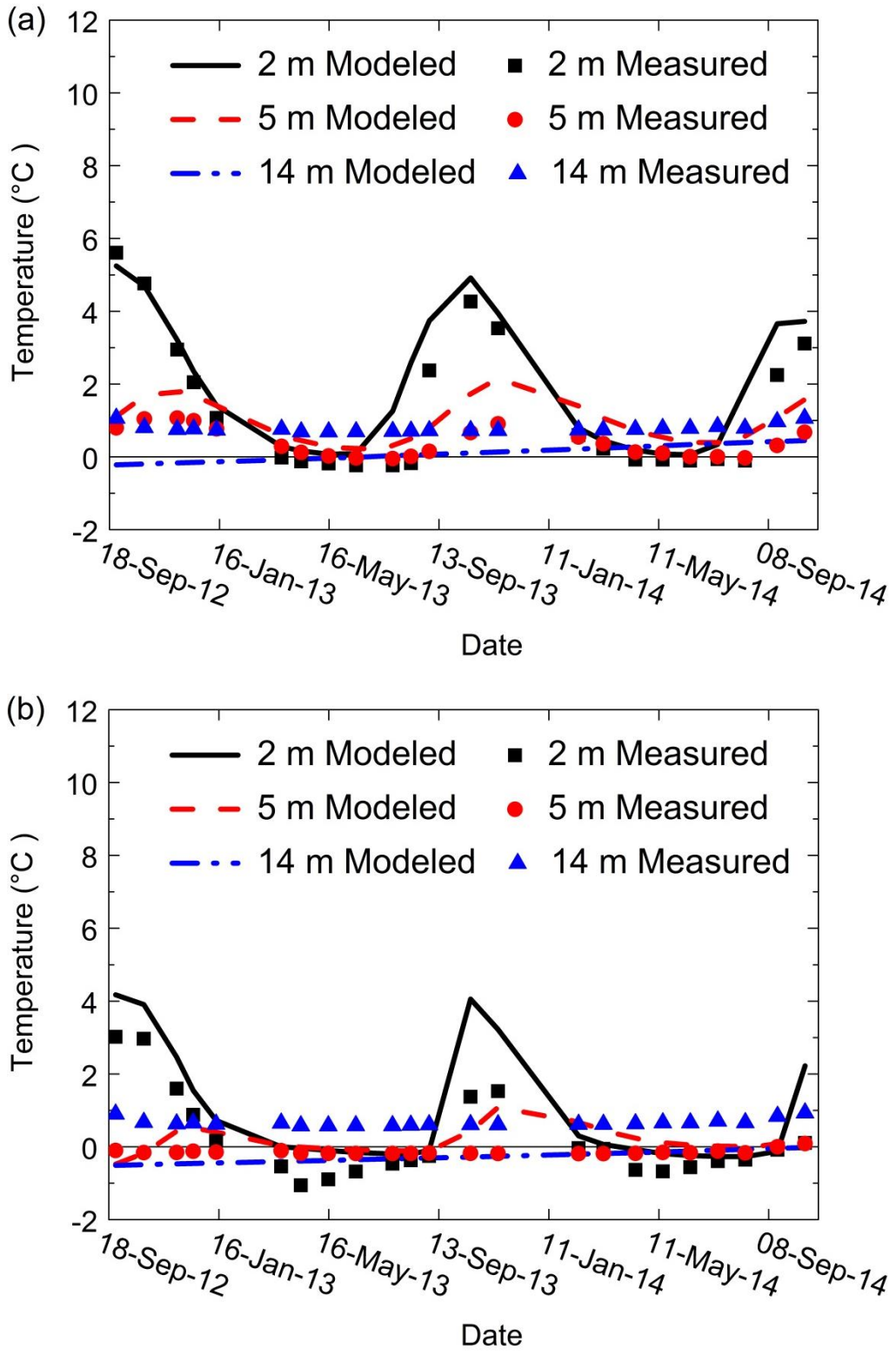

Figure 10: The measured and modeled temperatures versus time below the (a) shoulder and (b) centerline for the Climate boundary condition. Measured temperatures are after Flynn et al. (2015a)

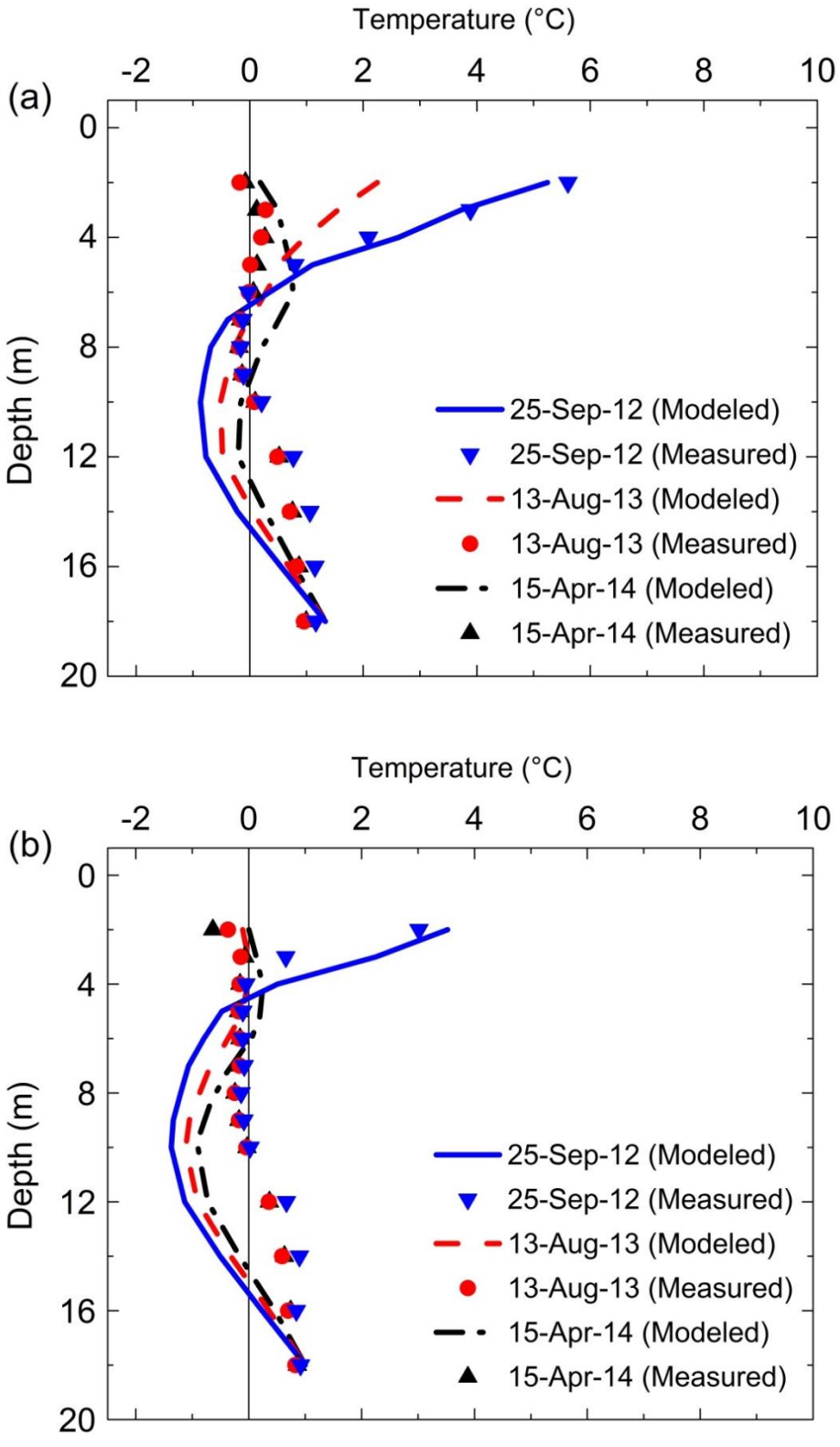

Figure 11: The measured and the modeled temperatures with depth below the (a) shoulder and (b) centerline for the Climate boundary condition. Measured temperatures are after Flynn et al. (2015a)

temperatures are colder than the measured temperatures by an average of 1°C to 2°C, leading to uncertainty about the actual position of the bottom of the frost bulb. Measured temperatures suggest it is at about 10 m depth to 11 m depth; modeling suggests it is lower, at 14 m depth. This difference is more noticeable at the centreline of the embankment. This may be due to the assumed thermal properties of the frozen silty clay material in the frost bulb and the assumed linear variation of the bottom boundary condition between the centreline and the shoulder.

A general comparison of the measured and modeled results shows that simulated temperatures below the toe and mid-slope are closer to measured temperatures than those below the shoulder and centreline. We believe this may be due to the frost bulb beneath the shoulder and centreline of the embankment. As mentioned earlier, the outer part of the bulb undergoes phase changes during freezing and thawing seasons. A better simulation of the temperatures inside the frost bulb requires improved understanding of the thermal properties of the silty clay, particularly in the narrow range of temperatures at which phase change occurs.

3.7.3 The Frost Bulb

The modeling shows existence of a frost bulb beneath the road surface but not beneath the mid-slope or toe. Figure 12(a) shows the extent of the simulated frost bulb in September 2012. This is consistent with the observations during a drilling program in September 2012, when ice-rich soil was found underneath the shoulder between depths 6 m and 9 m (Figure 12(b)). The actual location of the frost bulb can be approximately estimated from the 0°C isotherm measured by the thermistors. The measured temperatures show that the vertical extent of the frost bulb is between the depths of 4m

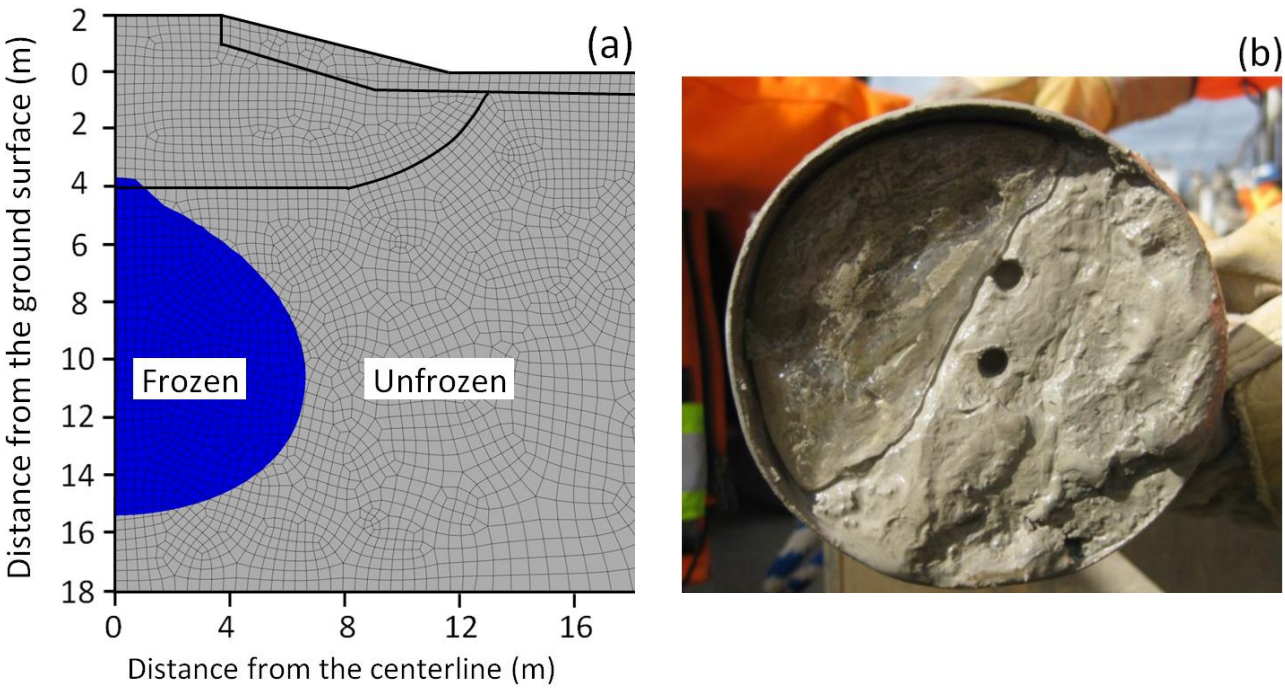

Figure 12: (a) The modeled location of the frost bulb underneath the embankment in September 2012; (b) Frozen ground and ice encountered beneath the shoulder in September 2012 (Courtesy of Flynn et al., 2015a)

and 11m below the ground surface at the centreline, and between 6m and 10m depth below the shoulder of the embankment (Flynn et al., 2015a). The model has simulated very well the location of the top of the frost bulb but it estimated the thickness to be larger than was observed. As suggested previously, we believe this to be associated with uncertainties in estimating thermal properties of the silty clay below the frost bulb, and to the assumed linear variation of base temperatures imposed as the bottom boundary condition between the centreline and the toe of the embankment.

Figure 13 illustrates the size, location and the yearly variation of the simulated frost bulb from January 2012 to August 2014, here taken as the 0^{o}C isotherm. The modeling shows that the boundary of the frost bulb changes seasonally in both lateral and vertical

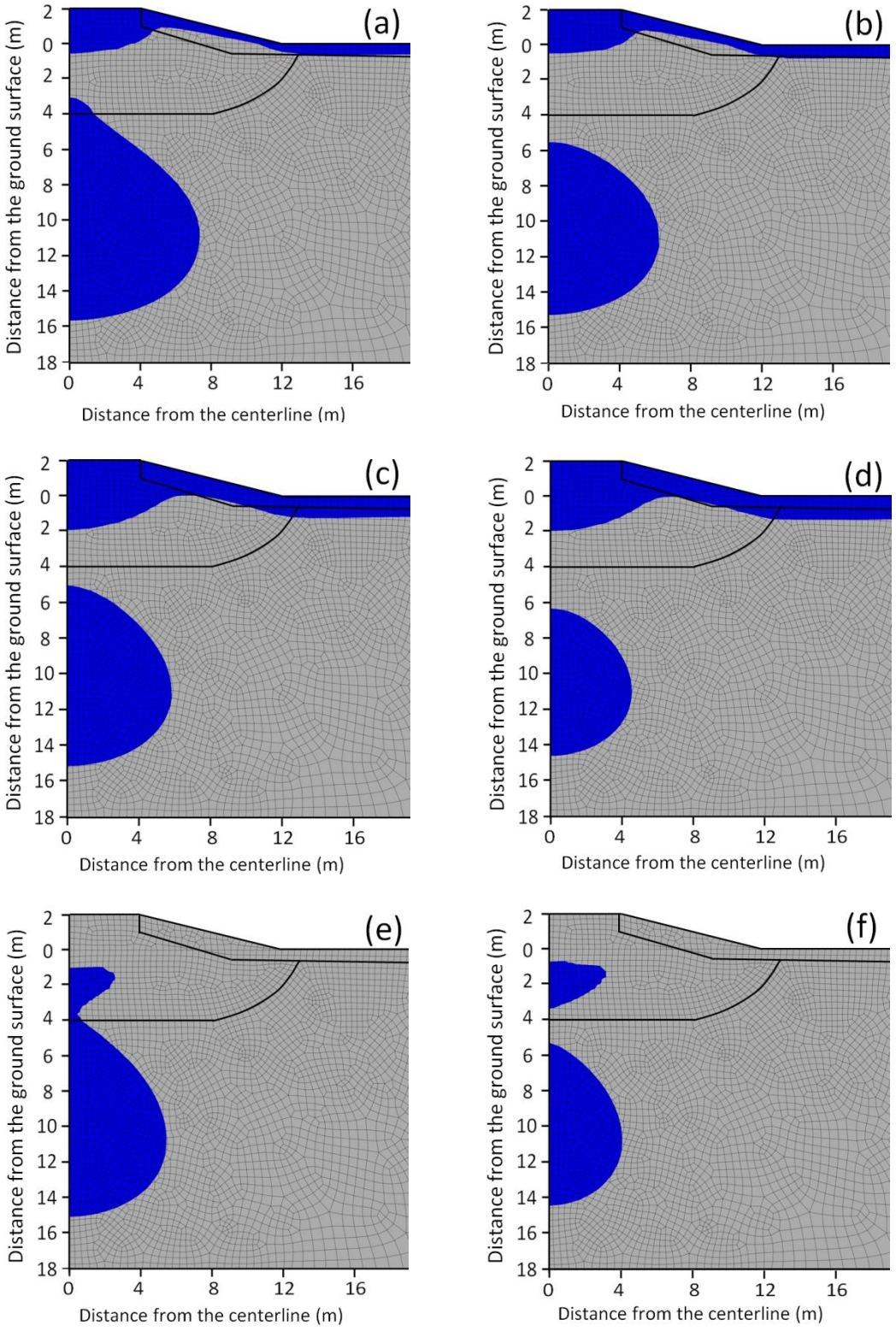

Figure 13: The size and location of the frost bulb in (a) Jan 2012; (b) Jan 2013; (c) Apr 2013; (d) Apr 2014; (e) Aug 2013; (f) Aug 2014.

directions. However, the changes are not equal in all directions; the highest and lowest changes occur at the top and bottom of the frost bulb respectively. The figure also shows the extent of freezing regions in the seasonally-active zone below the ground surface.

3.7.4 Discussion

The existence of the frost bulb under the gravel of the embankment, but not under the side slope or natural ground surface, can likely be attributed to clearing of snow from the road surface in freezing seasons and moving it over to the slope. Heat then can move easily from the gravel road to the atmosphere because insulation from snow cover has been removed. In contrast, snow cover on the slope and clay surfaces (Figure 2) insulates the ground and allows more heat to remain (Fortier et al., 2011). Reduced heat extraction allowed more rapid degradation of permafrost under the surfaces of the surrounding natural ground and side slope than under the gravel surface of the roadway.

In freezing seasons, the frost bulb increases in size; in thawing seasons, it gets smaller, but it currently retains a frozen core year-round. The absence of insulating snow cover on the road in winter and the relatively high thermal conductivity and n-factors of the gravel mean heat can flow easily into and out from the top of the embankment. This makes the top of the frost bulb beneath the road melt and freeze more rapidly than frozen soil below the side slope, where the thermal conductivity and n-factors are lower. Latent heat also influences transitions between frozen and unfrozen soil. As well as these yearly effects, we should also consider longer term trends associated with climate warming.

3.8. PREDICTION

Flynn et al. (2015a) showed net downward average annual temperature gradients over several years and therefore net heat flow into the embankment and its foundation. This means a general warming over time and future degradation of the frost bulb (Flato and Boer, 2001). Simulated ground temperatures and records from the various drilling programs at our research site suggest that the frost bulb has degraded in size over time and is likely to completely thaw in future. The degradation may in part be the reason for ongoing settlements that require frequent maintenance of the road surface.

The Canadian Center for Climate Modeling and Analysis (CCCma) has developed several simulation models for climate prediction and climate change. The authors used the CCCma's third generation Coupled Global Climate Model (CGCM3.1/T47 IPCC SRES A2 Scenario Data) from 2010 to predict future air temperatures. The third generation model was used since it substantially updated the atmospheric component compared with earlier models (CCCma, 2015).

When considering predicted temperatures at the research site over a 50-year period, CGCM3.1 predicts an increase in mean average air temperature of approximately 0.00015°C/day (0.055°C/year), or a total increase of approximately 2.7°C. This is slightly higher than an increase of about 2°C for the same area predicted by the Climate Change Office, 2005 (see also NRC, 2003).

Figure 14 shows mean average air temperatures predicted by CCCma (2015) for the 50 years from September 2012 to September 2062. The figure includes a fitted linear trend line with an air temperature increase rate of 0.00015°C/day.

Thermal modeling was performed using CCCma (2015) air temperatures to predict future degradation of the frost bulb. Figure 15 shows results of the modeling at 2 metres below the toe of the embankment where all temperatures are above zero and permanently frozen soil has already disappeared. The modeled and measured temperatures match reasonably for the period between September 2012 and October 2014 during which temperature measurements were available. While the results are good in freezing seasons, modeled temperatures are higher than measured temperatures in thawing seasons. This can be the reason why the model predicts rapid degradation of the remaining frost bulb between the centreline and shoulder within one year after the end of the 12-year analysis shown in Figure 13; that is, between 2014 and 2015. It should be mentioned that this prediction assumes that the long-term frozen properties of the frost bulb do not change significantly. Limitations on using the CCCma model (CCCma, 2015) and the observation that it produces warmer temperatures in thawing seasons (Figure 15) can affect the reliability of the prediction.

Another way of considering future degradation of the remaining frost bulb can be based on actual measured temperatures. These show that average temperatures inside the frost bulb vary only between -0.1°C and -0.3°C during the two-year period of the second monitoring program (Flynn et al., 2015a). This suggests that annual heat flows into and out from the ‘warm’ frost bulb may involve levels of latent heat and are not yet affecting temperatures. The frost bulb may be progressing towards of complete degradation.

In figures not shown here, our modeling suggests the predicted climate warming at the research site (from CCCma, 2015; Climate Change Office, 2005; NRC, 2003) in the next two decades will be sufficient to raise the temperature of the remaining frost bulb

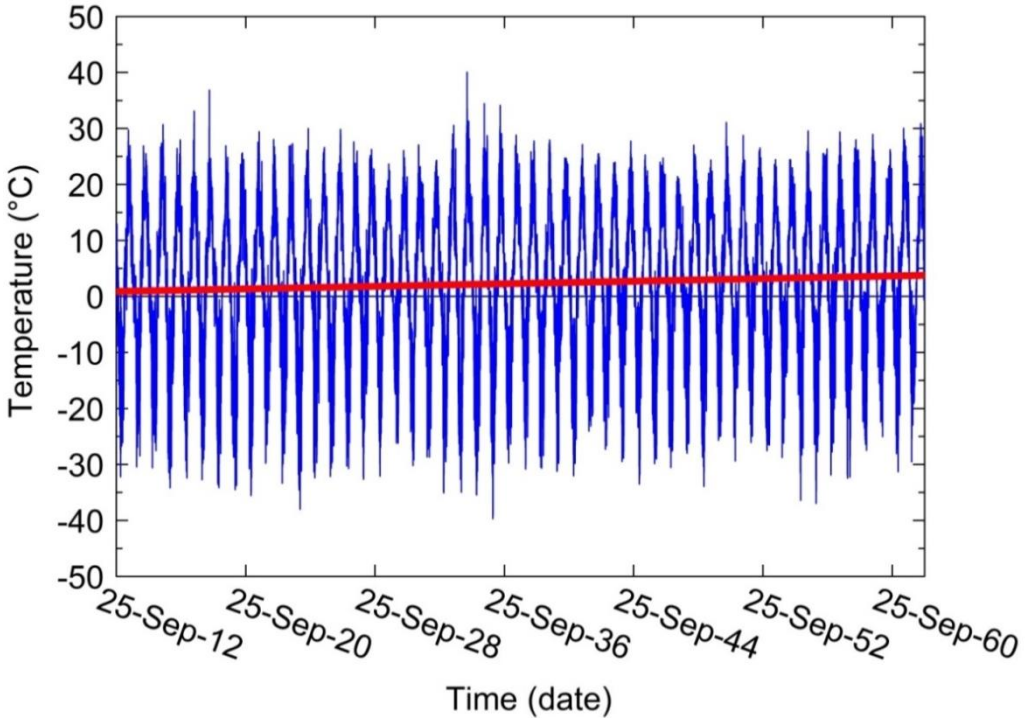

Figure 14: Predicted air temperature by CCCma for the next 50 years from September 2012 to September 2062 and a 0.00015 °C/day fitted linear trend line

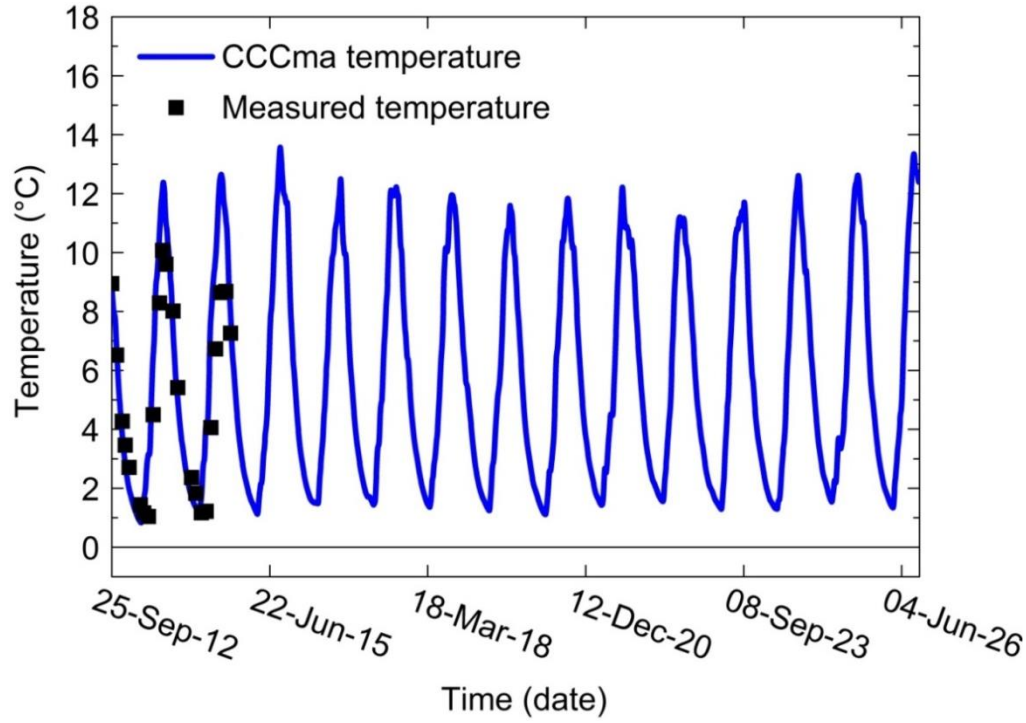

Figure 15: Temperature versus time at 2 m below the toe of the embankment. Measured temperatures are after Flynn et al. (2015a)

beneath the roadway and cause it to disappear entirely. A similar result has been proposed by Flynn et al. (2015a) using a lower warming rate of 0.0001^{o}C and different software.

Melting of the frost bulb in a fine-grained soil produces excess pore water pressures due to the overburden pressure. This is followed by thaw consolidation, which can result in differential settlements along the road alignment because soil conditions are rarely uniform. The net result is an uneven road (Figure 2), traffic safety issues, and the need for frequent maintenance. The thermal modeling in this study will also be used in predicting embankment deformations, information that will be valuable for future road maintenance and design of new embankments.

3.9. CONCLUSIONS

A numerical thermal model has been developed to investigate the ground thermal regime under a road embankment in northern Manitoba, Canada. Data from field instruments and laboratory testing programs were used in calibrating the model. Instrumentation and monitoring provided temperature data for 6 years at the toe and mid-slope of the embankment, and 2 years at the shoulder and centreline.

The model simulated the ground thermal regime under the embankment with good accuracy. The depth of zero annual temperature amplitude beneath the embankment was estimated to be about 8 metres, which is consistent with the measured temperatures. A zone of frozen soil or frost bulb is present beneath the embankment. It varies seasonally, but is gradually degrading over time and is likely to be the main reason for ongoing movements of the embankment. The model estimated reasonably well the shape, location, and seasonal changes of the frost bulb. Based on predicted

future air temperatures, the frost bulb will disappear completely within 20 years, and perhaps much sooner.

REFERENCES

ABAQUS Analysis user's manual 6.12-1, Dassault Systems Simulia Corp., Providence, RI, USA; 2012. (http://www.3ds.com/products-services/simulia/products/abaqus/)

Alfaro, M.C., Ciro, G. A., Thiessen, K. J., Ng, T., 2009. Case Study of Degrading Permafrost beneath a Road Embankment. *Journal of Cold Regions Engineering*, ASCE, 23(3), 93–111.

Andersland, O.B., Ladanyi, B., 2004. Frozen Ground Engineering, 2nd ed. John Wiley and Sons, Inc, Hoboken, NJ.

Anderson, D. M., Tice A. R., 1973. The unfrozen interfacial phase in frozen water systems. *Ecological Studies: Analysis and Synthesis*, vol. 4, Hadar, A. (ed.). Springer: New York, 107–124.

Batenipour, H. et al., 2014. Deformations and ground temperatures at a road embankment in northern Canada. *Canadian Geotechnical Journal*, 51(3), 260–271.

Brown, R.J.E., 1969. Distribution of Permafrost in Canada, T*hird Canadian Conference on Permafrost, Division of Building Research*, National Research Council, Ottawa.

Canadian Centre for Climate Modeling and Analysis (CCCma), 2015. 3rd Generation Coupled Global Climate Model (CGCM3.1/T47 IPCC SRES A2 Scenario Data), 2010. University of Victoria. (http://cccma.ec.gc.ca/)

Climate Change Office, 2005. Government of Canada. (http://www.climatechange.ge.ca/english/default.asp)

Darrow, M.M., 2011. Thermal modeling of roadway embankments over permafrost. *Cold Regions Science and Technology*, 65(3), 474–487.

Farouki, O., 1985. Ground thermal properties. *Proc., Thermal Design Considerations in Frozen Ground Engineering*, ASCE, New York, pp. 186–203.

Flato, G. M., Boer, G. J., 2001. Warming asymmetry in climate change simulations. *Geophysical Research Letters*, 28(1), 195–198.

Flynn, D., Kurz, D., Alfaro, M., Graham, J., and Arenson, L., 2015a. Forcasting ground temepratures under a highway embankment on degrading permafrost. Journal of Cold Regions Engineering, ASCE. (submitted)

Fortier, R., LeBlanc, A., Yu, W., 2011. Impacts of permafrost degradation on a road embankment at Umiujaq in Nunavik (Quebec), Canada. *Canadian Geotechnical Journal*, 48(5), 720–740.

Geo-slope, 2010, Thermal Modeling with TEMP/W 2007, Geo-slope International Ltd., Calgary, Alberta, Canada.

Johansen, Ø. 1975. Thermal conductivity of soils. Ph.D. dissertation, *Norwegian Technical University, Trondheim*; also, U.S. Army Cold Regions Research and Engineering Laboratory Transl. 637, July 1977.

Kersten, M. S., 1949. Laboratory Research for the Determination of the Thermal Properties of Soils. *ACFEL Technical Report 23, AD71256* (Also: Thermal properties of soils. University of Minnesota Engineering Experiment Station Bulletin No. 28)

Kurz, D., Alfaro, M. and Graham, J. 2015. Thermal Conductivities of Frozen and Unfrozen Soil in the Active Layer. Cold Regions Science and Technology. (*submitted*)

Li, Q., Sun, S., Xue, Y., 2010. Analyses and development of a hierarchy of frozen soil models for cold region study. *Journal Of Geophysical Research*, 115, 1-18.

Li, J-P. and Yu, S., 2008. Analysis of the thermal stability of an embankment under different pavement types in high temperature permafrost regions. *Cold Regions Science and Technology*, 54(2), 120–123.

Lunardini, V. J., 1981. Heat Transfer in Cold Climates, Van Nostrand Reinhold Company, NY.

McRoberts, E. C. 1974. Ground Thermal Regime. *Recent advances in permafrost engineering: Lecture notes and reference list*, Department of Civil Engineering, University of Alberta, Edmonton, Alberta, Canada.

Michalowski, R. L., Zhu, M., 2006. Frost heave modeling using porosity rate function. *International Journal for Numerical and Analytical Methods in Geomechanics*, 30, 703-722.

NRC. 2003. National annual temperature scenario: 2050. The atlas of Canada, Natural Resources Canada. (http://atlas.gc.ca)

Zhu, M. , Michalowski, R.L., 2005. Simulation of Heat Transfer in Freezing Soils Using ABAQUS. *Abaqus Users' Conference*, pp.1–7.

CHAPTER 4: Modeling of Highway Embankment Deformations due to Degrading Permafrost

Arash Gholamzadeh and Marolo Alfaro

Submitted to **ASCE Journal of Geotechnical and Geoenvironmental Engineering** for publication as an Article

In this chapter, the stress-deformation modeling part of the research is presented in the form of a journal paper. The paper consists of the following sections:

1- INTRODUCTION

2- LABORATORY TEST AND INSTRUMENTATION PROGRAMS AT THE TEST SITE

3- MODELING PROCEDURE

4- CONSTITUTIVE MODEL

5- STRESS-DEFORMATION MODELING

6- MATERIAL PROPERTIES

7- BOUNDARY CONDITIONS

8- RESULTS AND DISCUSSION

9- CONCLUSIONS

ABSTRACT

Degradation of permafrost is a major cause of excessive deformations and instabilities of linear transportation infrastructures such as highways, rail lines, and airport runways located in cold regions. A numerical model was developed to simulate the deformations of an embankment due to degrading permafrost. The model was calibrated with a fully instrumented test section along a highway that has settled considerably. Two types of stress-deformation modeling were performed. One was a fully-coupled analysis, where the thermal and consolidation analyses were performed in a fully-coupled manner in a single analysis, and the other was a sequentially-coupled analysis where the thermal and mechanical analyses were performed sequentially. The model was able to capture the vertical and horizontal deformations of the highway embankment. The results show that the fully-coupled analysis simulates lower deformations than the sequentially-coupled analysis. The reason is attributed to the colder temperatures simulated by the fully-coupled analysis which results in stiffer and consequently less compressible soil. The comparison between the simulated deformations using the two analyses can be useful as a basis for a more conservative design by the sequential analysis.

4.1. INTRODUCTION

Permafrost areas occupy around 40% to 50% of Canada's total land surface of 10 million square kilometers (Brown, 1960). Figure 1 shows the permafrost types and their distributions in Manitoba. Railroads, highways, pipelines and airport runways have been, and continue to be, constructed in this large area of permafrost. The infrastructure has to rely on the underlying permafrost for their foundation. Changes in the thermal regime of the permafrost, either from climate change or land use changes, can have significant effects on the stability and serviceability of the transportation infrastructure. Provincial Road 391 (PR 391), which is located in northern Manitoba (Figure 1), is an example of a road embankments built on degrading permafrost. Some sections of this road embankment are experiencing large irregular deformations which have resulted in serviceability and safety issues (Figure 2).

Thaw settlement is one of the common reasons for damage to road embankments built on degrading permafrost (Alfaro et al., 2009; Fortier et al., 2011). Numerical modeling of thaw consolidation has been the focus of many early researchers (Morgenstern and Nixon, 1971; Harlan, 1973; Guymon and Luthin, 1974; Taylor and Luthin, 1978). They proposed mathematical models for simulating heat and water flow in freezing soils. The model proposed by Harlan (1973), for example, coupled the heat and mass (water) transport equations in freezing soil medium using the interdependency of the equations when phase change occurs.

Coupled thermo-mechanical models have been recently developed to simulate the thermal and stress-deformation behaviour of embankments on permafrost. Recently, researchers (Qi et al., 2012; Ming and Li, 2012; Wang et al., 2015) have developed

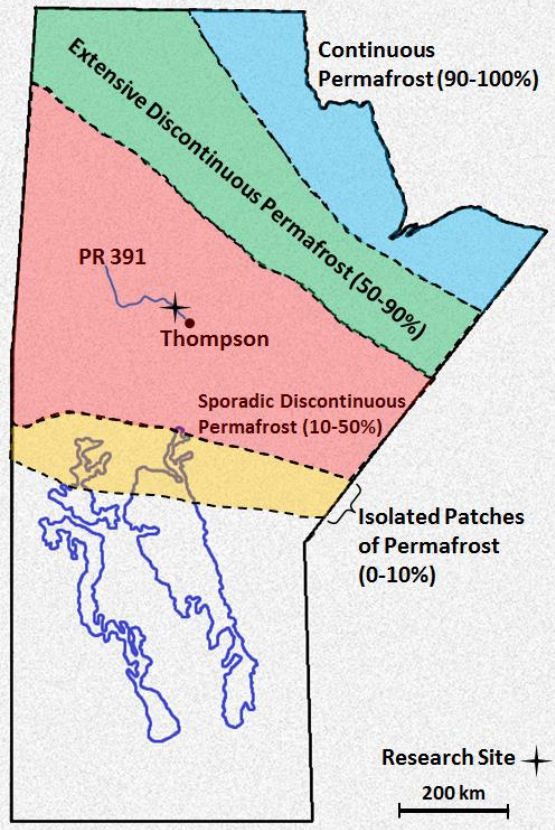

Figure 1: Permafrost types and distribution in Manitoba and location of the research site.

Figure 2: Unstable section of PR 391 in northern Manitoba (courtesy of Batenipour, 2014).

numerical models to simulate thaw consolidation of permafrost foundations under highway embankments.

This paper presents the results of a numerical modeling of a section along PR 391 road embankment in northern Manitoba. The model used the Finite Element computer program ABAQUS/CAE. The road is in a region of discontinuous permafrost and thawing has led to large irregular deformations resulting in serviceability and safety issues. Instruments were installed to measure ground temperatures, pore water pressures, and deformations. Thermal and mechanical properties of the soils have been measured in the laboratory. Monitoring data and laboratory results have been reported in earlier works (Batenipour et al., 2014; Kurz et al., 2014; Flynn et al., 2015a). The recorded ground temperatures show the existence of a frozen section (frost bulb) underneath the road embankment. The existence of the frost bulb was also confirmed during drilling and sampling at the site. Numerical modeling (Gholamzadeh et al., 2015; Flynn et al., 2015a) also confirmed the existence of the frost bulb beneath the embankment. Figure 3 shows the location and the size of the frost bulb based on the thermal modeling carried out by Gholamzadeh et al. (2015). This paper will focus on the effects of the thawing of this frost bulb on the deformations of the road embankment using numerical modeling. Two types of analyses were performed: 1) fully-coupled analysis, and 2) sequentially-coupled analysis. The results of the two analyses were compared with the monitored data from the instrumented test site of PR 391 road embankment.

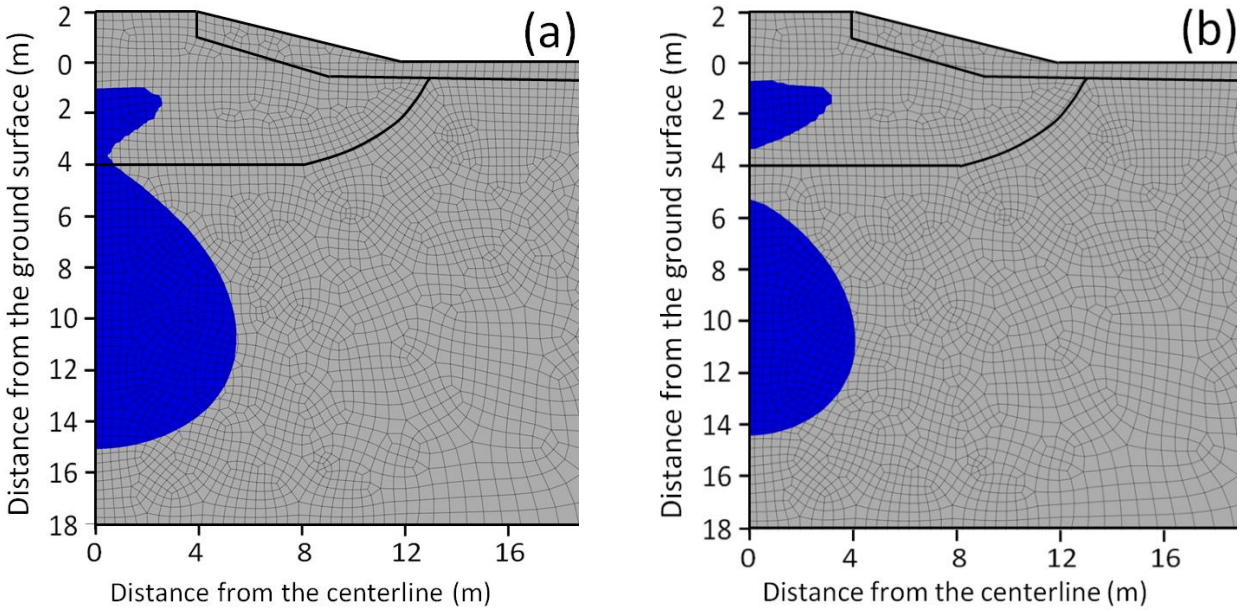

Figure 3: The location and size of the frost bulb under PR 391 road embankment from thermal modeling: (a) August 2013 and (b) August 2014. (After Gholamzadeh et al., 2015)

4.2. LABORATORY TEST AND INSTRUMENTATION PROGRAMS AT THE TEST SITE

The research site is along PR 391 located 18 km northwest of Thompson, Manitoba, at approximately N55°50' latitude and W98°01' longitude. This road is located in a region of discontinuous permafrost (Figure 1). It was originally constructed as compacted earthen road in the mid-1960s and converted to a gravel road in the early 1970s. In 1980s, it was upgraded to a bituminous asphalt surface. Degradation of permafrost beneath the road embankment has led to large ongoing irregular deformations and issues with traffic safety. Because of this, the portion of the road at the test site has been reverted to gravel surface (Figure 2).

4.2.1 Laboratory Testing Programs

Two extensive laboratory programs were completed in order to determine the mechanical and thermal properties of the soils at the site. In the first laboratory program, Isotropically-Consolidated Undrained (CIU) triaxial tests and one-dimensional oedometer tests were conducted on soil samples taken from different depths beneath the toe of the embankment (Batenipour et al. 2014). These tests provided the required mechanical properties of the soils. Thermal conductivity tests were carried out on frozen and unfrozen soil samples. The tests were conducted and reported by Kurz et al. (2015). These tests provided the thermal conductivities of the soils at the site at both frozen and unfrozen states. The results of the two laboratory programs were used in the numerical modeling.

4.2.2 Instrumentation and monitoring programs

Two comprehensive instrumentation and monitoring programs were conducted in 2008 and 2012 to monitor the performance of the road embankment. Table 1 and Figure 4 summarize and show the details of the two instrumentation programs, respectively. The first set of instruments, shown as dashed lines in Figure 4, were installed in October 2008 (Batenipour et al. 2014). They included vibrating wire (VW) piezometers installed beneath the toe to measure pore water pressures and a slope inclinometer (SI) and settlement plates at the toe to measure lateral and vertical deformations. The initial monitoring program provided data over three winters and two summers before it was terminated in April 2011 (Batenipour et al., 2014). Additional instruments, shown as square dots in Figure 4, were installed in September 2012 (Flynn et al., 2015a). The new instruments included vibrating wire (VW) piezometers beneath the centreline,

Table 1: A summary of the instrumentation and monitoring programs at PR 391 research site.

Field program	Start date	End date	Installed instruments	Location	Data collection	Researcher
First	October 2008	April 2011	Slope inclinometer and VW piezometer	Toe	Manual download	Batenipour et al. (2014)
Second	September 2012	October 2014	Horizontal and vertical SAA and VW piezometer	Shoulder and centerline	Remotely via satellite	Flynn et al. (2015b)

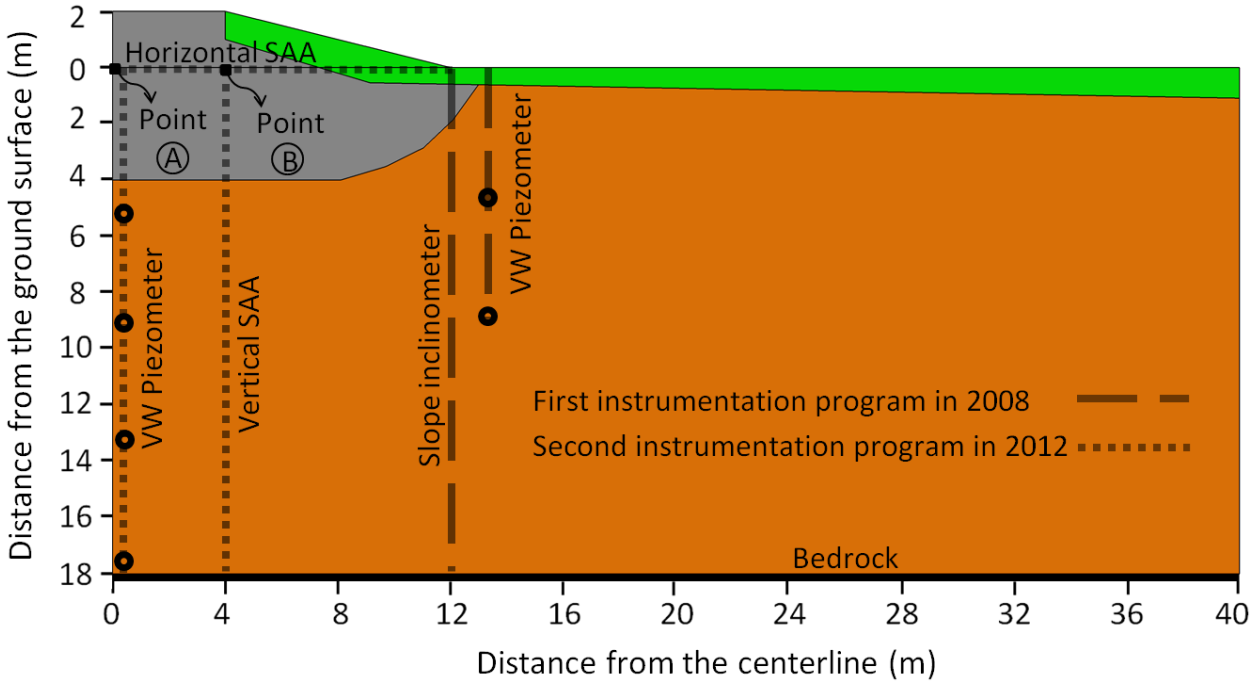

Figure 4: Instrumentation at PR 391 research site

Shape-Accel-Arrays (SAAs) vertically beneath the shoulder and horizontally beneath the embankment from the toe to the centreline to measure lateral and vertical displacements. It should be mentioned that almost all the instrumentation installed in the first monitoring program were still functional in the second monitoring program. The

results of the instrumentation programs were used to calibrate the numerical model developed in this research.

4.3. MODELING PROCEDURE

The frost bulb beneath the embankment (Figure 3) has been found to thaw (Gholamzadeh et al., 2015; Flynn et al., 2015a). A fully-coupled and a sequentially-coupled thermo-hydro-mechanical analysis were performed to investigate the operating mechanisms of deformations due to the thawing frost bulb beneath the road embankment. In the fully-coupled analysis, thermal and stress-deformation analyses are solved in a fully-coupled manner in a single analysis. Therefore, thermal, mechanical and hydraulic material properties were assigned to the model at the same time. In the sequentially-coupled analysis, thermal modeling is first performed to induce the temperature distributions in the soil medium. The results of the thermal modeling are then used to perform a stress-deformation modeling using temperature-dependent material properties. In the first stage, the thermal properties and in the second stage the mechanical and hydraulic properties of the soils were assigned to the model. The thermal modeling stage of the sequentially-coupled analysis has been conducted and described in detail in Gholamzadeh et al. (2015).

4.4. CONSTITUTIVE MODEL

Modified Drucker-Prager Cap (MDPC) was chosen as the constitutive model to capture the elasto-plastic behaviour of soils at the site. This model is the Drucker-Prager plasticity model with an addition of a cap yield surface which provides an inelastic hardening mechanism to account for plastic compaction (ABAQUS manual, 2012). The

MDPC yield surface consists of three different segments as illustrated in Figure 5. These segments are as follows:

4.4.1 Drucker-Prager shear failure (F_s)

Drucker-Prager shear failure segment is a line in *p-t* plane with the following equation (ABAQUS manual, 2012):

$$F_s = t - p\,tan\,\beta - d = 0 \qquad \text{[Eq.1]}$$

where *t* is the deviatoric stress, *p* is the equivalent pressure stress, β is related to the friction angle and *d* is related to the material cohesion. The deviatoric stress is defined as follows:

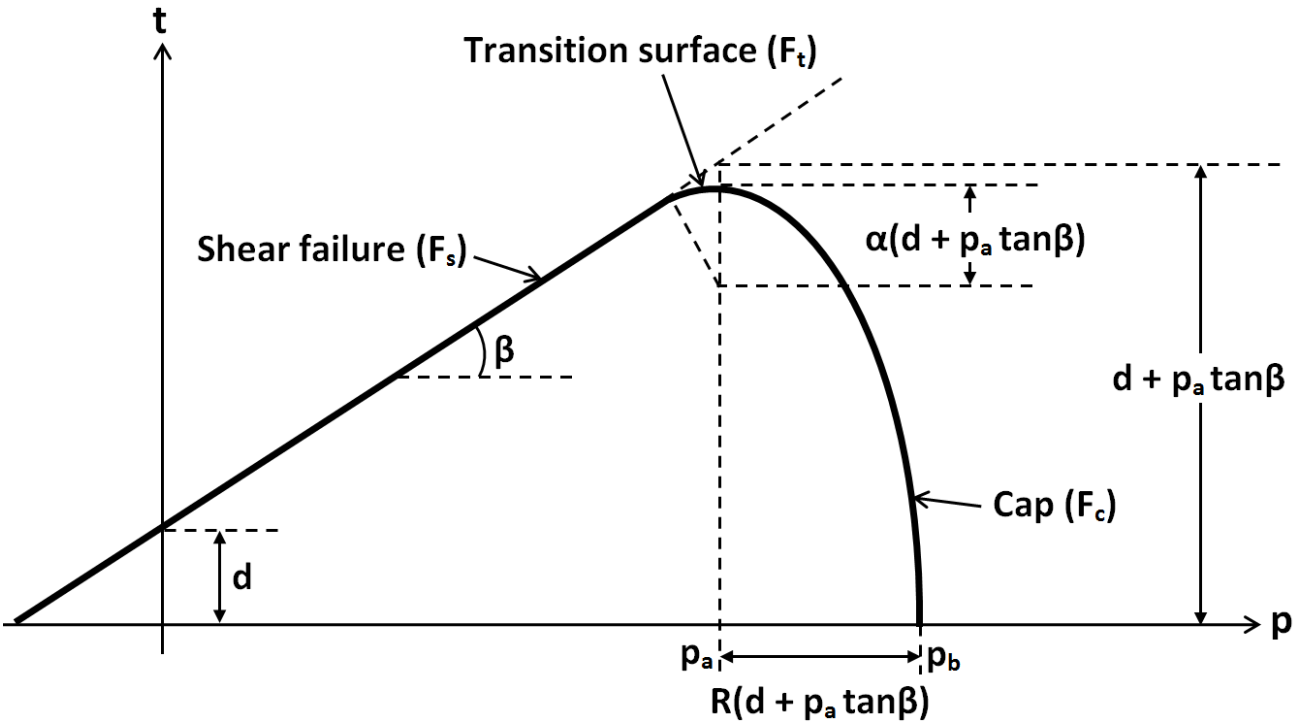

Figure 5: Modified Drucker-Prager Cap (MDPC) yield surface in p-t plane (Repreduced with permission from ABAQUS©, 2012, Dassault Systemes Simulia Corp). The parameters are: d is related to material cogesion; β is related to the material friction angle; α is the transition parameter; R is the cap eccentricity; p_a is the evolution parameter; p_b is the hydrostatic compression yield stress.

$$t = \frac{q}{2}\left[1 + \frac{1}{K} - \left(1 - \frac{1}{K}\right)\left(\frac{r}{q}\right)^3\right] \quad \text{[Eq.2]}$$

where q is the shear stress and K is a material parameter that controls the dependence of the yield surface on the value of the intermediate principal stress and can get a value $0.778 \leq K \leq 1$. A default value of K is 1 which results in $q = t = \sigma_1 - \sigma_3$. The values of β and d can be related to the classical Mohr-Coulomb parameters φ (friction angle) and c (cohesion) depending on whether the stress conditions in the problem are triaxial or plane-strain.

For plane-strain condition, which is the case for the numerical model in this research, β and d are defined as follows (ABAQUS manual, 2012):

$$\beta = Arc\ tan\left(\frac{3\sqrt{3}\ tan\varphi}{\sqrt{9+12\ tan^2\varphi}}\right) \quad \text{[Eq.3]}$$

$$d = \frac{3\sqrt{3}\,c}{\sqrt{9+12\ tan^2\varphi}} \quad \text{[Eq.4]}$$

For triaxial stress condition, which is used in triaxial test simulations, β and d are defined as follows:

$$\beta = Arc\ tan\left(\frac{6\sin\varphi}{3-sin\varphi}\right) \quad \text{[Eq.5]}$$

$$d = \frac{18\,c\ \cos\varphi}{3-\sin\varphi} \quad \text{[Eq.6]}$$

It is clear that for both stress conditions, if $c=0$ then $d=0$.

4.4.2 Cap yield surface

The cap segment of the MDPC yield surface is defined by the following equation (ABAQUS manual, 2012):

$$F_c = \sqrt{[p - p_a]^2 + [\frac{Rt}{(1+\alpha-\frac{\alpha}{cos\,\beta}}]^2} - R\big(d + p_a(tan\beta)\big) = 0 \qquad \text{[Eq.7]}$$

where *α* is the transition parameter*, R* is the cap eccentricity parameter which controls the shape of the yield surface, p_a is an evolution parameter that represents the volumetric inelastic strain driven hardening/softening and p_b is the hydrostatic compression yield stress. The evolution parameter is given by:

$$p_a = \frac{p_b - Rd}{1+R(tan\beta)} \qquad \text{[Eq.8]}$$

where p_b, *R* and *d* parameters are as defined previously. In the cap yield surface section, the hardening/softening law is defined as a function which dictates how the volumetric plastic strain gradually develops as the hydrostatic compression yield stress (p_b) increases. In other words, the cap hardening behaviour defines how the hydrostatic compression yield stress $p_b(\varepsilon_{Vol}^{Pl})$ evolves if the material yields in the cap region. It is important to note that the range of the defined values for p_b should be wide enough to include all the values of effective stress that the material might experience during the analysis. An isotropic-consolidated triaxial test should be conducted for directly establishing this relationship. Alternatively, the following exponential cap hardening function can be used as the relationship between the hydrostatic compression yield stress and the corresponding volumetric plastic strain (Wood, 1990):

$$\varepsilon_{Vol}^{p} = \frac{\lambda - \kappa}{1+e_o}\, ln\frac{P\prime}{P\prime_0} \qquad \text{[Eq.9]}$$

where *λ* and *κ* are the slopes of the normally consolidated (NC) and unloading/reloading (URL) lines respectively in *ln(p')-e* space, e_o is the initial void ratio, p'_o is the initial hydrostatic mean effective stress and *p'* is the hydrostatic mean effective stress. The

values of λ and κ can be determined from an oedometer test by obtaining the compression line (C_c) and the unloading/reloading line (C_s) and using the following relationships: $C_c = 2.303\ \lambda$ and $C_s \approx 2.303\ \kappa$. The value of $\varepsilon_{Vol}^{Pl}|_o$ should also be defined which is the initial volumetric plastic strain at the start of the analysis.

4.4.3 Transition yield surface

The transition yield surface is defined at the intersection between the cap yield surface and the failure surface by the following equation (ABAQUS manual, 2012):

$$F_t = \sqrt{[p - p_a]^2 + [t - (1 - \frac{\alpha}{(cos\,\beta)})(d + p_a\,(tan\beta))]^2}\ - \alpha\big(d + p_a\,(tan\beta)\big) = 0 \qquad \text{[Eq.10]}$$

where α is the transition parameter which is a small number typically between 0.01 to 0.05. The transition yield surface provides a smooth transition between the shear failure and cap surfaces (Figure 5). Other parameters have been defined earlier.

When using MDPC constitutive model, the following criteria must be satisfied:

1) $q_o < (P_o'\ tan\,\beta) + d$ [Eq.11]

2) $P'_b > Rd$ [Eq.12]

where q_o is the initial shear stress and other parameters have been defined earlier. The first equation states that all the initial stresses must lie under the Drucker-Prager yield surface. The second equation is derived from the fact that the evolution parameter must be positive at all times *($p'_a > 0$)*.

To summarize, the required MDPC model parameters are $\boldsymbol{d}$, $\boldsymbol{\beta}$, $\boldsymbol{R}$, $\boldsymbol{\varepsilon_{Vol}^{Pl}|_0}$, $\boldsymbol{\alpha}$, $\boldsymbol{K}$ which all have already been defined.

4.5. STRESS-DEFORMATION MODELING

Site investigation at the site carried out by previous researchers (Batenipour et al., 2014; Flynn et al., 2015a) provided an approximate ground profile. The road is approximately 2 m high above the natural ground surface and the water table is generally at the ground surface. There is approximately 6 m of gravel fill below the centreline of the road, partly from the original construction and partly from the re-grading during maintenance operations. Foundation soils consist of 1 m of clayey peat-silt underlain by silty clay and then gneissic bedrock at 18 m depth (Batenipour et al., 2014; Flynn et al., 2015a). The silty clay is firm, brown and moderately-plastic near the ground surface. It changes to soft, grey, low-plastic clay at depth. The Plasticity Index (I_P) ranges from 17% to 32%. The clay medium is divided further into 11 different layers based on drilling information and from the results of triaxial and oedometer tests. It should be mentioned that the first 10 meters of the clay medium can be modeled as a single layer with averaged mechanical properties for engineering practice uses. Figure 6 shows the geometry and the soil layers used in the modeling. Due to assumed symmetry, only half of the embankment geometry is considered in the modeling.

4.6. MATERIAL PROPERTIES

The following is a description of how the mechanical, thermal and hydraulic material properties are handled in the numerical modeling:

4.6.1 Mechanical and Hydraulic Properties

The elastic deformations in the model are characterized by Young's modulus and Poisson's ratio for all the materials. For unfrozen states of the clay soils, the Young's modulus was obtained from the stress-strain relationships (q-ε) of the triaxial test results

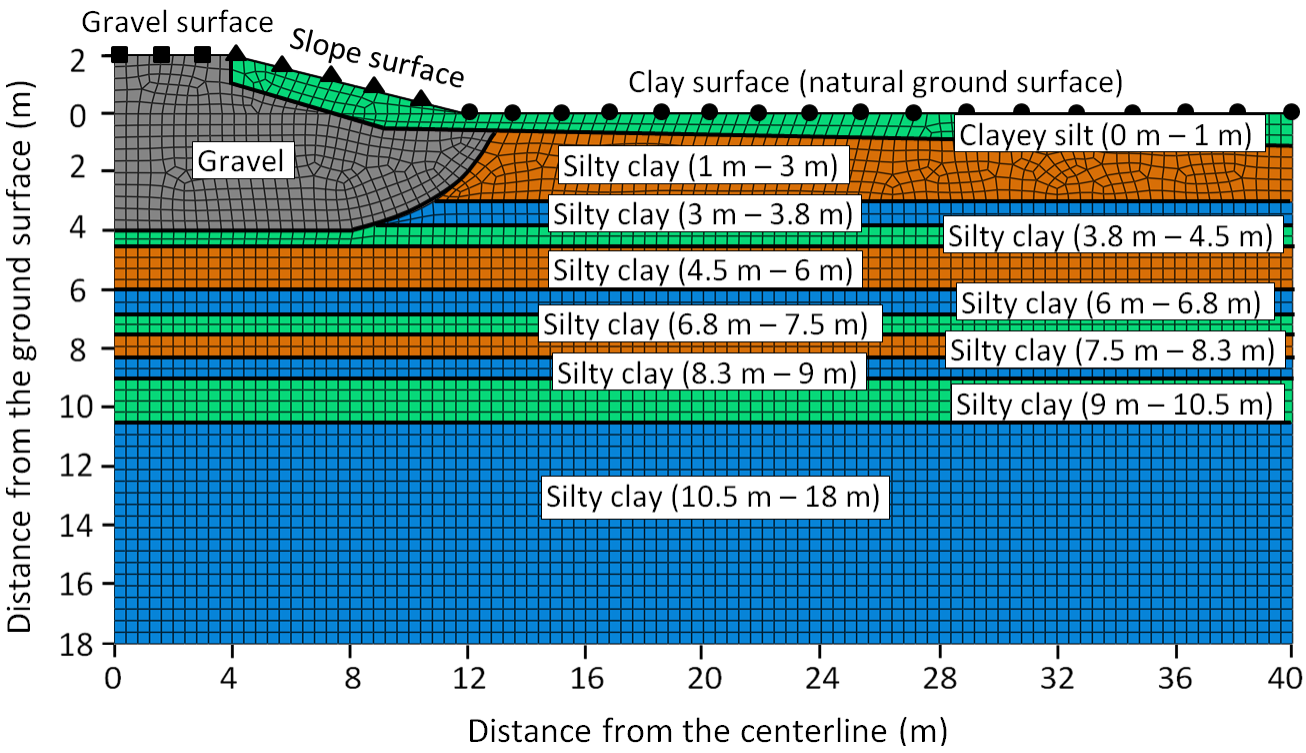

Figure 6: Final geometry of the model with the layers and Finite Element mesh

reported by Batenipour et al. (2014). For the frozen states, the elastic modulus was obtained from the available data in literature (for example, Tsytovich, 1975). The plastic deformation is characterized by the MDPC constitutive model described earlier. The values of β were calculated using Equation 3. No cohesion intercept was reported in the triaxial tests ($d \approx 0$). The results of the oedometer tests were used to establish the cap hardening relationships using Equation 9. Table 2 shows an example of the cap hardening relationship for the clay soil at depths between 9m and 10.5m (10th layer). The cap eccentricity parameter (R) was calibrated by simulating the isotropically-consolidated undrained (CIU) triaxial tests using MDPC constitutive model. The simulations were done using different R values for each layer. Figure 7 shows an example of the simulated and measured stress paths in q-p space which is for the clay

Table 2: An example of the Cap Hardening relationship

P_b' (KPa)	98	100	102	104	106	108	110	112	114	116	118	120	122
ε_v^p ($\times 10^{-4}$)	0	5	10	14	19	23	28	32	36	41	45	49	53

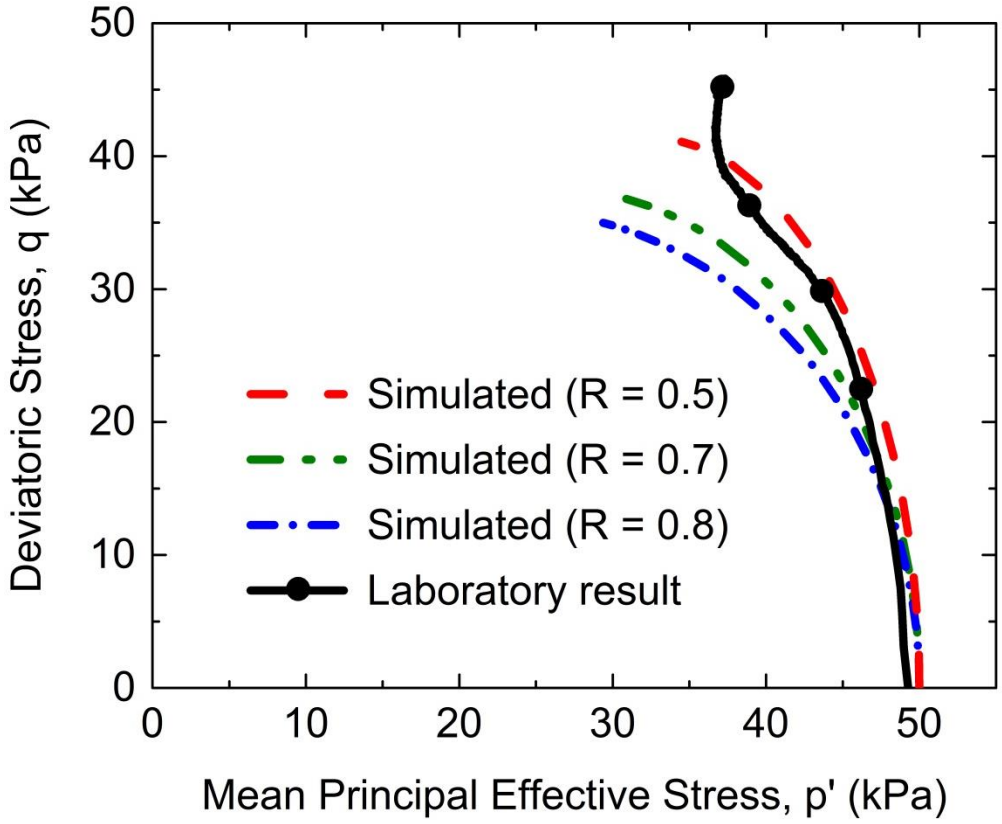

Figure 7: Cap eccentricity (R) calibration procedure for the 7.5m – 8.3m (8th layer). A comparison of q-p' relationships between the observed and simulated triaxial test results. Laboratory results are after Batenipour et al. (2014)

soil at depths between 7.5m – 8.3m (8th layer). Table 3 tabulates the mechanical and hydraulic properties of the soil layers used in the modeling. Hydraulic conductivity values were obtained from literature (for example, Tarnawski and Wagner, 1996) and were assigned for both frozen and unfrozen states.

Table 3: Summary of the mechanical and hydraulic properties of materials used in the modeling

Depth (m)	Constitutive model	d		ß (°)	R	$\varepsilon_{Vol}^{Pl}\|_0$	α	K	Elastic modulus			ν	NC line (λ)	U/R line (κ)	Hydraulic conductivity (m/s)	
		Froz (MPa)	*Unfroz (MPa)*						*Frozen (MPa)*	*Unfrozen (MPa)*	*Unfrozen (MPa)*[1]				*Frozen*	*Unfrozen*
Gravel	LE[2]	-	-	-	-	-	-	-	4000	40	-	0.25	-	-	1E-8	1E-3
0 - 1	LE	-	-	-	-	-	-	-	1600	20	-	0.3	-	-	1E-12	1E-7
1 - 3.0	LE	-	-	-	-	-	-	-	1200	18	-	0.3	-	-	1E-13	1E-8
3 - 3.8	LE	-	-	-	-	-	-	-	1200	17	-	0.3	-	-	1E-13	1E-8
3.8 - 4.5	MDPC[3]	1400	0	43	0.9	0	0	1	1200	10	3.2	0.3	0.146	0.030	1E-13	1E-8
4.5 - 6	MDPC	1300	0	46	0.9	0	0	1	1200	10	3	0.3	0.130	0.027	1E-13	1E-8
6 - 6.8	MDPC	1400	0	45	0.7	0	0	1	1200	13	3.2	0.3	0.107	0.023	1E-13	1E-8
6.8 - 7.5	MDPC	1400	0	43	0.7	0	0	1	1200	15	3.6	0.3	0.100	0.019	1E-13	1E-8
7.5 - 8.3	MDPC	1500	0	40	0.5	0	0	1	1200	11	3.1	0.3	0.097	0.020	1E-13	1E-8
8.3 - 9	MDPC	1500	0	40	0.7	0	0	1	1200	15	4.2	0.3	0.093	0.023	1E-13	1E-8
9 - 10.5	MDPC	1400	0	41	0.8	0	0	1	1200	25	9	0.3	0.059	0.009	1E-14	1E-9
10.5 - 18	LE	-	-	-	-	-	-	-	120	27	27	0.3	-	-	1E-14	1E-9

[1]The elastic modulus of the area under the gravel fill between centerline and mid-slope
[2]Linear Elastic
[3]Modified Drucker-Prager Cap

In order to consider the creep effects of the clay soil under the embankment, the built-in Singh-Mitchell creep model in ABAQUS/CAE was used. The model relates the strain rate and time using the following equation:

$$\mathring{\varepsilon} = Ae^{(\theta q)}(\frac{t_1}{t})^m \quad \text{[Eq.13]}$$

where $\mathring{\varepsilon}$ is the strain rate, A is the strain rate at time t_1, θ is the slope of the linear portion of the logarithmic strain rate versus deviator stress plot, q is the deviator stress, t_1 is a unit time and m is the slope of the logarithm of strain rate versus logarithm of time. Obtaining the model parameters requires conducting triaxial creep tests on samples from different depths above the frost bulb. In this research, the model parameters were obtained from literature (for example Morsy et al., 1995) for soils with similar values of C_α taken from the work of Batenipour et al. (2014). The adopted parameters in the model are A= 9.38 (%/day), t_1= 1 (day), θ= 5e-5 (1/Pa), m= 1 for the unfrozen state and A= 9.38E-3 (%/day), t_1= 1 (day), θ= 5e-7 (1/Pa), m= 1 for the frozen state.

4.6.2 Thermal Properties

The required thermal properties for a transient fully-coupled analysis are thermal conductivity, heat capacity and density for the soil solid grains (ABAQUS manual, 2012). Thermal conductivity and density of the saturated frozen and unfrozen states of the soils were measured and reported in Kurz et al. (2015). Using these results, thermal conductivity of the solid grains of the soil was back calculated based on the available relationships in the literature (for example in Lunardini, 1981; Farouki, 1985). Also required in the analysis are the temperature-dependent thermal properties of pore fluid water. The required thermal properties of water are latent heat, solidus and liquidus temperatures, thermal conductivity and heat capacity. Solidus temperature is defined as

the temperature below which the material is ‘frozen’ and liquidus temperature is the temperature above which the material is ‘unfrozen’ (ABAQUS manual, 2012). The solidus and liquidus temperatures were chosen based on the observations in the field and reported values in the literature. The recorded temperatures show that the average temperatures inside the frost bulb vary between -0.1°C and -0.3°C during the two-year period of the second monitoring program (Flynn et al., 2015a). Based on this observation and reported values in the literature (for example in Farouki, 1985 and Geo-Slope International, 2010), the solidus and liquidus temperatures of the clayey silt material were assumed to be -3°C and 0°C, respectively. The corresponding values for silty clay were assumed to be -4°C and 0°C. The solidus and liquidus temperatures of the gravel material were assumed to be -0.75°C and 0°C, respectively (Geo-Slope International, 2010). It should be noted that small variations of these values were used in the modeling but were found to have negligible effects. Table 4 summarizes the thermal material properties used in the fully-coupled analysis.

In a sequentially-coupled analysis, the material properties are defined based on the analysis type of each stage. In the thermal modeling stage, the thermal material properties of the soils are required. The thermal properties are the heat capacity, thermal conductivity and latent heat of the saturated frozen and unfrozen states of the soils. Detailed description of each property used in the thermal modeling stage can be found in Gholamzadeh et al. (2015). In the stress-deformation modeling stage, the required material properties are the mechanical and hydraulic properties which were presented in Table 3.

Table 4: Summary of the thermal properties of materials used in the fully-coupled analysis

	Pore Fluid (water)	Gravel solid grains	Clay solid grains
Solidus Temp (°C)	Clayey silt: -3°C Silty clay: -4°C Gravel: -0.75°C	-	-
Liquidus Temp (°C)	0	-	-
Latent Heat (J/kg)	334000	-	-
Thermal Conductivity (J/day·m·°C)	192000 at -3°C 48470 at 0°C	400000	240000
Specific Heat (J/kg·°C)	2045 at -3°C 4210 at 0°C	650	710
Density (kg/m^3)	1000	2700	2700

4.7. BOUNDARY CONDITIONS

The applied mechanical boundary conditions were zero horizontal and vertical displacements at the bottom and zero horizontal displacement at both vertical sides of the model. The hydraulic boundary conditions were zero pore water pressure on the natural ground surface and a default 'no-flow' boundary condition at the bottom and sides of the model. The thermal boundary conditions were applied on the top and bottom of the model. The left and right boundaries were defined from symmetry as a default 'no-heat-flow' boundaries. For the top thermal boundary condition, the seasonally changing ground surface temperatures are needed which is directly affected by air temperatures applied on the top surface of the model. The mean daily air temperatures were obtained from climate data recorded by Environment Canada at their weather monitoring station at Thompson Airport, less than 10 km away from the test

site. Conversion of air temperatures to temperatures just below the ground surface used modifying n-factors. The surface modifying n-factors are site-specific and can vary depending on many factors such as surface type, wind speed (Lunardini, 1981), and snow cover (Fortier et al., 2011), among others. Three distinct surface types were identified based on the materials at the site. The surfaces are shown in Figure 6 and are as follows:

1. The clay surface, which is the surface of the surrounding natural ground. This surface is covered with snow in freezing seasons and is under bushes and short plants in thawing seasons.
2. The slope surface, which is the surface from the shoulder down to the toe of the embankment. This surface is also covered with snow in freezing seasons and is under bushes and short plants in thawing seasons.
3. The gravel surface of the road pavement. This surface is free of snow and vegetation throughout the year.

Freezing and thawing n-factors were considered for each surface type which are presented in Table 5. The base boundary condition used average measured temperatures at 18 m depth below the ground surface. Constant temperatures of 1°C and 1.9°C were applied to the bottom of the model below the centreline and toe of the embankment respectively. A linear variation of base temperature was assumed between these two locations. The constant 1.9°C temperature was also applied to the base of the model extending from below the toe to the right boundary of the model.

Table 5: Summary of the n-factors used in the thermal modeling (from Gholamzadeh et al., 2015)

SURFACE	Freezing (n_f)	Thawing (n_t)
Clay	0.08	1
Slope	0.1	1.1
Gravel	1	1.2

4.8. RESULTS AND DISCUSSION

4.8.1 Vertical displacements

Figure 8 shows the simulated and measured vertical displacements at the shoulder and centerline of the embankment (Points A and B in Figure 4) for fully-coupled and sequentially-coupled analyses. The simulated displacements reasonably match the measured displacements at both locations. However, the results of the modeling are more accurate at the shoulder of the embankment than the centerline. This can be due to the uncertainties regarding the mechanical properties of the soil located over the frost bulb at the centerline of the embankment. The material in this region has been subject to constant freeze-thaw cycles by the degrading frost bulb (Gholamzadeh et al., 2015).

The measured settlements in Figure 8 show sharp upward movements in each spring beginning around mid-April and lasting 4 to 8 weeks. The numerical model was not able to capture the measured upward movements. This requires further studies including experimental tests to understand the operating mechanisms that caused the upward movements of the foundations during spring thaw. The authors believe that this behaviour can be explained by considering the change in effective stress during the thawing seasons. Figure 9 shows the ground water condition at 13.2 m and 17.5 m

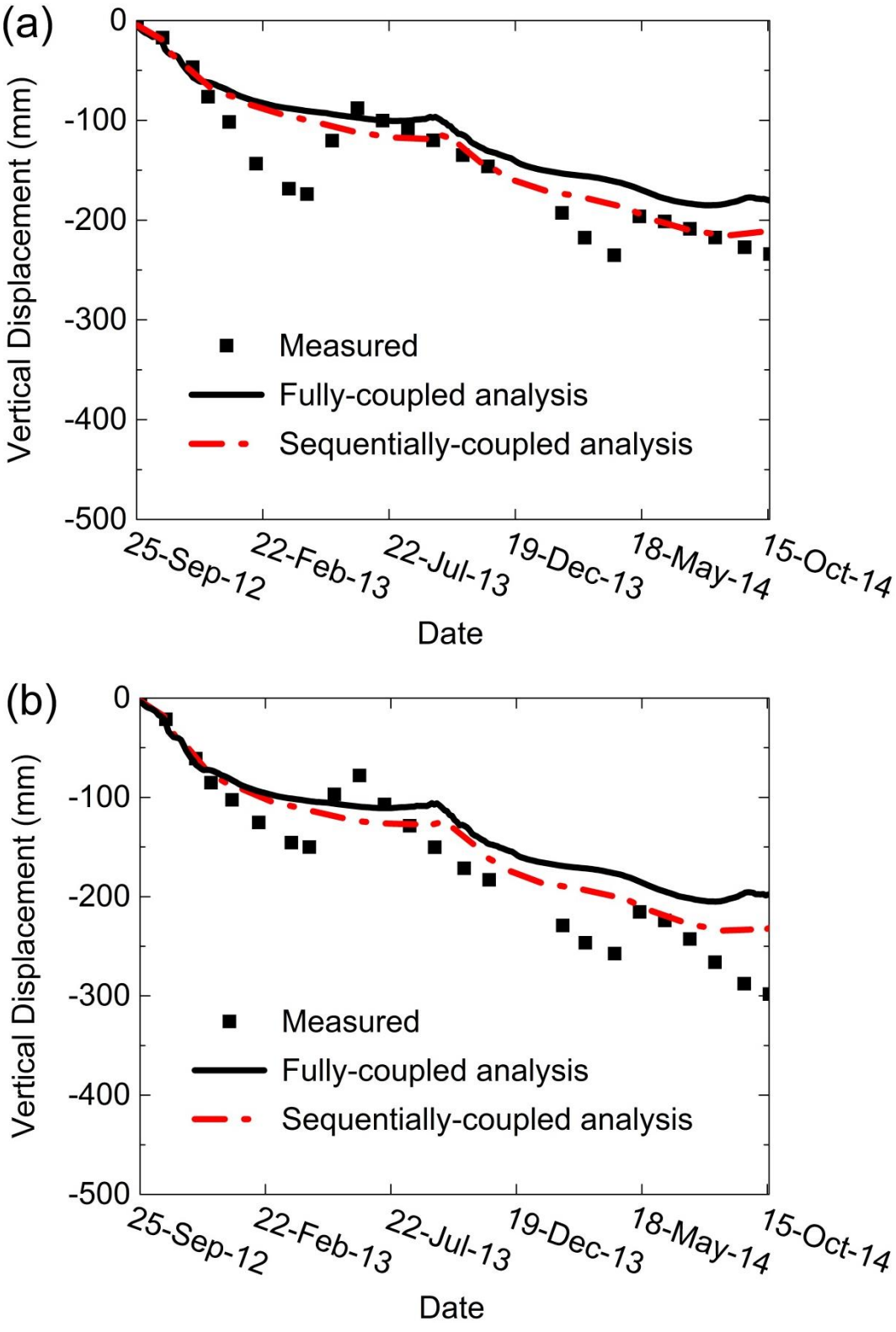

Figure 8: Modeled and measured vertical displacements at the (a) shoulder and (b) centerline beneath the embankment (refer to points A and B in Figure 4). Measured values are after Flynn et al. (2015b).

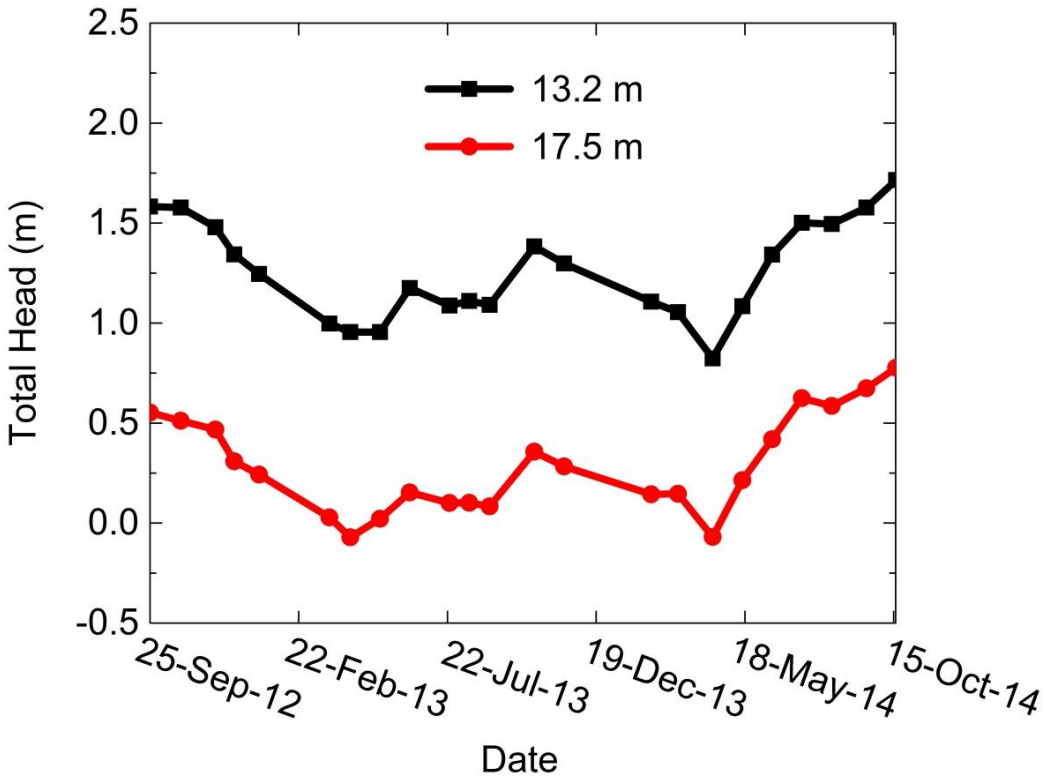

Figure 9: Total heads measured by the piezometer at 13.2 m and 17.5 m beneath the centerline of the embankment (After Flynn et al., 2015b)

beneath the centerline of the embankment plotted on the same time scale as the vertical displacement plots in Figure 8 (Flynn et al., 2015b). Total head calculations in this plot used the elevation at the toe of the embankment as the datum. As can be seen in Figure 9, total head increases during the times of spring melt which corresponds to the times of sharp upward movements in Figure 8. Since total stress (**σ**) is constant, increase in pore water pressure (**u**) due to spring melt can reduce the effective stress ($\boldsymbol{\sigma}' = \boldsymbol{\sigma} - \boldsymbol{u}$). The reduction in effective stress makes the soil behave as if it is unloaded and can consequently result in higher void ratios and expansion of the soil.

Another explanation for the upward movements proposed by Flynn et al. (2015b) is that the clay layer swelled under the embankment and caused the upward spike observed in

each spring. During the spring melt, unfrozen water coming from the thawed region around the frost bulb can accumulate in the clay layer. These observations were consistent with the observations by Konrad and Roy (2000) on clay subgrades. They noted that water cannot easily drain through the impervious still-frozen soil. The frozen soil swelled in response to the increased water availability from ground ice thawing. The swelling depends on the quantity of meltwater, the swelling index of the subgrade, and the volume of the subgrade (Konrad and Roy, 2000). The numerical model was not able to capture the measured upward movements. Further studies are needed to include the above-indicated operating mechanisms.

Figures 10 and 11 respectively illustrate the contours of the vertical effective stress and the displacement vectors from the fully-coupled analysis in July 2014. Both figures also include the approximate location of the simulated frost bulb (dashed line). As figure 10 shows, the stresses are concentrated in the area under the embankment close to the centerline. This area, as shown in Figure 11, has undergone the largest displacements. Figure 11 also shows that the magnitudes of displacements reduce significantly to negligible amounts in the frost bulb and the lower silty clay regions. This is due to the fact that the material of the frost bulb is considerably less compressible compared to the unfrozen soil above it. Weaker material and concentration of stress in the area under the embankment between the gravel fill and the frost bulb causes the soil in this area to deform significantly. This has also caused yielding and plastic deformations of the soil in this area, as shown in Figure 12. This figure shows the contours of the maximum principal plastic strains in February 2014 and July 2014, and as can be seen, the soil in the area between the gravel fill and the frost bulb has undergone plastic deformations.

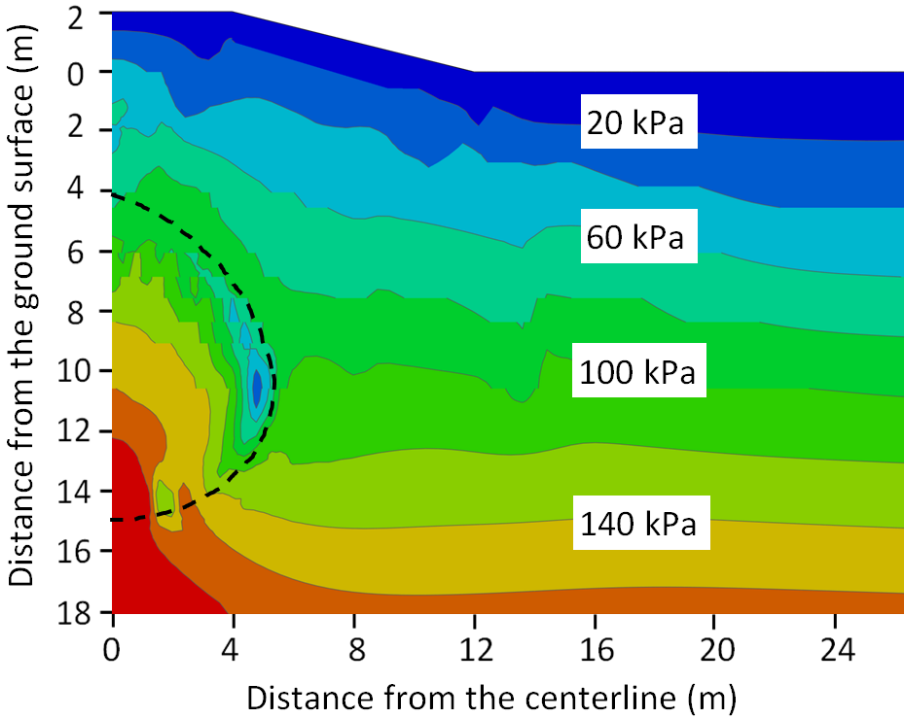

Figure 10: Contours of the vertical effective stress in July 2014 from the fully-coupled analysis. Dashed line delineates the approximate location of the simulated frost bulb

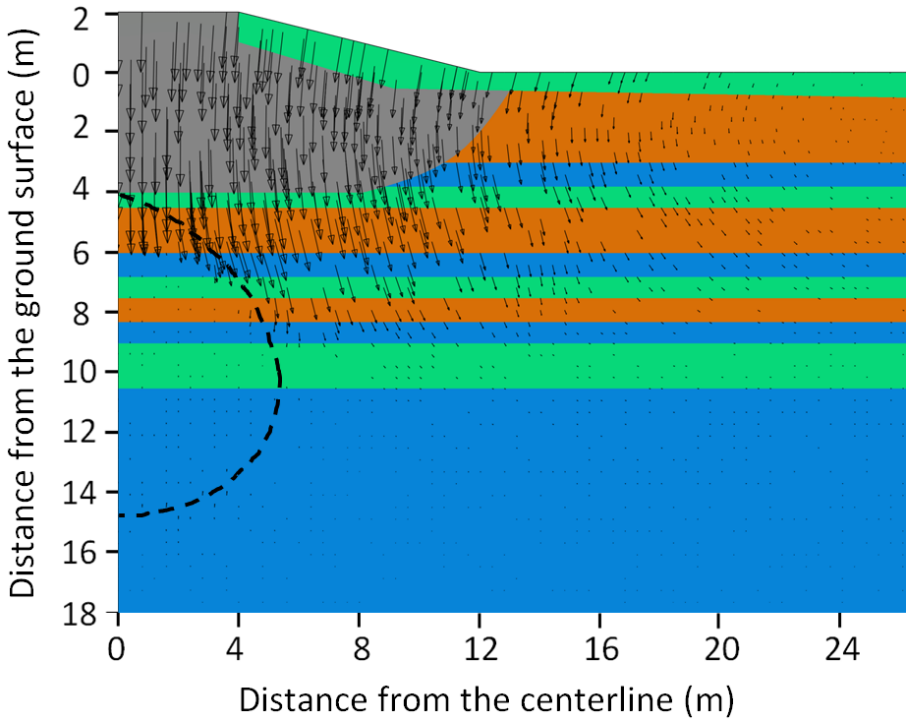

Figure 11: Displacement vectors from the fully-coupled analysis in July 2014. Dashed line delineates the approximate location of the simulated frost bulb

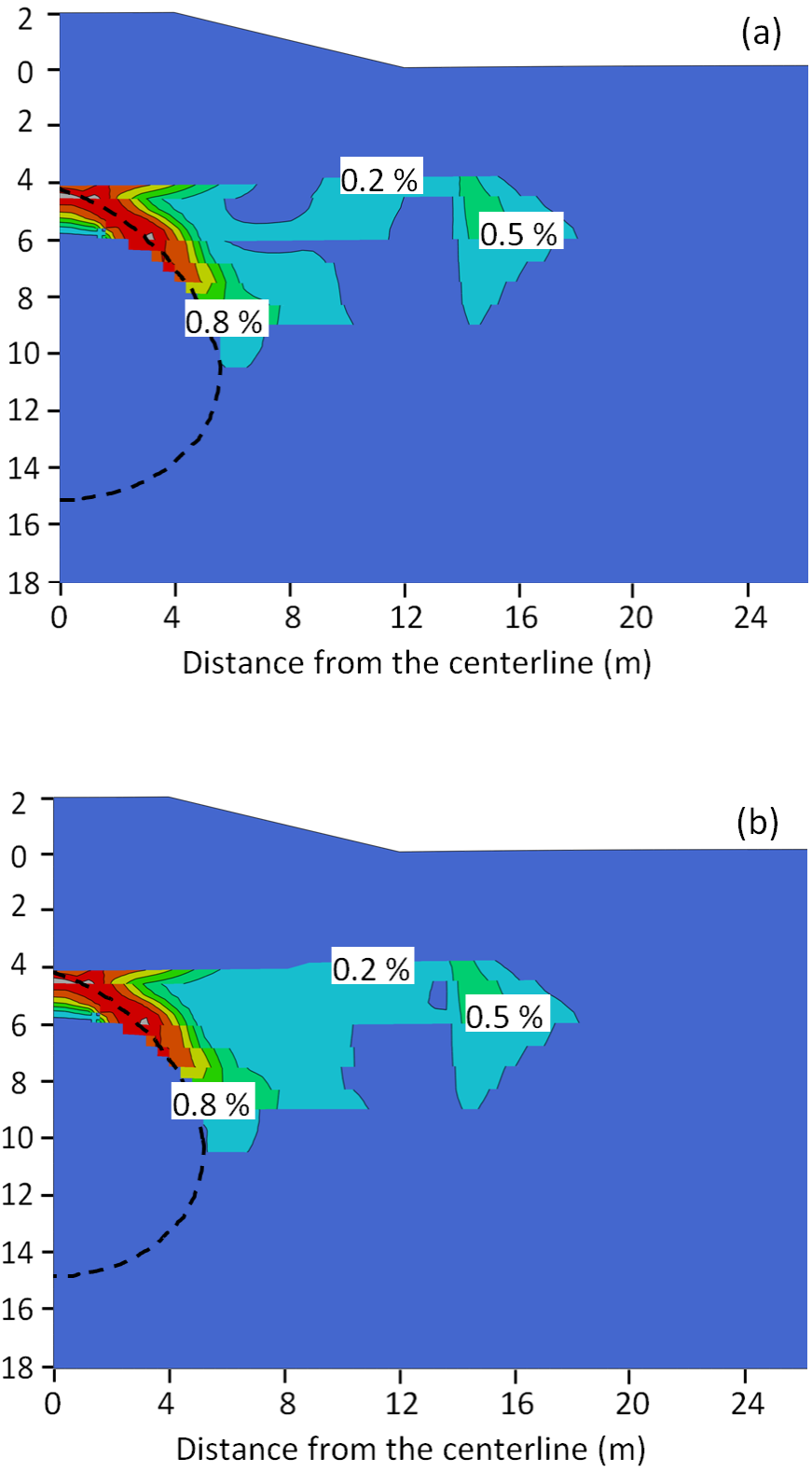

Figure 12: The contours of the plastic strains in (a) February 2014 and (b) July 2014 (the contours interval is 0.3%).

The deformation in this area is the reason for the ongoing settlements on the road surface.

As can be seen in Figure 8, sequentially-coupled analysis simulates slightly larger displacements compared to the fully-coupled analysis. This result is consistent with the results by Xu et al. (2009) reported in ABAQUS (2012). They studied thaw consolidation of permafrost around a warm pipeline. The difference of simulated settlements between the fully- and sequentially-coupled analyses is attributed to the difference in simulated ground temperatures. The simulated ground temperatures by fully-coupled analysis are colder than those simulated by the thermal modeling as part of the sequentially-coupled analysis. Figure 13 shows the comparisons of ground temperatures between the two analysis approaches at three points located inside and in the vicinity of the frost bulb (the approximate location of the frost bulb is depicted in Figure 3). The first point was chosen inside the simulated frost bulb at a depth of 10 m under the centerline of the embankment. The second and third points were chosen in the vicinity of the simulated frost bulb at depths of 14 m and 11 m under the centerline and the shoulder, respectively. The fully-coupled analysis simulates colder temperatures at all three locations. The effect is more noticeable for locations around the frost bulb (Figures 13(b) and (c)). In these locations, the temperatures simulated by the fully-coupled analysis were found to remain frozen for longer compared to those by the sequentially-coupled analysis. Colder temperatures result in stiffer and consequently less compressible soil in fully-coupled analysis which in turn produces lower deformations.

The comparison between the simulated settlements using the two analyses can be useful as a basis for a more conservative design by the sequential analysis. This finding

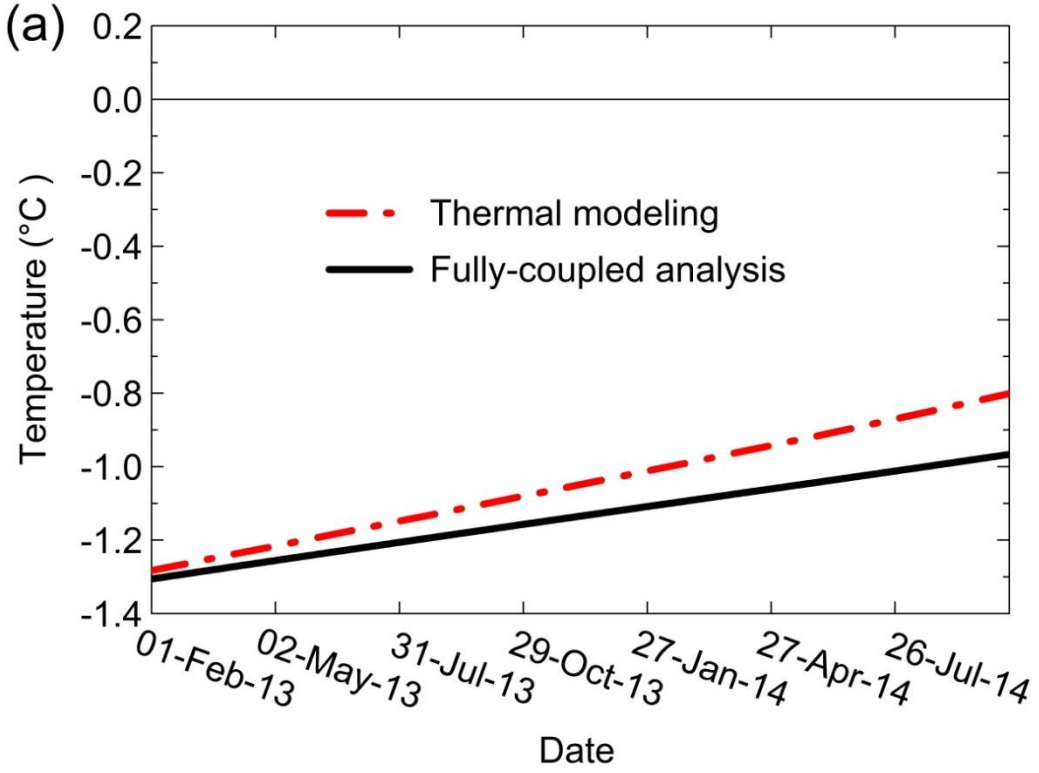
(a)
0.2
0.0
-0.2
-0.4
-0.6
-0.8
-1.0
-1.2
-1.4
Temperature (°C)
Thermal modeling
Fully-coupled analysis
01-Feb-13
02-May-13
31-Jul-13
29-Oct-13
27-Jan-14
27-Apr-14
26-Jul-14
Date

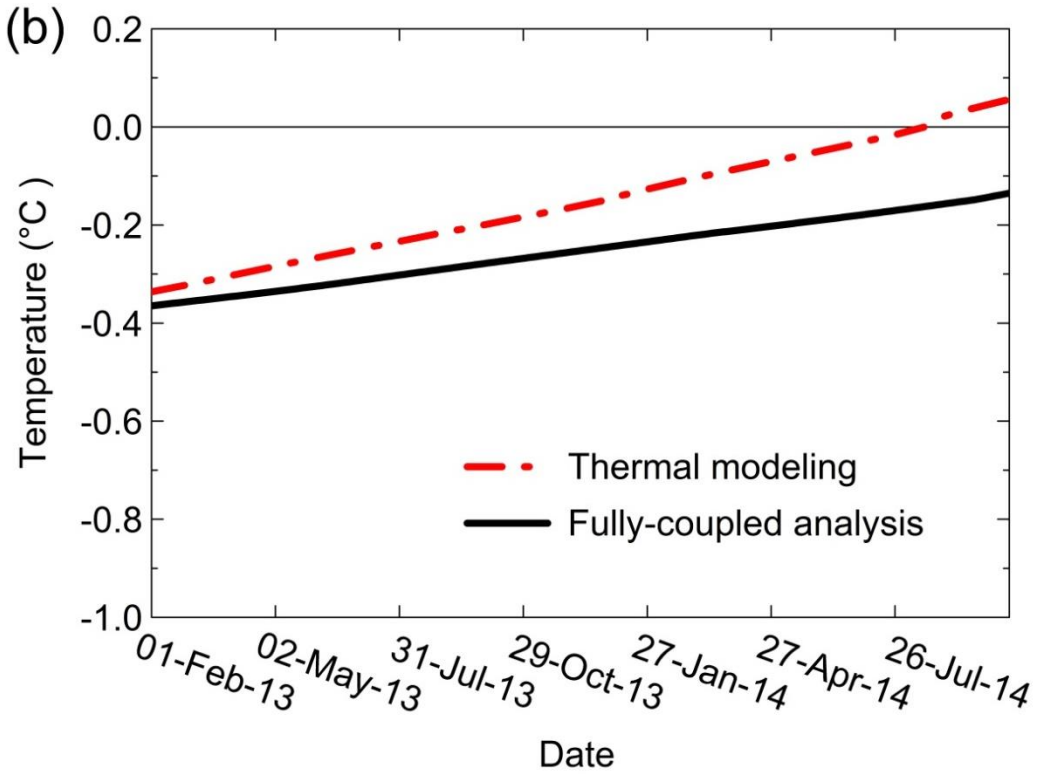
(b)
0.2
0.0
-0.2
-0.4
-0.6
-0.8
-1.0
Temperature (°C)
Thermal modeling
Fully-coupled analysis
01-Feb-13
02-May-13
31-Jul-13
29-Oct-13
27-Jan-14
27-Apr-14
26-Jul-14
Date

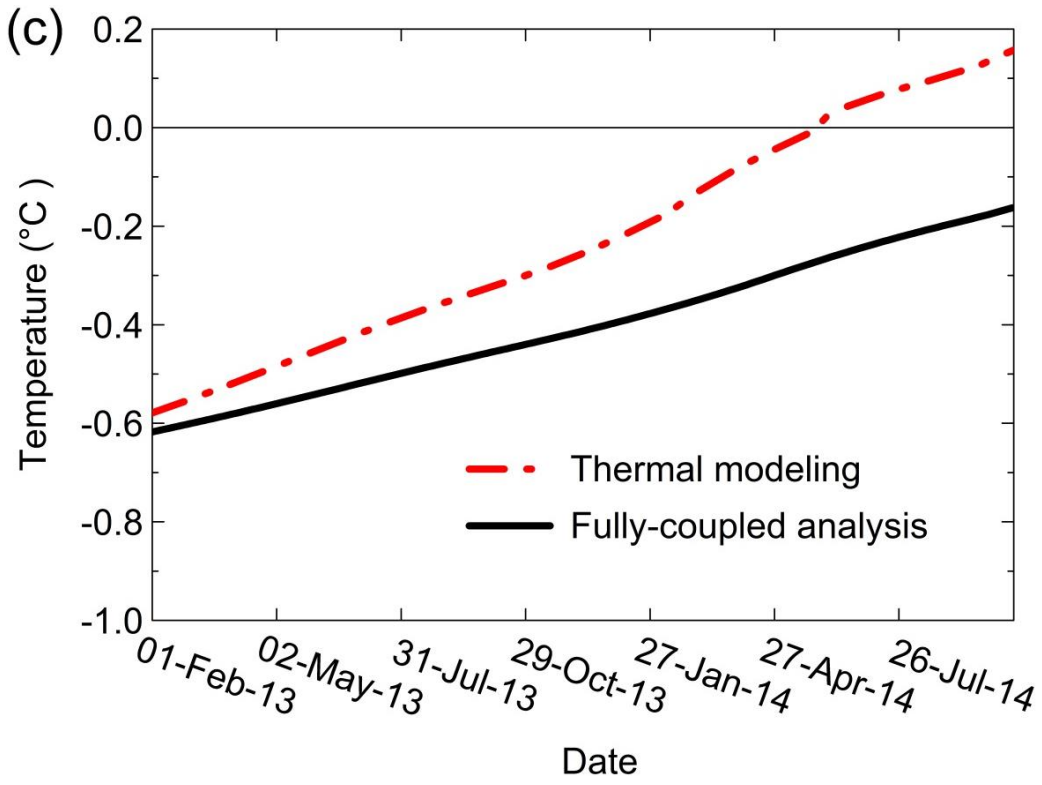

Figure 13: Comparison between simulated temperatures by thermal modeling (first stage of the sequential analysis) and fully-coupled analyses at three points. (a) 10 m beneath the centerline inside the frost bulb; (b) 14 m beneath the centreline outside the frost bulb; and (c) 11 m below the shoulder outside the frost bulb.

is also useful when designs are based on numerical results of some computer programs which are not capable of conducting fully-coupled analyses.

The contribution of creep was found to be minimal. As stated previously, the creep parameters in this research were taken from the literature. Considering the complexities and uncertainties regarding the creep behaviour of the soils over the frost bulb, further creep tests should be performed. Creep tests should include triaxial creep tests and should be conducted on samples from different depths under the gravel fill and above the frost bulb.

4.8.2 Lateral Displacements

Figure 14 shows the measured and simulated lateral displacements at the shoulder and the simulated displacements at the toe of the embankment from October 2012 until October 2013. Lateral displacements at the shoulder were measured using the vertical ShapeAccelArray (Measurand, 2012). Those at the toe were measured using slope inclinometers (SI). The simulated lateral displacements agree reasonably well with the measured values by SAA located at the shoulder. The maximum deflections are restricted to the area between the depths of around 4 m to 8 m. The gravel and the frozen materials are stiffer than the surrounding unfrozen soil under the gravel fill. This zone, which remains unfrozen during the whole time frame of the second instrumentation program, is located between the bottom of the gravel fill and the top of the frost bulb. The load from the weight of the road embankment and the gravel fill causes the unfrozen soil to spread laterally. The amount of the lateral displacements decrease at locations away from the frost bulb. This can be the reason why the lateral displacements at the toe are lower compared to those beneath the shoulder of the embankment (Figure 14). It is also seen that the amount of lateral spreading increases with time as the embankment and the gravel fill gradually settles.

4.9. CONCLUSIONS

A numerical model was developed and calibrated to investigate the deformation mechanisms of a road embankment in northern Manitoba, Canada. The data from field instrumentation and laboratory testing programs were used in calibrating the model. The model reasonably simulated the vertical and lateral displacements of the road embankment. The conclusions are summarised as follows:

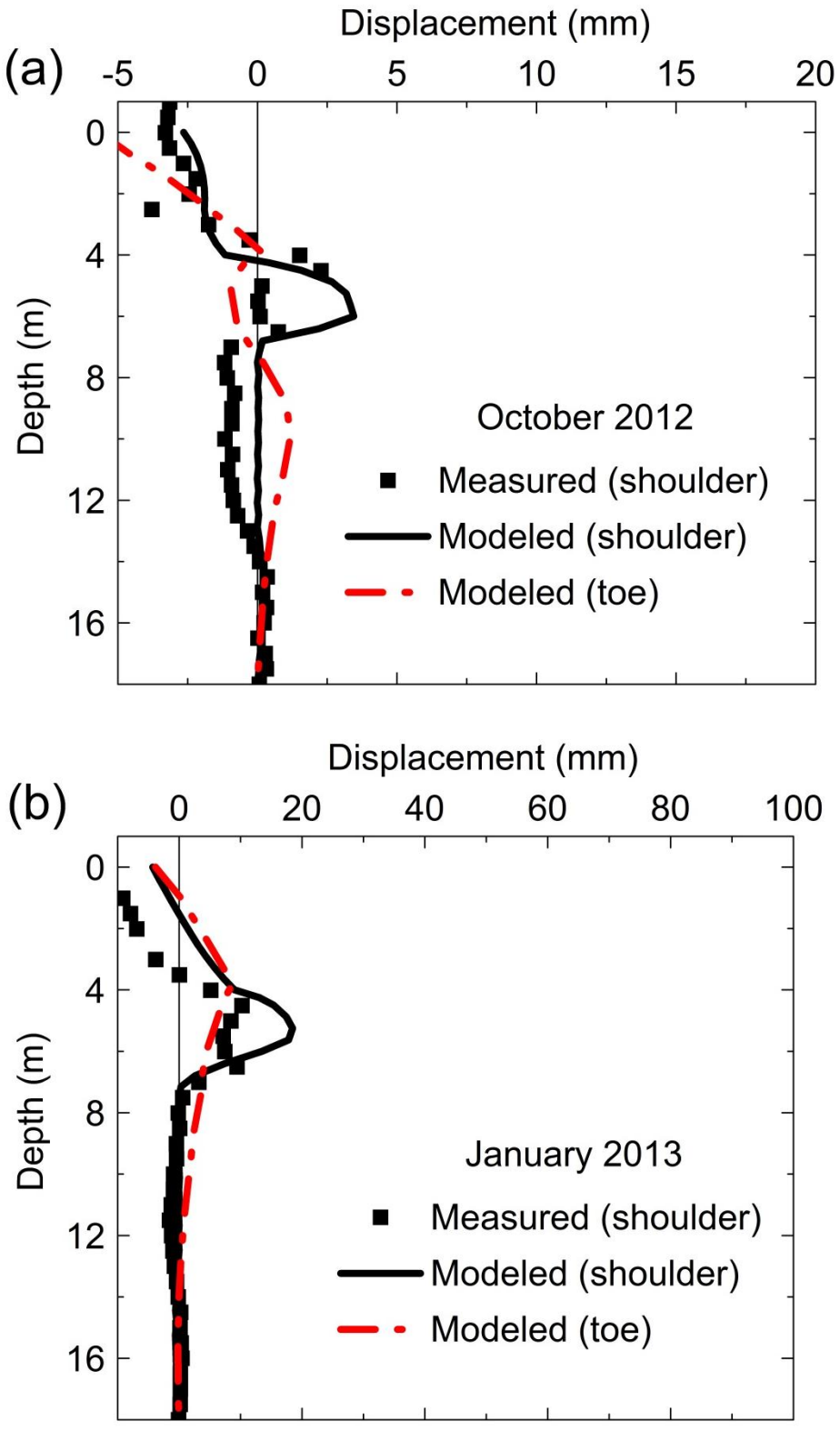
(a)
Displacement (mm)
-5
0
5
10
15
20
Depth (m)
0
4
8
12
16
October 2012
Measured (shoulder)
Modeled (shoulder)
Modeled (toe)
(b)
Displacement (mm)
0
20
40
60
80
100
Depth (m)
0
4
8
12
16
January 2013
Measured (shoulder)
Modeled (shoulder)
Modeled (toe)

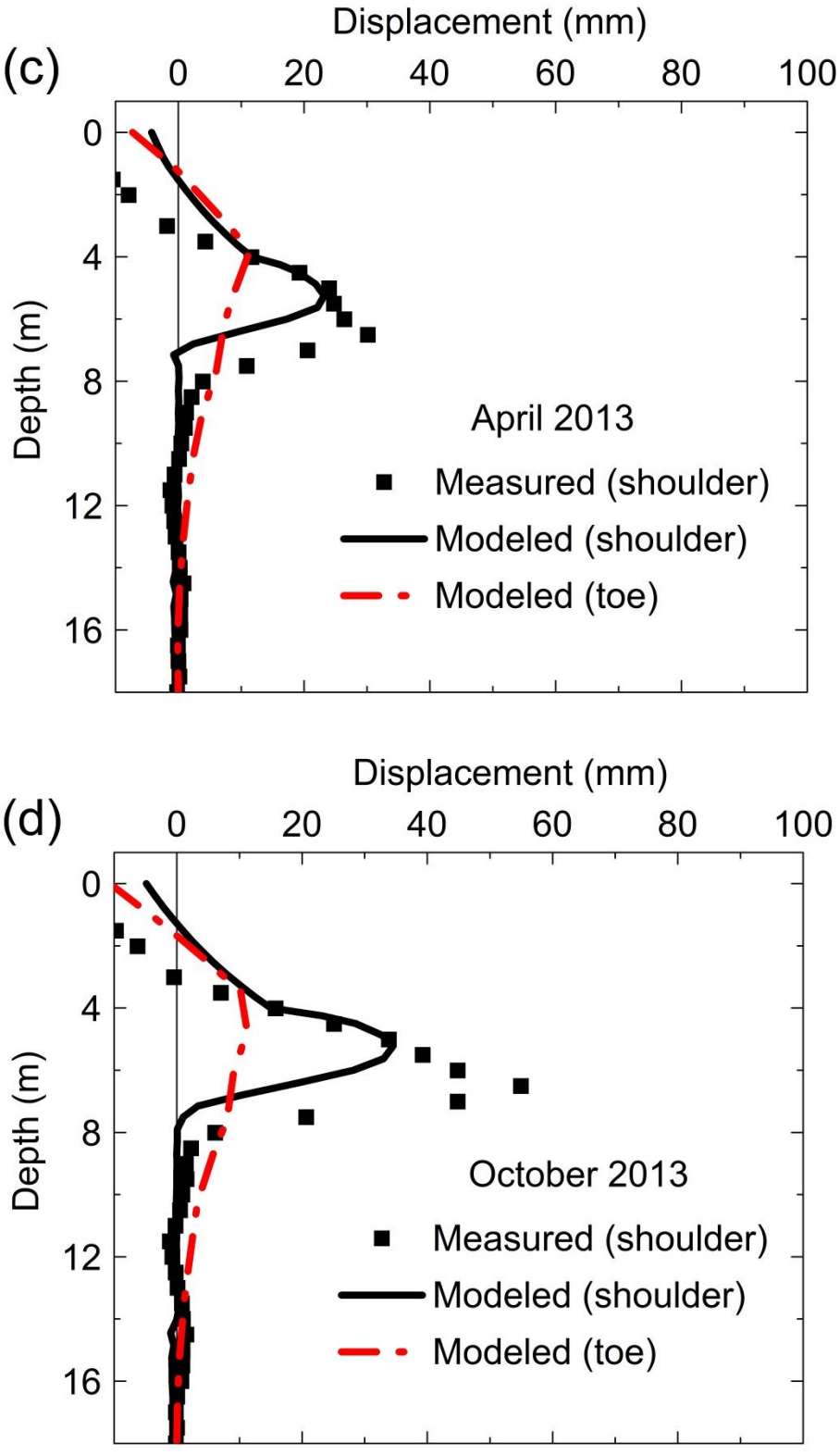

Figure 14: Measured and modeled lateral displacements at the shoulder, and the modeled displacements at the toe of the embankment at different times. Measured values are after Flynn et al. (2015b).

1) Gradual degradation of the frost bulb under the embankment affects the mechanical behaviour of the soil below the embankment and the associated deformations of the embankment. Fully-coupled analysis simulates slightly lower displacements compared to the sequentially-coupled analysis. This is attributed to the colder ground temperatures simulated by the fully-coupled analysis compared to those by sequentially-coupled analysis.
2) Lateral deformations are mainly due to the lateral spreading of the unfrozen soil under the shoulder of the embankment. The amount of lateral deformations are lower at the toe of the embankment compared to the shoulder.
3) The measured settlements show sharp upward movements in each spring beginning around mid-April and lasting 4 to 8 weeks. This can be due to the reduction of effective stress which is caused by the increase in pore water pressure during spring melt. Another possible explanation is that the clay layer may have swelled under the embankment in response to the increased water availability from ground ice thawing. During the spring melt, unfrozen water that originates in the thawed region around the frost bulb can accumulate in the clay layer. The numerical model was not able to capture the measured upward movements. This requires further studies including experimental tests to understand the operating mechanisms that caused the upward movements of the foundations during spring thaw. The mechanism can be implemented into the model in order to capture the behaviour.

REFERENCES

ABAQUS Analysis user's manual 6.12-1, Dassault Systems Simulia Corp., Providence, RI, USA; 2012. (http://www.3ds.com/products-services/simulia/products/abaqus/)

Alfaro, M.C., Ciro, G. A., Thiessen, K. J., Ng, T. (2009). Case Study of Degrading Permafrost beneath a Road Embankment. *Journal of Cold Regions Engineering*, 23(3), 93–111.

Batenipour, H., Alfaro, M., Kurz, D., Graham, J. (2014). Deformations and ground temperatures at a road embankment in northern Canada. *Canadian Geotechnical Journal*, *51*(3), 260–271.

Farouki, O. (1985). Ground thermal properties. *Proc., Thermal Design Considerations in Frozen Ground Engineering*, ASCE, New York

Flynn, D., Alfaro, M., Graham, J., and Arenson, L. (2015b) Observed deformations of an existing highway embankment on degrading permafrost. *Proc. 68th Annual Geotechnical Conference*, Quebec City, Quebec (in press)

Flynn, D., Kurz, D., Alfaro, M., Graham, J., and Arenson, L. (2015a) Forcasting ground temepratures under a highway embankment on degrading permafrost. *Journal of Cold Regions Engineering, ASCE*. (submitted)

Fortier, R., LeBlanc, A., Yu, W. (2011). Impacts of permafrost degradation on a road embankment at Umiujaq in Nunavik (Quebec), Canada. *Canadian Geotechnical Journal*, 48(5), 720–740.

Geo-slope (2010), Thermal Modeling with TEMP/W 2007, Geo-slope International Ltd., Calgary, Alberta, Canada.

Gholamzadeh, A., Alfaro, M., Graham, J. (2015). Modeling of Permafrost Degradation under a Road Embankment. *Cold Regions Science and Technology*, Manuscript submitted for publication.

Guymon, G. L., Luthin, J. N. (1974). A coupled heat and moisture transport model for Arctic soils. *Water Resources Research*, *10*(5), 995.

Harlan, R. L. (1973). Analysis of coupled heat-fluid transport in partially frozen soil. *Water Resources Research*, *9*(5), 1314.

Kurz, D., Alfaro, M. and Graham, J. (2015). Thermal Conductivities of Frozen and Unfrozen Soil in the Active Layer. *Cold Regions Science and Technology*. Manuscript submitted for publication

Lunardini, V. J. (1981). Heat Transfer in Cold Climates, Van Nostrand Reinhold Company, NY.

Measurand Shape Advantage. (2012). *ShapeAccelArray Brochure*. Measurand Shape Advantage.

Ming, F, Li, D. (2012). Thaw Settlement Analysis of Permafrost Embankment with Different Pavement Materials. *Cold Regions Engineering*, 532–541.

Morgenstern, N. R., Nixon, J. F. (1971). One-dimensional Consolidation of Thawing Soils. *Canadian Geotechnical Journal*, *8*(4), 558–565.

Morsy, M. M., Morgenstern, N. R., Chan, D. H. (1995). Simulation of creep deformation in the foundation of Tar Island Dyke. *Canadian Geotechnical Journal*, *32,* 1002-1023.

Qi, J., Yao, X., Yu, F., Liu, Y. (2012). Study on thaw consolidation of permafrost under roadway embankment. *Cold Regions Science and Technology*, *81*, 48–54.

Tarnawski, V.R., Wagner, B. (1996). On the predication of hydraulic conductivity of frozen soils. *Canadian Geotechnical Journal*, 33, 176-180.

Taylor, G. S., Luthin, J. N. (1978). A model for coupled heat and moisture transfer during soil freezing. *Canadian Geotechnical Journal*, 15, 548–555.

Tsytovich, N. A. (1975). The Mechanics of Frozen Ground (trans.), eds. G.K. Swinzow and G. P. Tschebotarioff. New York: Scripta/McGraw-Hill. (In Russian: Moscow: Vysshaya Shkola Press, 1973.)

Wang, L., Wang, W., Yu, F. (2015). Thaw consolidation behaviours of embankments in permafrost regions with periodical temperature boundaries. *Cold Regions Science and Technology*, *109*, 70–77.

Wood, D. (1990). Soil behaviour and critical state soil mechanics. Cambridge, England: Cambridge University Press.

Xu, J., Abdalla, B., Eltaher, A., Jukes, P. (2009). Permafrost Thawing-Pipeline Interaction Advanced Finite Element Model. *Proceedings of the ASME 2009 28th International Conference on Ocean, Offshore, and Arctic Engineering, OMAE2009–79554*. Honolulu, Hawaii, USA.

Zheng, B., Zhang, J., Qin, Y. (2010). Investigation for the deformation of embankment underlain by warm and ice-rich permafrost. *Cold Regions Science and Technology*, *60*(2), 161–168.

CHAPTER 5: CONCLUSIONS AND RECOMMENDATIONS

In this chapter, a summary of all the conclusions and recommendations for future work is presented. Two numerical models were developed and calibrated in order to investigate the thermal and mechanical behaviour of PR 391 road embankment in northern Manitoba, Canada. Data from comprehensive field instrumentation and laboratory testing programs were used in calibrating the models. Both models reasonably simulated the observed behaviour of the road embankment.

5.1. THERMAL MODELING

For the thermal modeling, the conclusions are as follows:

1) A thermal numerical model has been developed to investigate the ground thermal regime under a road embankment in northern Manitoba, Canada. Data from field instruments and laboratory testing programs were used in calibrating the model. Instrumentation and monitoring provided temperature data for 6 years at the toe and mid-slope of the embankment, and 2 years at the shoulder and centreline.
2) The model simulated the ground thermal regime under the embankment with reasonable accuracy. The depth of zero annual temperature amplitude beneath the embankment was estimated to be about 8 metres, which is consistent with the measured temperatures. A zone of frozen soil or frost bulb exists beneath the embankment. It varies seasonally, but is gradually degrading over time and is likely to be the main reason for ongoing movements of the embankment. The model estimated reasonably well the shape, location, and seasonal changes of the frost

bulb. Based on the predicted future air temperatures, the model results show that the frost bulb will disappear completely within 20 years, and perhaps much sooner.

5.2. STRESS-DEFORMATION MODELING

For the stress-deformation modeling, the conclusions are as follows:

1) Gradual degradation of the frost bulb under the embankment affects the mechanical behaviour of the soil below the embankment and the associated deformations of the embankment. Fully-coupled analysis simulates slightly lower displacements compared to the sequentially-coupled analysis. This is attributed to the colder ground temperatures simulated in the fully-coupled analysis compared to those using sequentially-coupled analysis.
2) Lateral deformations are mainly due to the lateral spreading of the unfrozen soil under the shoulder of the embankment. The amount of lateral deformations are lower at the toe of the embankment compared to the shoulder.
3) The measured settlements show sharp upward movements in each spring beginning around mid-April and lasting 4 to 8 weeks. This can be due to the reduction of effective stress which is caused by the increase in pore water pressure during spring melt. Another possible explanation is that the clay layer may have swelled under the embankment in response to the increased water availability from ground ice thawing. During the spring melt, unfrozen water that originates in the thawed region around the frost bulb can accumulate in the clay layer. The numerical model was not able to capture the measured upward movements. This requires further studies including experimental tests to understand the operating mechanisms that caused the upward movements of the foundations during spring

thaw. The mechanism can be implemented into the model in order to capture the behaviour.

5.3. RECOMMENDATIONS FOR FUTURE WORK

The results of the numerical modeling can be improved by the following future work:

1) The thermal and mechanical properties of the soil at the centerline of the embankment above the frost bulb should be determined. A better understanding of the properties of the soil in this region can help improving the results of the numerical models.
2) The creep properties of the soil under the gravel region should be determined by conducting triaxial creep tests on samples from different depths. Based on the assumed creep properties, the results of the numerical model show minimal effects of creep on the mechanical behaviour of the embankment. However, determining the creep properties can help better understanding of the creep effects and improving the results of the model.
3) Conducting experimental tests in order to understand the mechanism of heaving of the road during thawing periods of the year, as observed by the measured displacements. The mechanism can be implemented into the model in order to capture the behaviour.

REFERENCES

ABAQUS Analysis user's manual 6.12-1, Dassault Systems Simulia Corp., Providence, RI, USA; 2012. (http://www.3ds.com/products-services/simulia/products/abaqus/)

Alfaro, M.C., Ciro, G. A., Thiessen, K. J., Ng, T. (2009). Case Study of Degrading Permafrost beneath a Road Embankment. *Journal of Cold Regions Engineering*, 23(3), 93–111.

Andersland, O.B., Ladanyi, B. (2004). Frozen Ground Engineering, 2nd ed. John Wiley and Sons, Inc, Hoboken, NJ.

Anderson, D. M., Tice A. R. (1973). The unfrozen interfacial phase in frozen water systems. *Ecological Studies: Analysis and Synthesis*, vol. 4, Hadar, A. (ed.). Springer: New York, 107-124.

Anisimov, O., Reneva, S. (2006). Permafrost and changing climate: the Russian perspective. *Ambio*, *35*(4), 169–175.

Barbour, S. L., Krahn, J. (2004). Numerical Modeling – Prediction or Process? *Geotechnical News.* Obtained July 2015 from Geoslope website at: http://www.geo-slope.com

Batenipour, H., Alfaro, M., Kurz, D., Graham, J. (2014). Deformations and ground temperatures at a road embankment in northern Canada. *Canadian Geotechnical Journal*, 51(3), 260-271.

Brown, R.J.E. (1960). The distribution of permafrost and its relation to air temperature in Canada and the U.S.S.R. *Arctic*, *13*(3), 163-177.

Brown, R.J.E. (1969). Distribution of Permafrost in Canada, *Third Canadian Conference on Permafrost, Division of Building Research*, National Research Council, Ottawa.

Canadian Centre for Climate Modeling and Analysis (CCCma), 2015. 3rd Generation Coupled Global Climate Model (CGCM3.1/T47 IPCC SRES A2 Scenario Data). 2010. University of Victoria. (http://cccma.ec.gc.ca/)

Carslaw, H. S., Jaeger, J. C. (1947). Conduction of heat in solids. Clarendon Press, Oxford.

Climate Change Office (2005). Government of Canada. (http://www.climatechange.ge.ca/english/default.asp)

Darrow, M.M. (2011). Thermal modeling of roadway embankments over permafrost. *Cold Regions Science and Technology*, 65(3), 474-487.

Ding, Y. (1998). Recent Degradation of Permafrost in China and the Response to ClimaticWarming, in Lewkowicz, A. G. and Allard, M. (eds.), *Proceedings of the Seventh International Conference on Permafrost, Université Laval, Québec, Collection Nordicana,* 57, 225–231.

Farouki, O. (1985). Ground thermal properties. *Proc., Thermal Design Considerations in Frozen Ground Engineering*, ASCE, New York.

Flato, G. M., Boer, G. J. (2001). Warming asymmetry in climate change simulations. *Geophysical Research Letters*, 28(1), 195–198.

Flynn, D., Alfaro, M., Graham, J., and Arenson, L. (2015b). Observed deformations of an existing highway embankment on degrading permafrost. *Proc. 68th Annual Geotechnical Conference*, Quebec City, Quebec (in press)

Flynn, D., Kurz, D., Alfaro, M., Graham, J., and Arenson, L. (2015a). Forcasting ground temepratures under a highway embankment on degrading permafrost. Journal of Cold Regions Engineering, ASCE. (submitted)

Foriero, a., Ladanyi, B. (1995). FEM Assessment of Large-Strain Thaw Consolidation. *Journal of Geotechnical Engineering*, *121*(2), 126–138.

Fortier, R., LeBlanc, A., Yu, W. (2011). Impacts of permafrost degradation on a road embankment at Umiujaq in Nunavik (Quebec), Canada. *Canadian Geotechnical Journal*, 48(5), 720–740.

Geo-Slope. (2010). Thermal Modeling with TEMP/W 2007. Calgary, Canada: Geo-slope International.

Gholamzadeh, A., Alfaro, M., Graham, J. (2015). Modeling of Permafrost Degradation under a Road Embankment. *Cold Regions Science and Technology*, Manuscript submitted for publication.

Guymon, G. L., Luthin, J. N. (1974). A coupled heat and moisture transport model for Arctic soils. *Water Resources Research*, *10*(5), 995.

Harlan, R. L. (1973). Analysis of coupled heat-fluid transport in partially frozen soil. *Water Resources Research*, *9*(5), 1314.

Hildebrand, E. E. (1983). Thaw settlement and ground temperature model for highway design in permafrost areas. *Proceedings of the Fourth International Conference on Permafrost.* Washington, D.C.: National Academy Press, 492-497.

Houston, S.L., and Lin, H-D. (1987). A thermal consolidation model for pelagic clays. *Marine Geotechnology, 7,* 79–98.

Intergovernmental Panel on Climate Change (IPCC) website: http://climate.nasa.gov/effects/

Johansen, Ø. (1975). Thermal conductivity of soils. Ph.D. dissertation, Norwegian Technical University, Trondheim; also, U.S. Army Cold Regions Research and Engineering Laboratory Transl. 637, July 1977.

Kersten, M. S. (1949). Laboratory Research for the Determination of the Thermal Properties of Soils. *ACFEL Technical Report 23, AD71256* (Also: Thermal properties of soils. University of Minnesota Engineering Experiment Station Bulletin No. 28)

Konrad, J-M, Roy, M. (2000). Flexible pavements in cold regions: a geotechnical perspective. *Canadian Geotechnical Journal*, 37, 689–699.

Kurz, D., Alfaro, M. and Graham, J. (2015). Thermal Conductivities of Frozen and Unfrozen Soil in the Active Layer. Cold Regions Science and Technology. Manuscript submitted for publication

Kwong, Y. T. J. and Gan, T. Y. (1994). Northward migration of permafrost along the Mackenzie High-way and climatic warming. *Climatic Change*, 26, 399-419.

Li, Q., Sun, S., Xue, Y. (2010). Analyses and development of a hierarchy of frozen soil models for cold region study. *Journal Of Geophysical Research*, 115, 1-18.

Li, D., Wu, Z., Fang, J., Li, Y., Lu, N. (1998). Heat stability analysis of embankment on the degrading permafrost district in the East of the Tibetan Plateau, China Dongqing. *Cold Regions Science and Technology*, *28*. 183–188.

Li, J-P., Yu, S. (2008). Analysis of the thermal stability of an embankment under different pavement types in high temperature permafrost regions. *Cold Regions Science and Technology*, *54*(2), 120–123.

Ling, F., Zhang, T. (2004). A numerical model for surface energy balance and thermal regime of the active layer and permafrost containing unfrozen water. *Cold Regions Science and Technology*, *38*(1), 1–15

Lunardini, V. J. (1981). Heat Transfer in Cold Climates, Van Nostrand Reinhold Company, NY.

McRoberts, E. C. (1974). Ground Thermal Regime. *Recent advances in permafrost engineering: Lecture notes and reference list*, Department of Civil Engineering, University of Alberta, Edmonton, Alberta, Canada.

Measurand Shape Advantage. (2012). *ShapeAccelArray Brochure*. Measurand Shape Advantage.

Michalowski, R. L., Zhu, M. (2006). Frost heave modeling using porosity rate function. *International Journal for Numerical and Analytical Methods in Geomechanics*, 30, 703-722.

Ming, F, Li, D. (2012). Thaw Settlement Analysis of Permafrost Embankment with Different Pavement Materials. *Cold Regions Engineering*, 532–541.

Morgenstern, N. R., Nixon, J. F. (1971). One-dimensional Consolidation of Thawing Soils. *Canadian Geotechnical Journal*, *8*(4), 558–565.

Morgenstern, N. R., Smith, L. B. (1973). Thaw–Consolidation Tests on Remoulded Clays. *Canadian Geotechnical Journal*, *10*(1), 25–40

Morsy, M. M., Morgenstern, N. R., Chan, D. H. (1995). Simulation of creep deformation in the foundation of Tar Island Dyke. *Canadian Geotechnical Journal*, *32,* 1002-1023.

Natural Resources Canada (NRC) (2003). National annual temperature scenario: 2050. The atlas of Canada, Natural Resources Canada. (http://atlas.gc.ca)

Natural Resources of Canada (NRC). Permafrost in Canada. Atlas of Canada. Retrieved: July 2015 from Natural Resources Canada website at: http://www.nrcan.gc.ca/earth-sciences/geography/atlas-canada/selected-thematic-maps/16876

Nelson, F. E., Brigham, L.W.,Hinkel, K.M., Smith, O., Parker, W., Tucker, W., Romanovsky, V. E., Vinson, T., Shiklomanov, N.I. (2003). Climate Change , Permafrost , and Impacts on Civil Infrastructure. *U.S. Arctic Research Commission: Permafrsot Task Force Report*

Nixon, J. F., Morgenstern, N. R. (1974). Thaw–Consolidation Tests on Undisturbed Fine-grained Permafrost. *Canadian Geotechnical Journal*, *11*(1), 202–214.

Ostrekamp, T. E., Burn, C.R. (2003). Permafrost. *Encyclopedia of Atmospheric Sciences, 2nd Ed*. *Volume 4.* 1717-1729. Elsevier Ltd.

Osterkamp, T. E., Lachenbruch, A. H. (1990). Thermal Regime of Permafrost in Alaska and Predicted Global Warming. *Journal of Cold Regions Engineering*, *4*(1), 38–42.

Osterkamp, T. E., Romanovsky, V. E. (1999). Evidence for warming and thawing of discontinuous permafrost in Alaska. *Permafrost and Periglacial Processes*, *10*(1), 17–37.

Qi, J., Yao, X., Yu, F., Liu, Y. (2012). Study on thaw consolidation of permafrost under roadway embankment. *Cold Regions Science and Technology*, *81*, 48–54.

Tarnawski, V.R., Wagner, B. (1996). On the predication of hydraulic conductivity of frozen soils. *Canadian Geotechnical Journal*, 33, 176-180.

Taylor, G., S., Luthin, J., N. (1978). A model for coupled heat and moisture transfer during soil freezing. *Canadian Geotechnical Journal*, 15, 548–555.

Tsytovich, N. A. (1975). The Mechanics of Frozen Ground (trans.), eds. G.K. Swinzow and G. P. Tschebotarioff. New York: Scripta/McGraw-Hill. (In Russian: Moscow: Vysshaya Shkola Press, 1973.)

Van Everdingen, R. O. (1998). Multi-language glossary of permafrost and related ground-ice terms. *International Permafrost Association (IPA).* Retrieved July 2015 from NSIDC website at: https://nsidc.org/fgdc/glossary/illustrations.pdf

Vitt, D. H., Halsey, L. a, Zoltai, S. C. (1994). The bog landforms of continental Western Canada in relation to climate and permafrost patterns. *Arctic and Alpine Research*, *26*(1), 1–13.

Wang, L., Wang, W., Yu, F. (2015). Thaw consolidation behaviours of embankments in permafrost regions with periodical temperature boundaries. *Cold Regions Science and Technology*, *109*, 70–77.

Wood, D. (1990). Soil behaviour and critical state soil mechanics. Cambridge, England: Cambridge University Press.

Xu, J., Abdalla, B., Eltaher, A., Jukes, P. (2009). Permafrost Thawing-Pipeline Interaction Advanced Finite Element Model. *Proceedings of the ASME 2009 28th International Conference on Ocean, Offshore, and Arctic Engineering, OMAE2009–79554*. Honolulu, Hawaii, USA.

Zheng, B., Zhang, J., Qin, Y. (2010). Investigation for the deformation of embankment underlain by warm and ice-rich permafrost. *Cold Regions Science and Technology*, *60*(2), 161–168.

Zhu, M. , Michalowski, R.L. (2005). Simulation of Heat Transfer in Freezing Soils Using ABAQUS. *Abaqus Users' Conference,* pp.1–7